THESIS

VULNERABILITY OF A COASTAL INDUSTRIAL COMMUNITY TO SEA LEVEL RISE, HURRICANES, AND CLIMATE CHANGE

Submitted by

Mohamed Abdelhafez

Department of Civil and Environmental Engineering

In partial fulfillment of the requirements

For the Degree of Master of Science

Colorado State University

Fort Collins, Colorado

Fall 2020

Master's Committee:

Advisor: Hussam Mahmoud
Co-advisor: Bruce R. Ellingwood

Erin Arneson

ABSTRACT

THE VULNERABILITY OF A COASTAL INDUSTRIAL COMMUNITY TO SEA LEVEL RISE, HURRICANES AND CLIMATE CHANGE

Approximately 10% of the world's population live and work in low-lying coastal regions that are less than 10 meters above sea level, and this percentage is likely to increase during the remainder of the 21st century. Along with this growth is the potential for increasing economic losses due to hurricanes, storm surge and sea-level rise (SLR) in an era of climate change. More than 80% of global commodities are traded by sea. In the United States, ports contributed $5.4 trillion to the U.S. economy, or around 26% of the GDP, and provided jobs, either directly or indirectly, to over 30 million individuals.

In this study, a new model for quantifying the functionality of the seaports subject to various hurricanes, storm surge and SLR due to a changing climate is implemented in a fault tree analysis. A hydrodynamic analysis to enable the impact of tropical cyclones and SLR on port facilities is validated using data from Hurricane Katrina. A series of plausible hazard scenarios is identified and their impact on the Port of Mobile, AL is assessed. The key findings show that if a Katrina-like hurricane were to occur late in the 21st Century, the damages to the Port of Mobile, AL would be increased by 5.5 times and 6.5 times by SLR under RCP 4.5 and RCP 8.5 scenarios when compared to the damages caused by historical Hurricane Katrina alone. Furthermore, the immediate post-disaster functionality of the port under the RCP 8.5 scenario would be reduced to virtually zero.

ACKNOWLEDGEMENTS

To the Fulbright program, AMIDEAST, and the Binational Fulbright Commission in Egypt, thank you for choosing me over thousands of applicants from Egypt, and for giving me this unique opportunity to do my M.Sc. at Colorado State University. Special thanks to my AMIDEAST advisor, who recommended me to apply to CSU. Now I can see that it was the best choice.

This work would never be possible without the support from my advisor Dr. Hussam Mahmoud and co-advisor Professor Bruce R. Ellingwood. I thank them heartily for their continuous support, motivation, and guidance.

I want to thank Professor Hussam Mahmoud, who accepted me as an M.Sc. student and believed in me without seeing any of my previous work. I also want to thank him not only for his technical guidance, support, and endless help but also for listening and for the helpful discussions, that helped me to develop a logical way of thinking not only in research but also in other life aspects.

I would like to thank Professor Bruce R. Ellingwood for giving me the honor of working under his supervision and for being his student. I am grateful for his guidance, patience, understanding, support and sharing the knowledge. I am also thankful for his academic advice and every lesson I learned from him through each meeting.

I want to express my thanks to my additional committee member, Dr. Erin Arneson, for her support and interest in the progression of this research.

I would like also to thank Dr. Bret Webb from the University of South Alabama for his guidance on the use of Delft3D and for the discussions regarding the coupled SLR and hurricane simulations. Dr. Yanlin Guo of CSU provided invaluable assistance and guidance regarding the hurricane simulation scenarios.

I was also honored to receive KENNETH G. MEDEARIS SCHOLARSHIP and would like to take this opportunity and thank both the provider and the selection committee for choosing me for this prestigious award.

Thanks also to all the people I met during the MSc, to CSU Fulbright family, and to my Egyptian friends, especially Emad and Abdo.

Finally, sincerely thanks to my family for their endless emotional and financial support. Thanks to my father, Professor Ali Abdelhafez, for encouraging me to follow my dream, for his unlimited support, and for believing in me even when I had doubts. Also, thanks to my mother, Jehan, for her support, care, and prayers that helped me to become the person I am today. Thanks to my brothers and best friends, Motaz and Eslam, for keeping me in your minds even with the long-distance barriers. Without my family, I would not be where I am today

TABLE OF CONTENTS

LIST OF TABLES

LIST OF FIGURES

CHAPTER 1. INTRODUCTION

1.1. Problem statement

Natural hazards worldwide occur about five times more often nowadays than in the 1970s (Golnaraghi et al., 2014). Over 3,900 natural climatological hazards (floods, droughts, tropical cyclones and storm surge, extreme temperatures, wildfires and others) caused the death of more than 1.9 million people and almost $2.4 trillion in damage, from 1970 to 2012 (Golnaraghi et al., 2014; Guha-Sapir et al., 2014). As more than 80% of natural hazards are climate-related events (UNISDR, 2013), increasing global temperatures may cause climatic changes that can intensify and amplify natural disasters, affecting society and biodiversity. Figure 1-1 shows the major natural hazards that are likely to be impacted by climate change in the future.

Figure 1-1: Effects of global warming due to climate change.

Sea-level rise (SLR) and its effects on coastal regions in the United States (U.S.) and other countries worldwide, especially in East Asia, have been a major concern since the 1980s, when the potential impacts of human-induced global warming became apparent to the scientific community, urban planners and governmental agencies. SLR, directly and indirectly, threatens ecosystems, human habitation and essential community services in low-lying coastal plains for up to half a billion residents worldwide (Neumann et al., 2015). Numerous researchers have studied the consequences of SLR on coastal regions floods (Revell et al., 2011; Le Cozannet et al., 2015), marine ecosystems (Kane et al., 2015; Clough et al., 2016), or marine protection systems (Isobe, 2013; Burcharth et al., 2014). Tropical cyclones[1], coastal storm surge, inundation, ground table salinization and saltwater intrusion, coastal erosion, destruction of wetlands, and other fragile coastal ecosystems all are consequences of global warming.

Hurricanes and flooding have caused approximately 80% of the losses due to natural hazards in the decade of the 2000s , while hurricanes alone accounted for about 0.77 million of the world's 1.94 million deaths (Golnaraghi et al., 2014) due to natural hazards from 1970 to 2012. Hurricanes are usually accompanied by storm surge, rain, and extreme wind that causes severe damage to a coastal community's-built environment. Flooding due to storm surge has caused almost half of the deaths due to hurricane events in the U.S. (Rappaport, 2014). For example, Hurricane Katrina in 2005 led to 1,833 deaths and total property damage of approximately $US 107 billion (Knabb

[1] Tropical cyclones are known as hurricanes in the North Atlantic Ocean and the eastern North Pacific and by typhoons in the western North Pacific around the Philippines, Japan, and China.

et al., 2006). Intense coastal flooding in the northeast U.S. triggered by Superstorm Sandy in 2012 led to 159 fatalities and at least $50 billion of direct and indirect economic losses (Blake et al., 2013). The frequency and intensity of natural disasters and the resulting damages are increasing because of population growth and economic development in coastal regions and the influence of global climate effects. Considering the predicted increase in hurricane intensity and frequency with the rising sea-level and anticipated population growth across lowland regions, more individuals and infrastructure will be put at risk by flooding from storm surge (Emanuel, 2013; IPCC, 2014).

In addition to the threat to coastal communities posed by SLR, as shown Figure 1-2, SLR also increases the impact of other climate-driven events such as high tide flooding and hurricanes. Sustainable and healthy coastal communities must be resilient against these expected hazardous events. The need to mitigate or adapt to such risks has led to the development of frameworks and tools to assess and enhance the resilience of coastal communities (U.S. EPA., 2017). Several studies have been conducted to assess the impacts of SLR and climate change on coastal communities and to develop mitigation strategies, mainly from the perspective of managing future infrastructure, resources and socio-economic growth (Hanson et al., 2011; Tebaldi et al., 2012; Bloetscher et al., 2016). However, only minimal emphasis has been placed on how to manage recovery after such extreme climatic events, which is an essential component of community resilience.

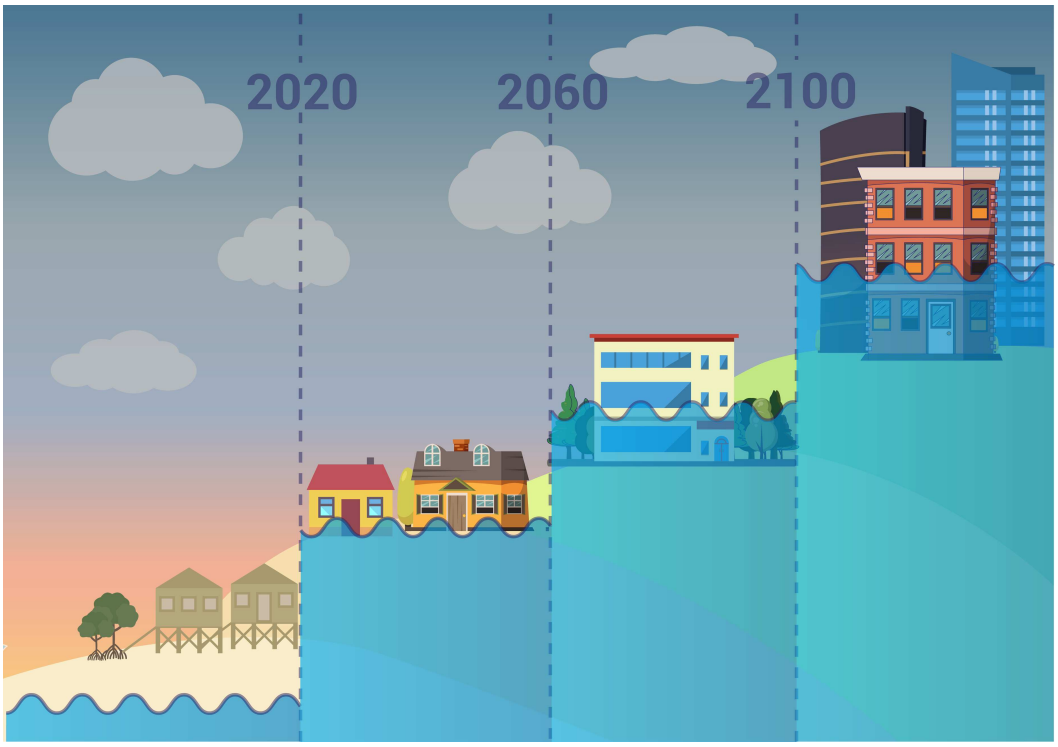

Figure 1-2: The increasing SLR threats to low-lying coastal communities from present days to after the year 2100.

A robust risk management strategy should involve an awareness of coastal activities, assets, and infrastructures and ensure continuation of the various economic activities within the community. Seaports are vital maritime assets that provide significant economic function, as more than 80% (by volume) of the global product is traded by sea (Shi and Li, 2017). However, around one-third of the global harbors are in areas at risk to severe tropical cyclones (Becker et al., 2012). Seaports are also prone to inundation, whether transient as a consequence of a hurricane or irreversible caused by an increase in sea level. In addition, coastal trade gives communities the accessibility to goods and services such as fuel and natural gas for essential life needs, which highlights the importance of recovery of port facilities. The Port of New York and New Jersey, for

example, was closed for several days following Superstorm Sandy (Smythe, 2014). Ports in the U.S. contribute $5.4 trillion in annual financial activity, almost 26 percent of the gross domestic product estimated for the fourth quarter of 2018 and, directly and indirectly, create jobs for more than 30 million people (AAPA, 2018). The Port of Mobile, AL, which is the major topic in this study, lies in a region of the Gulf of Mexico that has seen 28 severe (Simpson-Saffer Category 3 – 5) hurricanes in the past five decades, handled a total of 59 million tons of commodities and occupied the 11th place among the top 100 U.S. ports in terms of total tonnage of all categories in 2018 (USACE, 2018). The port is particularly important because it is the main coal facility of the Gulf Coast and the second largest in the U.S. (Harris et al., 2008).

1.2. Objectives and scope of research

It is clear from the preceding brief review that coastal port communities in the Southeast and Gulf Coast regions of the U.S. will be challenged by the impacts of a changing climate during the remainder of the 21st Century. While the vulnerability of port facilities has been recognized, only limited work has addressed the issue of port functionality and recovery in the aftermath of severe tropical cyclones in an era of SLR and other climate-driven effects which is essential to promote the maritime economy of the country (Becker et al., 2012; Chhetri et al., 2015; Ng et al., 2016; Sánchez-Arcilla et al., 2016).

This study presents a new approach to quantify the functionality and recovery processes of port facilities subjected to the threat of SLR and other climate-driven effects. This approach has four major aspects:

(1) A multi-hazard assessment of the coupled effects of SLR and Hurricane's storm surge is conducted using a hydrodynamic model;

(2) A new fault tree analysis (FTA) is constructed for the Port of Mobile, AL, which represents the physical port infrastructure - containers, cranes, storage facilities, rail and road connections - which must function as an integrated system to ensure that commodities and products transit the port efficiently, from cargo ships to ground transportation facilities, from which they can be distributed to customers, as schematically shown in Figure 1-3;

(3) Decision analysis is used in a simple example of a set of plausible future SLR and storm scenarios, using Hurricane Katrina as a base scenario event; and

(4) A simple illustration of a recovery assessment is conducted to give a sense of how the recovery the port functionality might be assessed in terms of the operating loss under various hurricane and global warming scenarios and risk mitigation strategies.

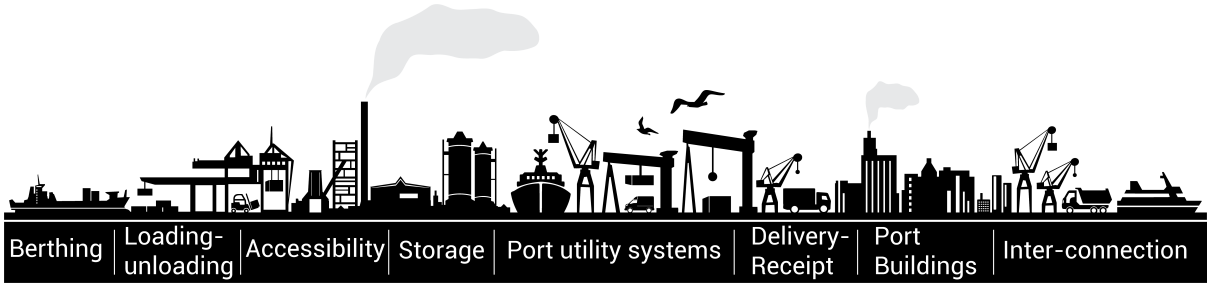

Figure 1-3: The seaport supply chain, showing the complexity of the subsystems.

Until recently, most community resilience research and implementation were focused on the performance of seaport during and after earthquake events (Na and Shinozuka, 2009; Shafieezadeh and Ivey Burden, 2014; Burden et al., 2016). The

fundamental aim of this research is to understand how future climate effects, including tropical cyclones and SLR, might affect storm surges and coastal flooding in coastal land regions and, in particular, ports that are essential to a healthy economy. An emphasis is placed on how to evaluate port functionality when impacted by such hazard events. To this end, the following tasks and subtask will be performed to achieve this goal:

- Task 1: Conduct Comprehensive Literature Review.
    - Assess the main causes of SLR.
    - Summarize existing tools for SLR projection.
    - Investigate the impact of SLR on coastal communities.
    - Provide an overview of the impact of hurricanes on coastal communities.
- Task 2: Develop and validate an advanced hydrodynamic model to simulate the hazard on coastal community.
    - Develop a comprehensive 2D hydrodynamic analysis model that captures the peak of the storm surge and the related inundation coupled with projected climate driven SLR scenarios for a coastal community.
    - Validate the output of the hydrodynamic model simulation with recorded water level data at gauge stations.
    - Conduct scenario analysis including hurricane coupled/uncoupled with projected SLR.

- Task 3: Quantify the functionality of the Port of Mobile through identification of essential components and systems and construction of a descriptive fault tree:
    - Identify the distinct types of the seaports.
    - Define the functionality of seaport.
    - Define fragilities to estimate the probability of damage state of each component and subcomponent under the risk of the studying scenarios.
- Task 4: Consider impact of scenario tropical cyclone on the Port of Mobile during the remainder of the 21st century under various projections of SLR.
    - Review each scenario results in terms of inundation extend and storm surge peak values.
    - Evaluate the performance of each even/subevent of the fault tree analysis (FTA) corresponding to each scenario.
    - Assess the functionality of each dock of the seaport and the whole seaport.
- Task 5: Critically appraise proposed framework and make recommendations for overcoming current limitations.

This study will focus on the hazard assessment of the physical impact by SLR and surge effect to a coastal industrial community. Damages due to the hurricane's wind load are not considered in this thesis, the wind profile is only used to drive the storm surge. Economic and social impacts are out of this analysis scope. The proposed framework

will help to increase the awareness of the effect of climate change on the coastal industries.

1.3. Organization of Thesis

The remainder of this thesis consists of seven chapters**:**

- **Chapter 2** briefly reviews SLR to understand emission scenarios and the recent efforts to predict future SLR related to those scenarios. In addition, the possible impacts of sea-level rise on coastal communities is described.
- **Chapter 3** Provides a review of some potential software that could be used to simulate future SLR and/or coupled with predicted cyclone intensity is also provided. The chapter illustrates the hydrodynamic simulation model used in this thesis (Delft3D) includes input data, setting up and validation of the model.
- **Chapter 4** describes the importance of seaport as a critical infrastructure and how as well as the seaport function are also described. The chapter describes the different component of the ports as well as the fragility and the recovery for each one. This chapter also develops the fault tree analysis for the functionality of the port of Mobile.
- **Chapter 5** discusses the output results from the multi-hazard assessment in terms of the inundation to the studied area by each scenario and the damages to the studied port. The chapter also reviews the output from the fault tree analysis as well as the recovery assessment afterward.

- **Chapter 6** states summary and conclusion of the thesis including the description of the model limitations and future work.

CHAPTER 2. BACKGROUND AND LITERATURE REVIEW

2.1. Impact of climate change on global and local SLR

Coastal communities will be challenged by a changing climate over the remainder of the 21st century. SLR is one of the main impacts of climate change, as it threatens the coastal communities with flooding and inundation hazards. SLR reflects both global and local SLR, the relative contributors varying with area (Gattuso et al., 2015).

2.1.1. Climate changes and its impact on SLR

One of the most significant climate change catalysts is carbon dioxide in the atmosphere, which has increased because of human activities, reaching over 400 ppm during the last five years (NOAA, 2019c). Greenhouse gases are comprised mainly of CO2 (82%), methane (10%) and other gases (8%), and are responsible for the imbalance in the Earth's climate system, in which the difference in energy absorbed and emitted is approximately 0.5 Watts/m^2 (Trenberth et al., 2014). As shown in Figure 2-1, the absorbed energies comprise of 198 W/m^2, 211 W/m^2, and 20 W/m^2, resulting in around 90% of being absorbed by the ocean, causing SLR from thermal expansion. Moreover, melting of polar ice sheets associated with the increase in temperature is also a contributor to SLR.

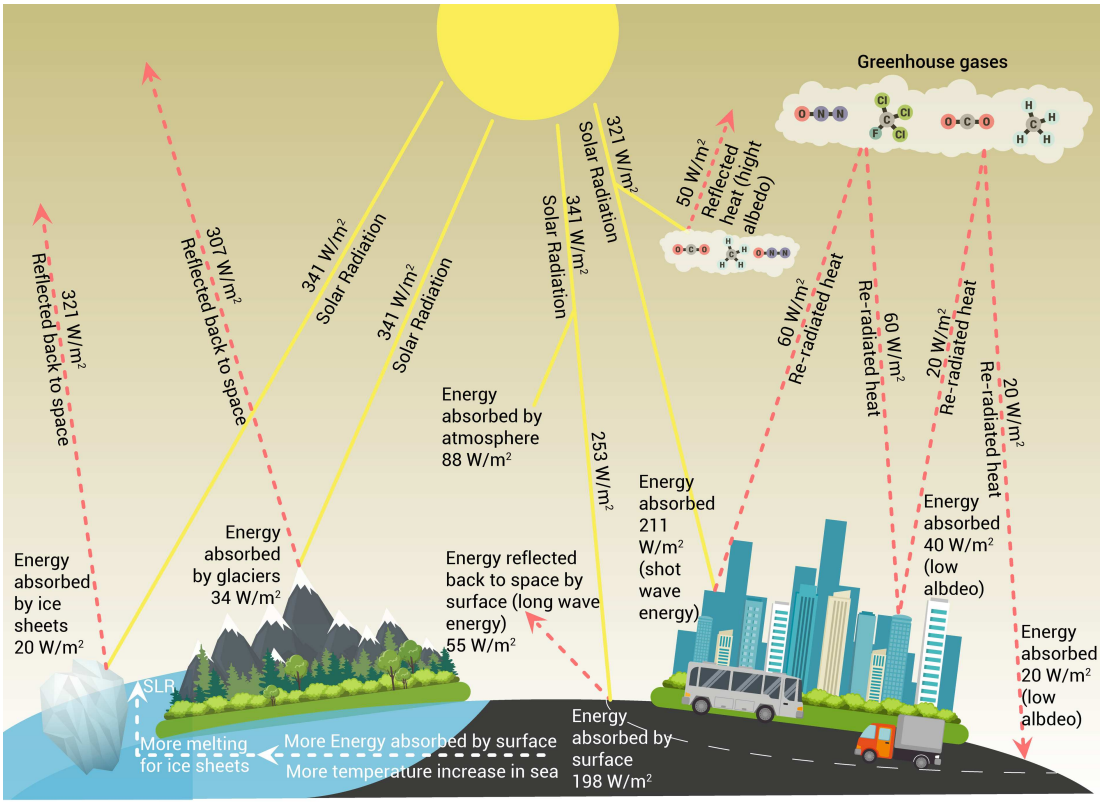

Figure 2-1: The effect of greenhouse gases on climate change and SLR with example illustrative numbers.

2.1.1.1. Factors driving global mean sea-level rise

Thermal expansion of ocean water due to its warming is caused by absorption of increased atmospheric heat, and has been the major cause for global mean sea-level (GMSL) rise during the last century, representing around half of the contribution to GMSL (Horton et al., 2015). The remaining half is caused by melting ice caps, mountain glaciers and the Greenland and Antarctic ice sheets (Church et al., 2013). Figure 2-2 illustrates the dominant factors contributing to SLR. Satellite altimetry since 1993 has shown that the Greenland and West Antarctic ice sheets are melting at an accelerating rate, suggesting that they will become increasingly important contributory factors in the future (Leuliette and Nerem, 2016). The capacity of the Greenland and West Antarctica ice

sheets may increase GMSL by around 7.4m and 57m, respectively, if fully melted (Fretwell et al., 2013). Moreover, a study by DeConto and Pollard (2016) showed that by the end of 21st-century, GMSL will rise by 1.14 ± 0.36m contributed only by Antarctica under extreme warming scenario. Records from global tide gauges during most of the 20th century had shown that GMSL rise was between 1.2 ± 0.3 mm/year and 1.7 ± 0.3 mm/year, while satellite altimetry showed an average increase of 3.4 ± 0.4 mm/year starting from 1993 – almost double of the records from the global tide gauges (Church et al., 2013). Groundwater has the smallest contribution to GMSL rise, around 0.4 mm/year, as water used for agriculture and domestic works flows to the ocean (Church et al., 2013).

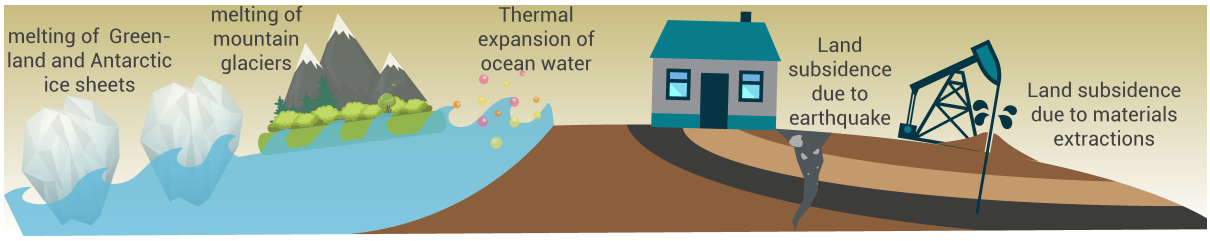

Figure 2-2: The main influencing causes of SLR.

2.1.1.2. Factors driving local mean sea-level rise

Relative sea-level rise (RSLR), is the elevation difference at any location between the height of the sea-level and the height of the land level. RSLR can reach as much as three times GSLR in some places (Cazenave and Cozannet, 2014). Variations in RSLR is mainly driven by local vertical land motion due to subsidence or uplift. Isostatic adjustments - the deformation of the Earth after ice and ocean mass redistributions along with sediment compaction, withdrawal of groundwater and some natural disasters (such as earthquakes) - are the leading causes of vertical land motions (Figure 2-2) (Kopp et

al., 2015). Land subsidence varies spatially and may impact the global pattern of SLR, e.g., observations showed that it is responsible for almost half of SLR in New York City (Peltier, 2004). Moreover, relative sea-level trends provided by the National Oceanic and Atmospheric Administration (NOAA) for most U.S. coastal tide gauges show that observed RSLR has exceeded the average projections made in the 1980s, reaching a maximum value of over 9 mm/year at the coastal region of the State of Louisiana. In comparison, RSLR reaches around 4 mm/year in the Mobile Bay region. Figure 2-3 illustrates the trends measured from tide gauges for the northern Gulf of Mexico, with values ranging from 6-9 mm/year in the Texas coastal zone to 3-6 mm/year in portions of Florida (NOAA, 2019a).

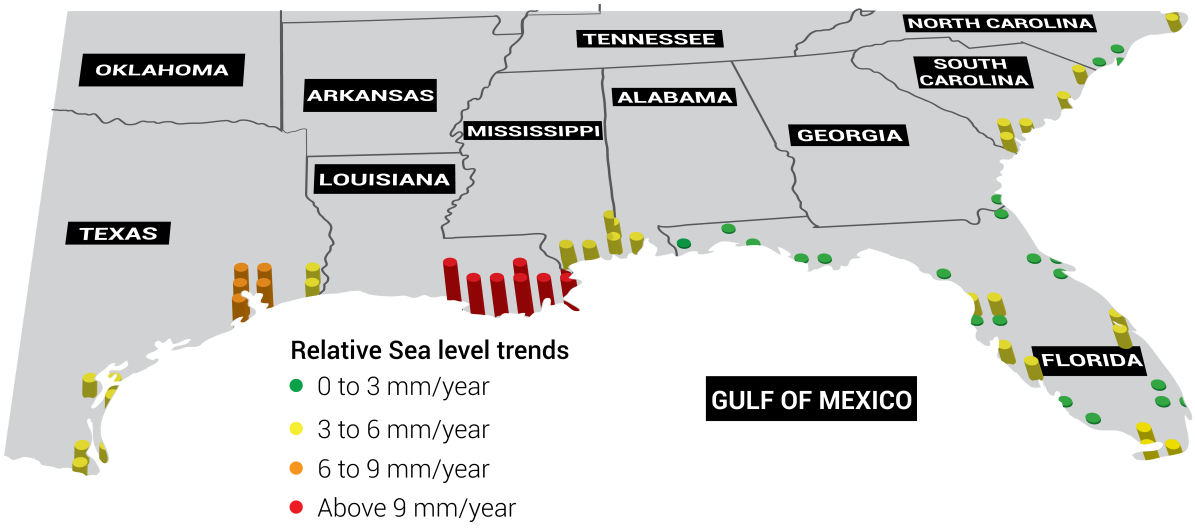

Figure 2-3: Relative sea-level trends at the Gulf Coast, from NOAA (2019a).

2.1.2. Understanding emissions scenarios used to project sea-level rise

Future sea-level rise predicted by the Intergovernmental Panel on Climate Change (IPCC) in their third and fourth assessment reports (AR3 and AR4) was based on

emission scenarios, or emission pathways that depend on specific warming and socio-economic hypotheses. For example, one pathway (A1F1) was based on a scenario involving very rapid economic and population growth, as well as fossil fuel-intensive usage (Nakicenovic and N., and Swart, 2000). The authors of AR4 concluded that the impact of Greenland and Antarctic ice sheets melting on GSLR was relatively small compared to the contribution from thermal expansion. Thus, the impact of ice sheet melting was neglected by the IPCC in AR4, which was reflected in their projection of SLR by 2100 to be around 0.59 m, based on pathway A1F1 (IPCC, 2007). More recent studies have sought a better understanding of how much SLR might have been underestimated by ignoring the contribution of melting ice. For example, using a composite of the IPCC AR4 global SLR estimate of ocean warming and the calculation of maximum possible loss of glaciers and ice sheets, two recent papers (Vermeer and Rahmstorf, 2009; Parris et al., 2012) have shown that global SLR by the end of the century may exceed 2.0 m with 90% confidence.

The IPCC introduced a new method in their Fifth Assessment Report (AR5) to represent emissions scenarios using representative concentration pathways, or RCPs. The projections of SLR in AR5 exceed those in AR4, mainly because of the advanced simulation of land-ice contributions that was developed in the Coupled Model Intercomparison Project Phase 5 (CMIP5) (IPCC, 2014). Radiative forcing describes the difference between the insolation (sunlight) absorbed by the Earth and the energy radiated back to space (albedo) in units of watts per square meter of the Earth's surface, and is used to summarize four new emissions scenarios: RCP 2.6, 6.0, 4.5, and 8.5 (Moss et al., 2010). RCP 2.6 represents the mildest scenario, and is based on the assumption

that greenhouse gases are reduced until they reach 0% of CO_2 by 2080, to comply with the Paris Agreement's primary objectives of the United Nations Framework Convention on Climate Change to lower mean global warming to below 2°C by 2100. In contrast, RCP 8.5 assumes that no action is taken to prevent additional emissions of CO_2 (van Vuuren et al., 2011), resulting in mean global warming of around 4.8°C by 2100. RCP 4.5 is an intermediate scenario and assumes that climate policies are invoked to achieve the goal of limiting emissions, concentrations and radiative forcing, leading to mean global warming of around 2.6°C by 2100 (IPCC, 2014). RCP 6.0 almost matches RCP 4.5 in predicting future SLR by 2060; thus, most studies use RCP 4.5 to represent this scenario (Church et al., 2013). Using these more recently developed RCPs, the likely range (over 66% probability) of GMSL rise by the end of the century is 0.26 – 0.55m for RCP 2.6 scenarios and 0.52 - 0.98 m for RCP 8.5 scenarios (IPCC, 2014). There is notable uncertainty (beyond the likely ranges) associated with the projection of sea-level rise, especially the rate and magnitude of the contribution of ice sheet loss, as presented in AR5's (IPCC, 2014). Kopp et al. (2014) concluded that the very likely range (over 90% probability) of future global SLR, by 2100, is 0.5–1.2 m for RCP 8.5. Since the extreme scenario in AR5 was questionable, other efforts have been made to construct a probability density function (PDF) to determine the likelihood of high risk events. Le Bars et al. (2017) predicted SLR by 2100 of as much as 2.92 m.

Many agencies of the U.S. Federal government have presented future spatial anticipated SLR scenarios in the U.S. based on the studies summarized above. For example, the U.S. Army Corps of Engineers (USACE) provides a sea-level change calculator tool that helps engineers and planners to apply three USACE scenarios (low,

intermediate, and high) of forecasted SLR in future coastal engineering projects at any one of 142 coastal tide stations in the U.S. (USACE, 2013). NOAA, presented six possible projections of SLR in its 2017 report - 30 cm, 50 cm, 100 cm, 150 cm, 200 cm, and 250 cm - denoted as Low, Intermediate-Low, Intermediate, Intermediate-High, High and Extreme, respectively (Sweet et al., 2017). The NOAA report provides expected relative SLR at most coastal locations in the U.S. at ten year intervals up to 2100. Figure 2-4 shows the differences in the NOAA and USACE projections of global mean SLR. Finally, the Department of Defense (DoD) adjusted the Parris et al. (2012) scenarios using recent IPCC AR5 projections for scenarios up to 1 m and using a semi-empirical method (Perrette et al., 2013) with RCP 8.5 for more than 1 m, resulting in five pathways (0.2, 0.5, 1.0, 1.5 and 2.0 m) of predicted SLR by 2100, providing options for designing and planning coastal military projects (Hall et al., 2016).

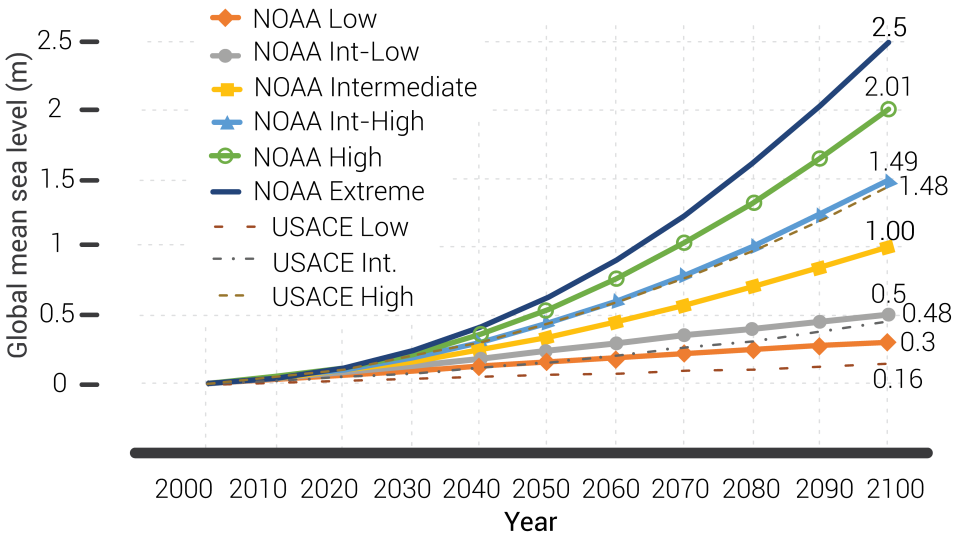

Figure 2-4: Comparison between NOAA and USACE projections for SLR up to year 2100 extracted from the tool developed by USACE.

2.1.3. Hazards associated with SLR

2.1.3.1. High tide flooding

One consequence of increases in relative sea-level (RSLR) is high tide flooding, which has increased during the last 30 years and has had a noticeable impact on coastal infrastructure. Annual rates rose from 1.3 days to 3 days per year in the southeast U.S., from 3.4 days to 6.0 days per year in the northeast U.S., and from 1.4 days to 2.5 days per year in the Western Gulf, respectively, in the last 15 years (Sweet et al., 2014). Because of RSLR, flash flooding no longer requires the occurrence of a powerful storm or hurricane (NOAA, 2018b). Figure 2-5 demonstrates the concept of high tide flooding and shows that before 1950, such flooding required the occurrence of storm surge from a tropical cyclone, while in the years following 2010 only a high tide was required to cause the same level of flooding. Sweet et al. (2018) forecast that under the NOAA Intermediate Low Scenario (see section 2.1.2), high tide flooding will occur as frequently as once every two days within the northeast and Southeast U.S., the Eastern and Western Gulf, and the Pacific Islands by the end of the 21st century.

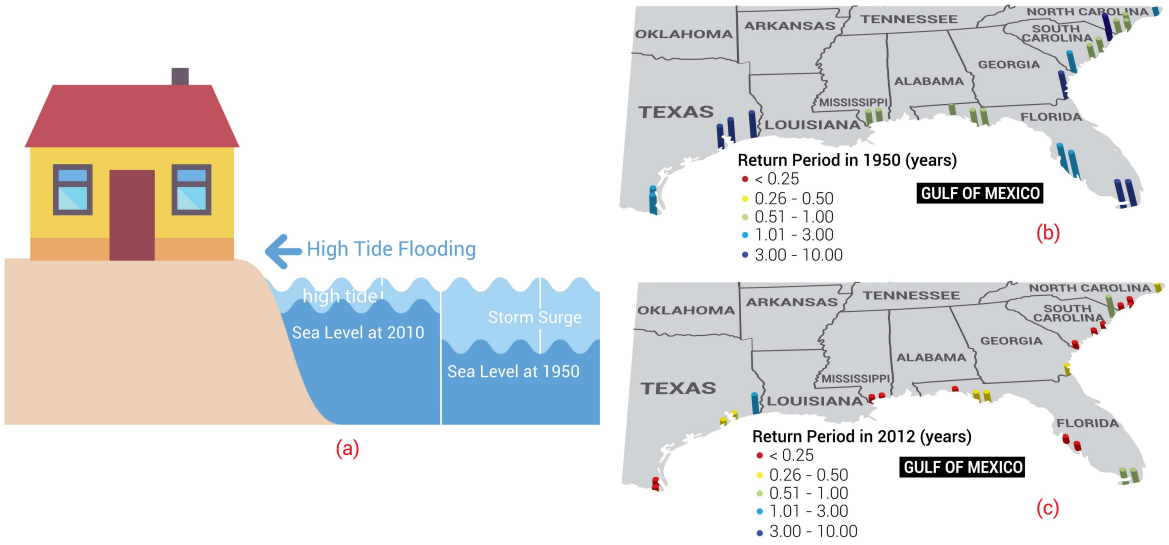

Figure 2-5: High tide flooding event (a) in relation to SLR and as a return period at NOAA gauges in (b) 1950 and (c) 2012.

2.1.3.2. Hurricanes

2.1.3.2.1. Definition of hurricanes

Hurricanes are rotating low-pressure weather systems that form in warm sea water (Williams, 1997). Those mechanisms rotate counterclockwise by the Coriolis effect (Earth rotation effect) in the northern hemisphere and rotate clockwise in the southern hemisphere (Graham and Riebeek, 2006). The term hurricanes may be used in any storms worldwide with a peak wind intensity greater than 33 m/s. Hurricanes are categorized based on the Saffir-Simpson scale (1970) in 5 different categories (Figure 2-6), depending on the maximum sustained wind speed, defined as the maximum one minute average wind speed, measured at an elevation of 10 m in an open exposure. Hurricanes in Categories 3 – 5 are classified as severe, and have a major impact on coastal infrastructure.

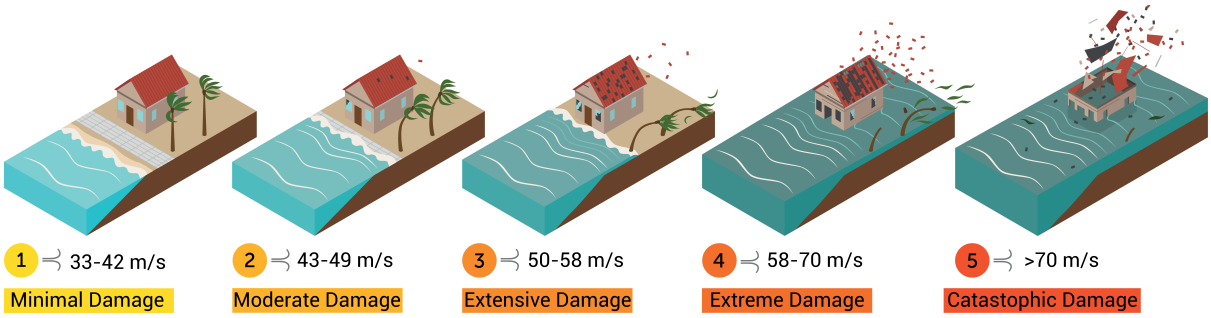

Figure 2-6: Simpson-Saffir Hurricane wind scale.

2.1.3.2.2. Storm surge

Storm surge is an unexpected rise in water, induced primarily by wind intensity and, to a lesser degree, by a hurricane low pressure (McInnes et al., 2002). The duration associated with a storm surge varies from a few minutes up to a few days (Webb, 2017). Storm surges pose the highest risk to life and property caused by a hurricane (Rappaport, 2014). Variations in storm surge are mainly driven by storm intensity, central pressure, hurricane forward speed, hurricane approach angle, landfall location, and hurricane size (NHC, 2020). Storm surge can also increase with the hurricane size, as showed by Irish et. al. (2008). Winds in a bigger hurricane move through a greater ocean area and carry more water, which leads to greater surge levels and a greater proportion of the coast gets inundated.

The coastal geography and landfall location play a significant part in the speed at which a hurricane moves along its track. As illustrated by Rego et. al. (2009), when the coast is open, a hurricane that advances quicker causes a higher storm surge, with less flood volume, than a hurricane that advances slowly. Conversely, if the coastline is "closed," such as in the form of a bay, a hurricane that advances slower causes a higher storm surge. When a hurricane hits the coast perpendicularly, it may create the highest

possible storm surge on the shoreline (Irish et al., 2008). The importance of this factor, along with landfall location factor, was also confirmed by Weisberg et. al. (2006) when their analysis found that the maximum surge occurred at the north of Tampa Bay when the landfall of the hurricane occurred at this location.

SLR can affect the impact of future storms on coastal infrastructure, causing higher surges and further flooding. Three studies have found that the peak of storm surge increases nonlinearly with the increase in SLR projection (Smith et al., 2010; Bilskie et al., 2016; Yin et al., 2017b) , while one study showed a linear relationship between increased storm surge and SLR (Yang et al., 2015). Thus, the relationship between SLR and storm intensity is not clear, which could be due to the variability of studied locations and hurricanes.

2.1.3.2.3. Impact of hurricanes on coastal communities

Coastal flooding during hurricanes (or tropical cyclones) has caused significant financial losses and disasters globally. Tropical cyclones account for approximately 47 percent of all billion-dollar events worldwide and represent 80 percent of the U.S. damages from cumulative extreme weather and climate disasters (Smith and Katz, 2013). The 1900 Galveston hurricane leading to the deaths of 8,000 people is still the most severe in U.S. history in terms of loss of life (NOAA, 2012). Hurricane Katrina, Harvey and Sandy inflicted more than $160, $125, and $70.2 billion in damages to the Gulf Coast, Texas, and New York (NY) and New Jersey (NJ), respectively (NOAA, 2018a). SLR has accounted for 8 out of 20 extreme recorded water levels in the New York Harbor region following 1990 (Talke et al., 2014). The New York City Metropolitan Area has seen a SLR of 30 cm since the end of 19th century; this increase is believed to be responsible

for almost 70 km^2 of additional inundation area due to Superstorm Sandy (Miller et al., 2013). The impact of storm surge in Lower Manhattan during Superstorm Sandy was particularly severe, the maximum water level at Battery reached 4.27 m.

When a hurricane occurs, it often produces severe storm surges that range from 1 to over 5 meters on average (The Hurricane Disaster—Potential Scale, 1974). However, as shown in Figure 2-7, if that same hurricane is combined with future projections of SLR, an extreme event is likely to be generated. In Figure 2-7 (a), the hurricane is not causing a significant problem when it is coupled with the current SLR. On the contrary, substantial damage could result when combined with future SLR as shown in Figure 2-7 (b). Even if the hurricane climatology does not change, SLR will decrease the return period of hurricane-induced flooding. Lin et al. (2016a) noted that a storm surge event of 2.8 m, similar to Superstorm Sandy, may occur in the NY region four times more by 2100 under RCP 4.5 emission scenario. Each of these occurrence will lead to more destructive results on city infrastructure (Yin et al., 2017a).

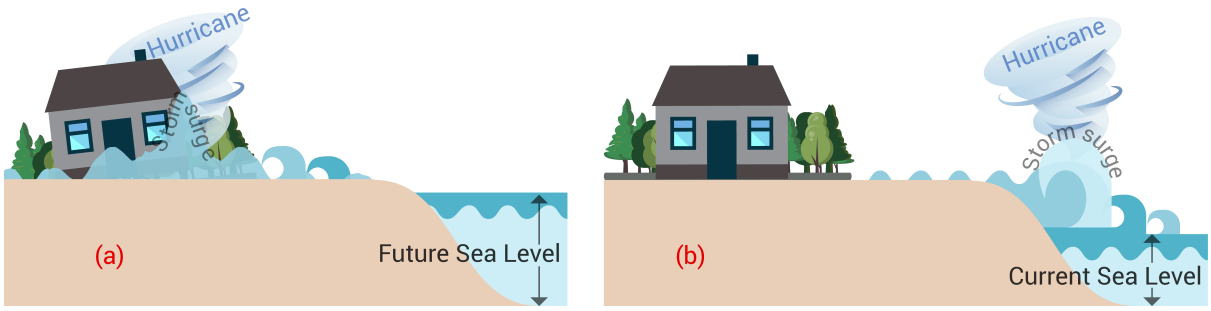

Figure 2-7: The effect of a hurricane combined with (a) current SLR and (b) future SLR.

2.1.4. Impacts of SLR on transportation, infrastructure, population near shorelines, and seaports

2.1.4.1. Transportation and infrastructure

Transportation is the most critical public infrastructure system because emergency facilities and services – police, fire and healthcare – are not available if public transportation is interrupted or damaged by flooding; nor can community response and recovery be initiated if other damaged infrastructure cannot be reached (Yin et al., 2017a). When an extreme natural event occurs, some cars can only operate on high-elevation roads or bridges. A recent study shows that the coupling of 100-year coastal floods with the predicted SLR by 2080 is likely to decrease the roadway accessibility by 28% and to double emergency response time by highway interruption in NY (Yin et al., 2017a).

2.1.4.2. Populations near shorelines

Many of the nation's commercial, industrial, and recreation facilities, military installations, and energy production facilities are located near shorelines. As of 2010, approximately 124 million individuals, 39% of the people in the U.S., resided in coastal shoreline counties, representing 10% of the entire U.S. land area (NOAA, 2013a). Worldwide, over 625 million (10 percent) of the global population live in low-lying coastal regions that are less than 10 meters over sea level, based on the world's population of the year 2000 (Neumann et al., 2015). Thus, inundation from even a moderate SLR scenario will have a destructive economic and social impact, especially on a vulnerable high-density population living and working in a low-lying coastal region. One possible impact may be increased relocation to inland locations (Hauer, 2017). For example,

Hauer et. al. (2016) projected that future SLR of 0.9 and 1.8m would put approximately 4 and 13 million citizens, respectively, living or working in coastal regions of the U.S. at risk. Heberger et al. (2012) estimated that the damage to buildings in the San Francisco Bay area affected by future SLR of 1 m to 1.4 m, coupled with a storm with a return period of 100 year, would be between $49 billion to $62 billion (in 2000 dollars). Even present coastal flood defenses are at risk of damage or collapse from future SLR, indicating that design criteria for such protective structures should be revised to meet the forecasted high rates of SLR (Rajabalinejad and Demirbilek, 2013).

2.1.4.3. Seaports

Seaports consist of the docks, piers, and other facilities that handle the exchange of goods and commodities between ocean-going ships and intermodal transportation systems that serve inland markets (USDOT, 2008). Over 80% (by volume) of the global commodities and goods are exchanged by sea (Shi and Li, 2017) and the economies of many countries depend on the status of their commercial ports and harbors. Any disruptions of their operations have both national and local impact – diminished commercial and industrial activities, loss of jobs, and population dislocation. The approximate asset value in major ports in coastal regions in the world (with over one million population) vulnerable to global warming in 2005 was $3 trillion, with Hanson et al. (2011) expecting an increase to $35 trillion or 9% of world GDP by 2070.

Coastal port operations are threatened directly by storms and SLR (Becker et al., 2013). The drop in functionality (i.e. lack of inoperability) due to the inundation of the docks and service ways, and the increase in water depth inside and outside the port is one of the enormous potential impacts of SLR on ports (Sánchez-Arcilla et al., 2016).

Hurricane-related storm surge has caused significant damage to ports in the past. For example, damages to the three ports of Mississippi State (Bienville, Gulfport, and Pascagoula) and in ports in South Louisiana by Hurricane Katrina alone were about $100 million (PEER, 2006) and $1.7 billion (Santella et al., 2010), respectively. Furthermore, operation in the Port of NY & NJ was halted for several days due to physical damages following Superstorm Sandy (Smythe, 2014), resulting in $2.2 billion in economic losses to the port (Strunsky, 2013). The damage to infrastructure and facilities caused by Hurricane Ike to ports in Texas was reported to be $2.4 billion (FEMA, 2008).

2.2. Community resilience under the impact of SLR

Growth in coastal communities requires not only increased investment in infrastructure, such as transportation, water/wastewater, power and telecommunications, and housing but also effective protective measures against coastal risks discussed in the preceding sections. SLR poses a significant threat to coastal communities, due not only to its standalone risk but also its role in increasing the incidence and intensity of other climatological events. Confronted with this threat, additional investments will be necessary in the coming decades to safeguard present and future populations, as well as civil infrastructure, and to ensure resilient coastal communities that can withstand and recover from extreme climatological events. While there are many ways in which coastal resilience can be defined and operationalized, including social and behavioral sciences perspectives as well as financial and ecological standpoints, this study provides an engineering focus on the resilience and performance of physical infrastructure of coastal communities and port facilities to SLR.

2.2.1. Defining community resilience

Assurance of community resilience has become an essential goal for policymakers and planners, in the aftermath of numerous large natural disasters in the past two decades. Bruneau et al. (2003) advocated a quantitative framework for measuring and defining seismic community resilience by identifying 4Rs — robustness, redundancy, resourcefulness (capability to determine problems) and rapidity (fast recovery). Koliou et al. (2018) conducted an extensive review of previous studies focusing on the impact of natural hazards on community resilience, in terms of the built environment as well as economic and social systems. Bhattachan et al. (2018) focused on coastal systems, describing the resilience from a rural coastal social-eco logical systems perspective as the capacity for climate change hazards to be absorbed and addressed while maintaining critical functions.

In this study, we adopt a definition which combines those proposed by the National Academies (NAP 2012) (National Research Council, 2012) and in Presidential Policy Directive 21 (Department of Homeland Security, 2013): *Resilience is the ability to prepare for and adapt to changing conditions and withstand and recover rapidly from disruptions.* As such, community resilience depends on the performance of the built environment and on supporting social, economic and public institutions which are essential for immediate response and long-term recovery within a community following a disruptive natural hazard event.

2.2.2. Community adaptation versus resilience corresponding to SLR

The customary way of thinking about community resilience involves a disruptive natural hazard event that shocks the community and causes widespread damage, to

which the community must respond and from which it must recover. Until recently, most community resilience research has been focused on the performance of communities during and after earthquake events (Lin et al., 2016b; Sharma et al., 2017; Koliou et al., 2018). A distinguishing feature of SRL and coastal inundation is that it occurs relatively slowly over time. Furthermore, there is a difference between the impact of SLR as a hazard in and of itself and as a hazard that may intensify the effects of other hazards, such as severe hurricane or storm surge events, in boosting their impact on coastal communities and their resilience. As a result, risk mitigation strategies and their financing, adopted for the long term, must consider a mix of approaches, ranging from protecting and hardening infrastructure to adaptation through long-term land-use planning.

CHAPTER 3. MODELS OF HURRICANE/STORM SURGE

Chapter 2 established the importance of commercial ports to the economies of nations worldwide, with particular emphasis on port facilities in regions of the Southeast U.S. and Gulf Coast susceptible to the threat of SLR and tropical cyclones. With this context of the present study established, Chapter 3 summarizes the workflow for assessing the impact of these natural hazards on commercial ports. Subsequently, a model of the hurricane/storm surge model is presented, which will be used in later chapters to examine the vulnerability of a typical port in the Gulf Coast to various scenario hazards driven by climate change during the remainder of the 21st Century.

3.1. Workflow of the study

This study builds a probabilistic method to estimate the functionality of the Port of Mobile (Chapter 4) under future SLR coupled with hurricane's storm surge (Chapter 3). Storm surge simulation of the hydrodynamics related to storm surge is an essential component of this workflow. A digital elevation model (DEM) that describes the variation of land elevations along with the seabed levels of the water areas is the first step needed for the hydrodynamic model. The quality of the final results depends on the resolution of the DEM file. For example, a DEM file that has geographical information for every 1 km represents a better simulation than another one that has information for every 100 km.

As noted previously, storm surge is a critical characteristic of a hurricane in an era of increasing SLR. The common way to define a hurricane is by providing its wind profile and hurricane track locations for specific time intervals, along with its associated wind speed intensities and pressure deficit. Usually, historical hurricanes lack enough

information to be used as a wind profile in storm surge simulation. Therefore, a wind profile generator is an essential tool to stimulate the wind profile of any historical hurricane by providing the available related information.

When performing scenario analysis of future hurricanes, SLR values must be estimated by one of the recently available projections (such as IPCC or NOAA, as discussed in Chapter 2). To obtain the storm surge values related to future scenarios of hurricanes coupled with SLR, previous data are simulated using Delft3D hydrodynamic simulation software (Caldwell and Edmonds, 2014). Before obtaining these values, a comparison of the model output data with a historical recorded water level at an observation station is performed to validate the hydrodynamic model. Then, by using the DEM file, an inundation map around the area of interest can be generated to calculate the maximum water depth values affecting that area.

In Chapter 4, the functionality of a port corresponding to the future climate scenarios is determined through the fault tree analysis (FTA), which utilizes the depth damage fragilities to calculate the drop in the port operability following a hurricane event. The final step is to apply these methodologies to the Port of Mobile in Chapter 5. Figure 3-1 summarizes all the steps used as a methodology in this study.

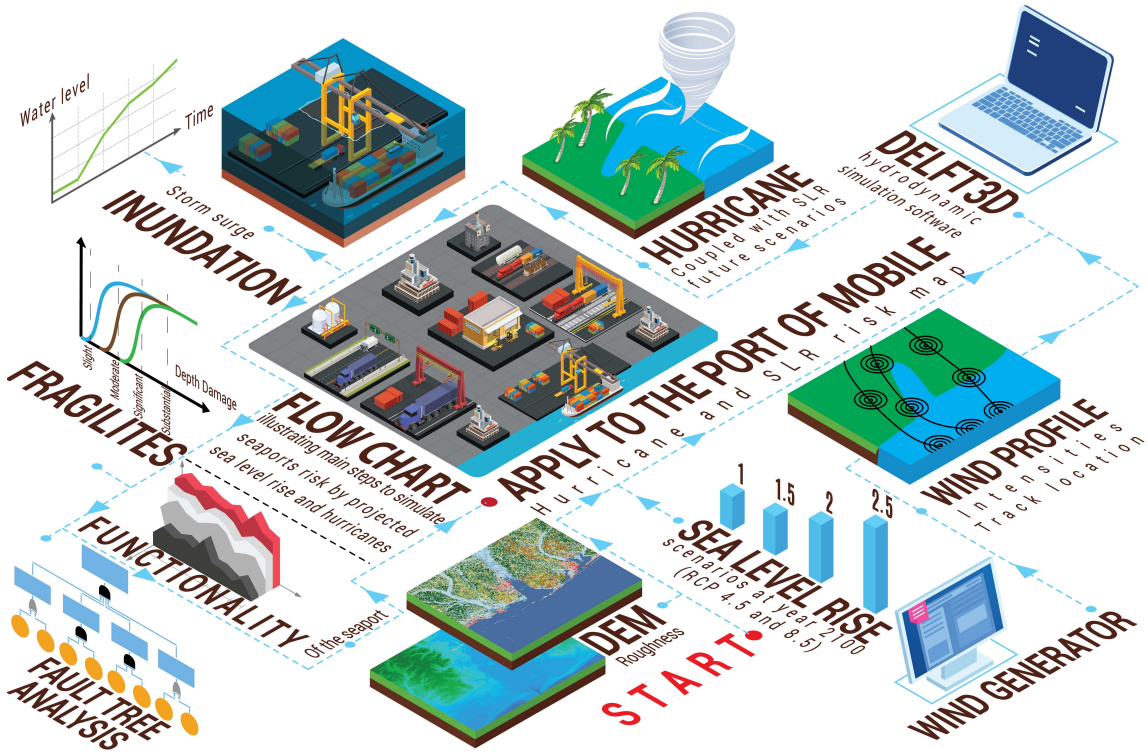

Figure 3-1: Flow chart illustrating the workflow of this study.

3.2. Modeling the effect of SLR and hurricane

3.2.1. Introduction

Flood hazard events and their effect have always been a major concern for communities situated near oceans and rivers. Consequently, storm surge and flood simulation software has been developed to help those communities understand and address this problem (Teng et al., 2017).

3.2.2. Software used to simulate storm surge

There are several storm surge modeling systems based on similar principles of computational fluid dynamics, including ADCIRC (Luettich et al., 1992) and Delft3D (Stelling, 1996), that are used mainly to capture the effect of tides, storm surge, waves (when coupled with SWAN (Booij et al., 1999), erosion, and SLR near the coast. Many of

these models require special training in the basic physics of flood and storm surge to utilize the model's inputs and its data effectively. Coastal inundation can be simulated using 1D, 2D, and 3D hydrodynamic models. 1D models, which represent only one of the spatial dimensions using 1D finite difference method (FDM) of the Navier-Stokes equations (Bates and De Roo, 2000). These equations define fluid accelerations, pressures, viscous forces and forces of friction in the fluid. 2D modeling is the most common method for simulating and designing coastal transportation infrastructure in the horizontal plane (Webb, 2017). Thus, we use the 2d modeling in this study to simulate the storm surge coupled with future SLR.

3.2.2.1. Delft3D

Delft3D is a physics-based hydrodynamic software that has been tested by simulating different coastal scenarios, including storm surge (Lesser et al., 2004). The accuracy of the analysis performance, however, relies on the feasibility of the relevant data, the configuration selected by the user, and the specified input variables. Thus, the model for storm surge simulation need to be properly validated with recorded data. Delft3D is an example of a 3D model which is capable to simulate hydrodynamic, sediment, morphology and water quality in all three dimensions (Stelling, 1996).

Delft3d solves the Navier-Stokes equations using the finite volume method (FVM), under the shallow water and the Boussinesq assumptions (Caldwell and Edmonds, 2014). The software's algorithm can identify the wet/dry regions which indicate the inundation area by a storm surge or coastal flooding. Many software packages are part of Delft3d suit that can be used separately or integrally to simulate different hydrodynamic components such as Delft3d-FLOW, Delft3D-SED, Delft3D-WAVE,

Delft3D-WAQ, and Delft3D-ECO for modeling: flow, sediment transport, waves, water quality, and water ecology, respectively (Caldwell and Edmonds, 2014). For the purpose of simulating current and future storm surge magnitude and extend induced by a hurricane and/or SLR, Delft3D-FLOW in 2D method can be utilized for computing non-steady hydrodynamic flow on a rectangular or curvilinear grid domain arising from external forces including wind, tides, and waves. Delft3D boundary conditions include features such as water elevation, discharge, wind stress, and atmospheric pressure.

Veeramony et al., (2017) have noted that by using the Delft3D graphical user interface, Delft dashboard (DDB), one can save preparation time to construct the required files for storm surge simulation analysis such as grids, bathymetry data, boundary condition, initial condition, wind forcing and other input data. Delft3D provides strong pre- and post-processing sub-software. Among the other pre-processing tools, Delft3D-RGFGRID and Delft3D-QUICKIN are included in the Delft3D suit package, which are used in orthogonal, curvilinear and bathymetric dataset generation, modification and visualization. For post-processing, the Delft3D-QUICKPLOT tool allows the visualization and animation of the simulation results (Caldwell and Edmonds, 2014).

Delft3D is able to deal with two kinds of grids, structured (rectangular) and unstructured (triangular, hexagons, and pentagons) grids. However, the stable verified version of Delft3D (Veeramony et al., 2016) can only use the structured grids. While Delft3D Flexible Mesh (Delft3D FM), which is still in beta version and not open to the public yet (Deltares, 2020), is capable of using unstructured grids. The difference between structure and unstructured meshes is that the structure grid is typically effective and simple to use, but grids around irregular topologies or essential regions are hard to

modify and improve. On the other hand, the unstructured meshes have more resolution and spatial discretion flexibility which allows a more accurate representation of the data and better results for the model simulation, but with a high computation time as a tradeoff.

3.2.2.2. ADCIRC

Similar to Delft3D, ADCIRC can simulate hydrodynamic coastal inundation with either 2D or 3D models. However, it solves the Navier-Stokes equations by using the finite element method (FEM) or the finite difference method (FDM) in the case of unstructured grid or structure grid, respectively (Luettich and Westerink, 2015). It also has similar capabilities, such as the ability to use cartesian or spherical co-ordinates systems in the horizontal direction, and the ability to deal with the same types of boundary conditions. ADCIRC has been used and verified for storm surge simulation modeling (Blain et al., 2010). When coupled to SWAN (Booij et al., 1999), ADCIRC can simulate waves when coupled with SWAN. Table 3-1 summarizes the advantages and disadvantages of the discussed models.

Table 3-1: Comparison between Delft3D and ADCIRC

	Simulation models	
	Delft3D	**ADCIRC**
Navier-Stokes equations solving method	Finite volume method (FVM)	Finite element method (FEM) and finite difference method (FDM)

2D and 3D capabilities	Yes	Yes
Grid types	Structured, Unstructured (beta version only)	Structured, Unstructured
Wind simulation	Yes	Yes
Parallel computers ability	Yes	Yes
Pre-processing software	Yes	No
Post-processing software	Yes	No
Coupling capabilities	Integrally simulating flow, sediment transport, waves, salinity, and water ecology.	Simulate waves when coupled with SWAN

Delft3D was tested and evaluated for storm surge and coastal flooding, specifically under hurricanes scenarios (Lesser et al., 2004). From Table 3-1, unlike ADCIRC, Delft3D has pre and post-processing tools that can enable the visualization of the model inputs and results graphically. Thus, Delft3D is a suitable storm surge modeling program for this thesis.

3.2.3. Selection of Scenario Hurricane

Two major hurricanes have affected the Alabama (AL) coastal region in the vicinity of Mobile significantly in the past two decades: Ivan (2004) and Katrina (2005). However, the surge induced by Katrina (at 3.4 to 3.8 m in downtown Mobile) resulted in disabled roads and inundated areas (Choate et al., 2014) and was larger than the surge from Ivan. Accordingly, the impact of a number of hurricane scenarios constructed from Hurricane

Katrina will be considered in performing a damage and loss assessment of the port of Mobile (Adhikari et al., 2020).

Katrina initiated as a tropical depression on 23 August 2005 near the Bahamas. Late on August 25, its strength increased to hurricane strength, and at 1200 August 28, Katrina was a Category 5 hurricane over the Gulf of Mexico (Figure 3-2), with maximum winds of 75 m/s and a central pressure of 909 millibars (NOAA, 2019b). Katrina's strength waned at its second landfall on the following day to Category 3 at 1100 August 29 over southeast Louisiana and Mississippi, with a maximum wind speed of 57 m/s and a central pressure of 920 millibars (Knabb et al., 2006). Figure 3-2 shows the hurricane Katrina storm path.

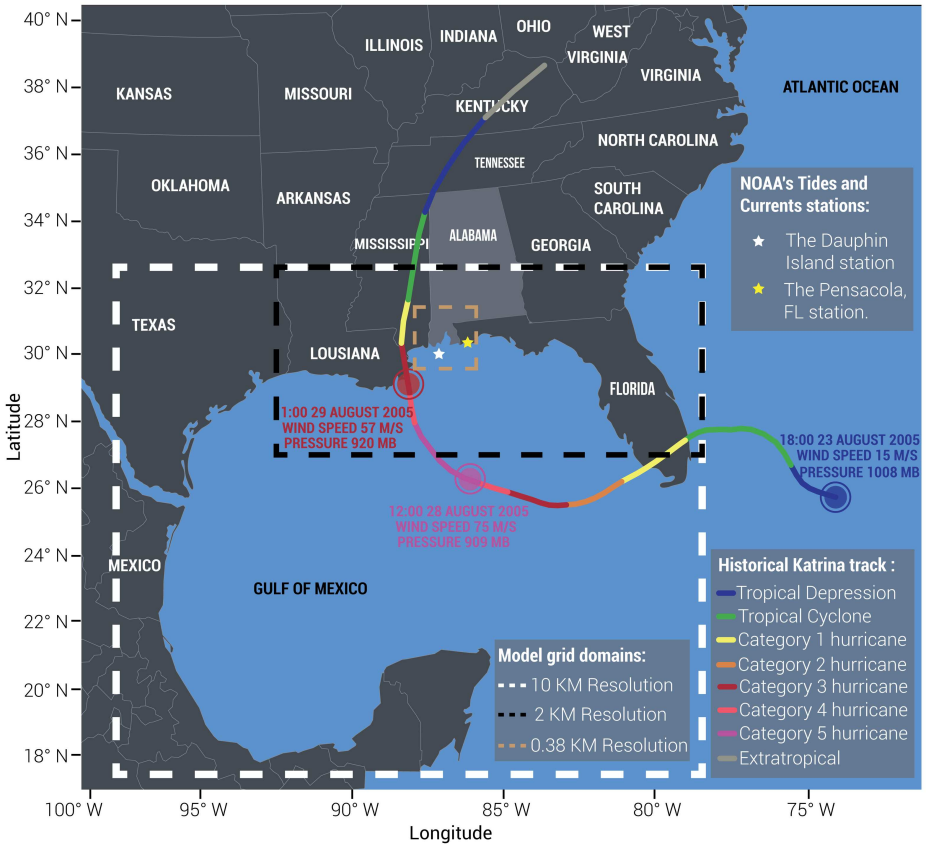

Figure 3-2: Modeling domains with Katrina original track

3.2.4. Model grid and bathymetry

To simulate the track of Hurricane Katrina, the domain for the hydrodynamic analysis should include the start of the hurricane in order to accurately capture the water propagated from the Gulf of Mexico (GOM). Accordingly, a nesting grid modeling technique is used to simulate a broad selection of spatial scales. Following a previous study (Veeramony et al., 2017), three different scale model domains shown in Figure 3-3 as (a), (b) and (c) are selected. A large lower resolution grid of about 10 km is chosen to cover the GOM region as the first stage of the analysis. Then the output information from the GOM model is passed to a higher resolution grid of about 2 km which covers the northern part of the Gulf (NG). Finally, the results of the previous two domains are passed to the highest resolution grid domain of about 0.38 km surrounding Mobile Bay (MB).

Bathymetry and topography data are based on the U.S. Coastal Relief Model (CRM) (NOAA., 2001), which has a horizontal resolution of 3 arc seconds (approximately 90 meters). The vertical datum in the CRM model is mean sea level. In areas where the CRM data are not available, the General Bathymetric Chart of the Oceans (GEBCO, 2010) (900 meters horizontal resolution) is used. The depths of the three nesting model domains are also shown in Figure 3-3.

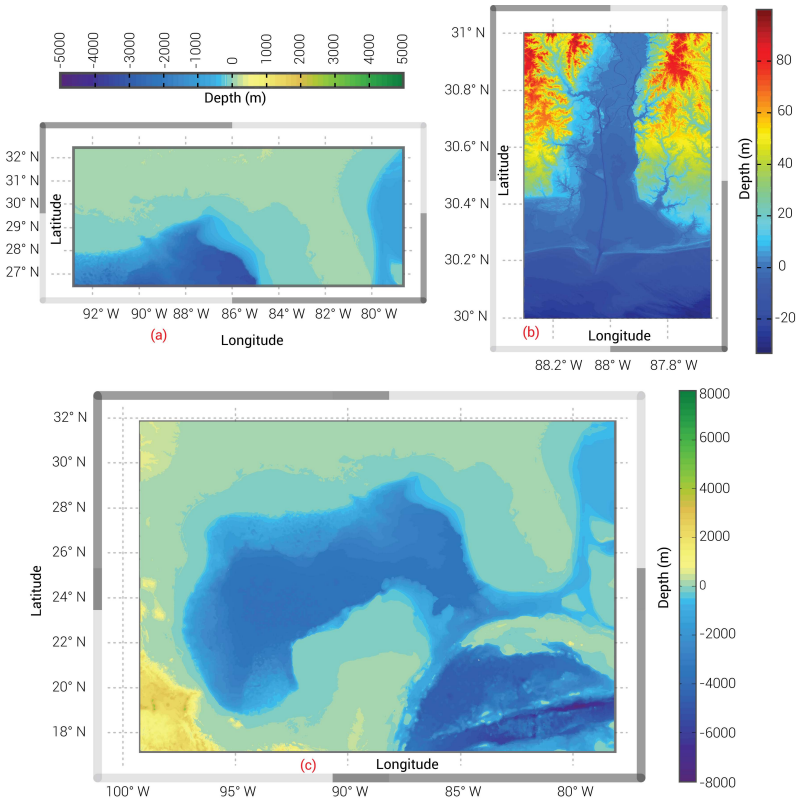

Figure 3-3: Bathymetry and topography for the three nesting domains used in this study: (a) NG domain, (b) MB domain, and (c) GOM domain.

3.2.5. Wind Profile

Delft3D is capable of calculating the wind profile, presented by a spiderweb grid data, by using the Wind Enhancement Schema (WES) approach (Heming et al., 1995) informed by analytical formulations by either Holland (1980), revised Holland (2008), or modified Rankine vortex (MRV) models (Phadke et al., 2003). The Holland model is employed in this study, following a previous study (Adhikari et al., 2020) to simulate current and future wind profiles for storm surge assessment because it is widely used in engineering applications. In this study, Hurricane Katrina track data are extracted from the National Hurricane Center second-generation HURDAT2 data set (NOAA, 2014). Note that the HURDAT2 data provides 1-min maximum sustained wind speeds. To

facilitate surge simulation, WES converts this wind speed to 10-min surface mean wind speed for the open-sea exposure.

According to the Holland's equation, the wind speed gradient $V_g(r)$, the mean horizontal wind speed in the lower atmosphere, can be expressed by:

$$V_g(r) = \left(\frac{AB(P_n - P_C)exp^{\left(-A/r^B\right)}}{\rho r^B} + \frac{r^2 f^2}{4}\right)^{0.5} - \frac{rf}{2} \quad (3\text{-}1)$$

where ρ and f are the air density and the Coriolis parameter, respectively. The coefficients A and B are scaling parameters. Parameter A physically determines the distance between the pressure or the wind profile and the origin, and parameter B describes the profile shape of the hurricane. P_C is the central pressure of the hurricane, and P_n is the ambient pressure. The distance from the center of the cyclone is represented by r. When the Coriolis force is small in the region of maximum winds compared with the pressure gradient and centrifugal forces, the air becomes in cyclostrophic equilibrium. The cyclostrophic wind speed $V_C(r)$, can be expressed by:

$$V_C(r) = \left(\frac{AB(P_n - P_C)\exp^{\left(-A/r^B\right)}}{\rho r^B}\right)^{0.5} \quad (3\text{-}2)$$

By assuming $dV_C/dr = 0$, the radius of maximum winds R_W can be obtained by:

$$R_W = A^{1/B} \quad (3\text{-}3)$$

Replacing Equation (3-3) back to Equation (3-2) gives a maximum wind speed (V_{max}) expression in function of parameter B and the pressure in the center of the hurricane as follows:

$$V_{max} = \left(\frac{B(P_n - P_C)}{\rho e}\right)^{0.5} \quad (3\text{-}4)$$

Where e is the base of the natural logarithm (=2.71828). The Delft3D-FLOW (Caldwell and Edmonds, 2014) and Holland (2008) provide full information on this method.

3.2.6. Bottom Roughness

The seafloor roughness factor is defined by the spatial variations of the Manning coefficient, which was extracted from the land use data using the National Land Cover Database (NLCD) and then transformed into compatible Manning's values by implementing the method developed by Mattocks and Forbes (2008). Figure 3-4 illustrates the interpolated manning values for each nesting model domain.

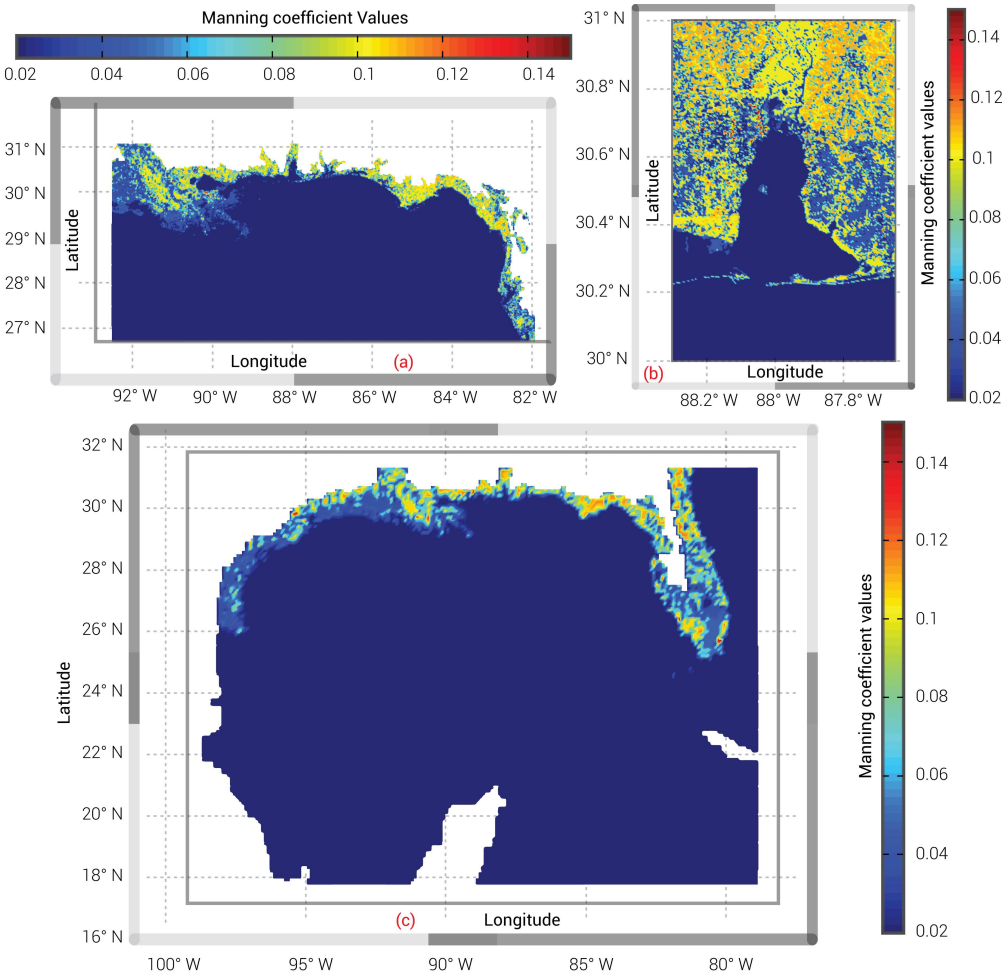

Figure 3-4: Manning coefficient values for the three nesting domains used in this study: (a) NG domain, (b) MB domain, and (c) GOM domain.

3.2.7. Boundary condition tidal forcing

Many boundary conditions for the open boundaries can be implemented in Delft3D to force the model domain. These include: water level, current, discharge, and Neumann, and Riemann (water level and current) boundaries (Caldwell and Edmonds, 2014). Tidal forcing can be applied as harmonic, astronomical or time series elements. In this study, the Riemann astronomical boundary condition is used, extracted from the TPXO 7.2 Global Inverse Tidal Model (Egbert et al., 1994; Egbert and Erofeeva, 2002), to define the 13 tidal components used to force the open ocean boundary of the Gulf of Mexico domain. For the NG and MB domains (see Figure 3-2), the Riemann time series were used to define their open boundary condition in order to pass the water level and current data from the Gulf of Mexico domain to the nested domains.

3.2.8. Selection of scenarios

The actual hydrodynamic parameters of water level and characteristics of the existing hurricane track were used in the baseline storm surge scenario, which is defined by the historical Hurricane Katrina track and wind field. A shifted track of historical hurricane Katrina from previous study (Adhikari et al., 2020) also was used in this study to represent the highest possible storm surge caused by Hurricane Katrina that could have hit the Port of Mobile (see Figure 3-5). The water levels for the future scenarios accounting for a changing climate were determined by the Army Corps of Engineers (USACE, 2020) projections for the Dauphin Island gauge station sea level rise (SLR) based on NOAA (Sweet et al., 2017) scenarios. Two SLR scenarios were selected - 1.21 m and 3.28 m - to represent the intermediate and extreme scenarios in NOAA's scale (Sweet et al., 2017) which correspond to about 3% probability of exceedance for RCP

4.5 and 0.1% probability of exceedance for RCP 8.5 in IPCC's scale (IPCC, 2014) by 2100, respectively. A total of six scenarios were utilized with different combinations of hurricane tracks and climate change projections (Adhikari et al., 2020). These scenarios are identified using the following designation $S_{KWXXXX\text{-}Y.Z}$: where S = scenario; K = Katrina; W = N or S (natural or shifted track); XXXX = year considered; and Y.Z = RCP.

Table 3-2 shows all the scenarios considered in this study. These scenarios will be used in the following chapters to examine the vulnerability and operability of the Port of Mobile to changes in climate.

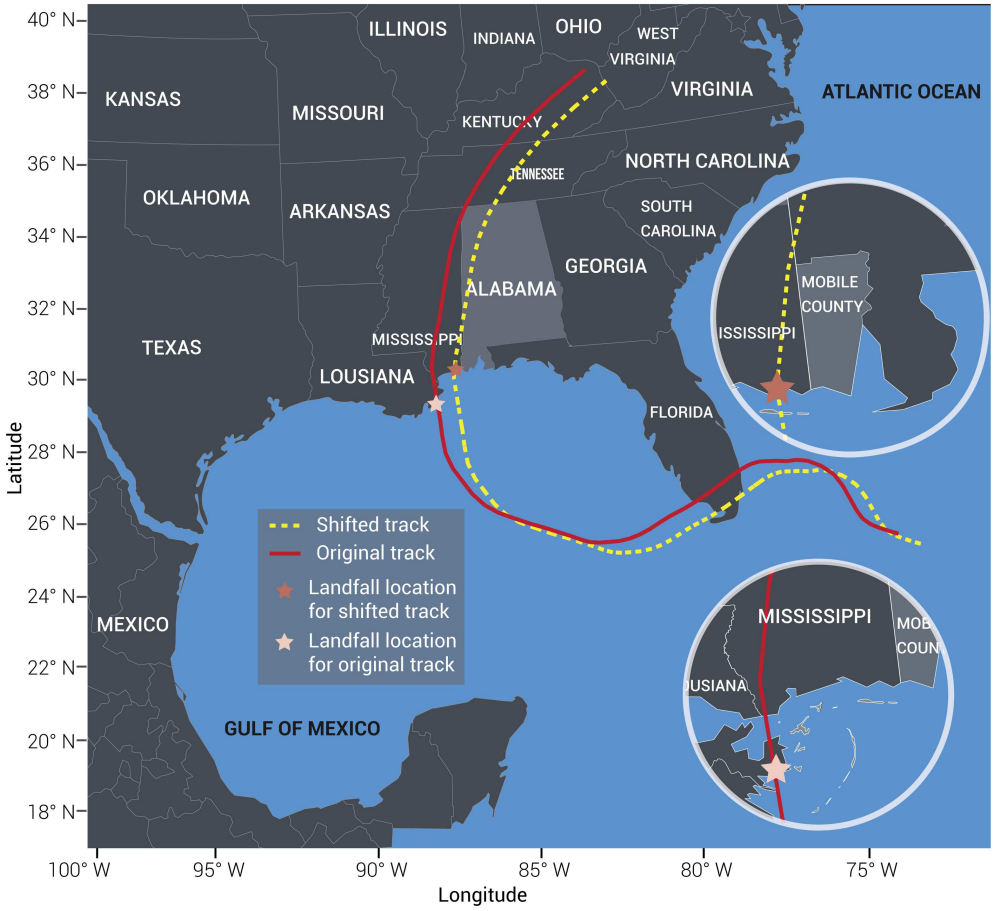

Figure 3-5: Hurricane Katrina's original and shifted track along with their landfall locations.

Table 3-2: List of 6 hurricane scenarios considered for this study

Scenarios	Hurricane name	Hurricane track	SLR		
			Value (m)	Year	Projection IPCC (NOAA)
S_{KN2005} **(baseline)**	Katrina	Natural	0.04	2005	-
S_{KS2005}	Katrina	Shifted	0.04	2005	-
$S_{KN2100\text{-}4.5}$	Katrina	Natural	1.21	2100	RCP 4.5 (intermediate)
$S_{KS2100\text{-}4.5}$	Katrina	Shifted	1.21	2100	RCP 4.5 (intermediate)
$S_{KN2100\text{-}8.5}$	Katrina	Natural	3.28	2100	RCP 8.5 (extreme)
$S_{KS2100\text{-}8.5}$	Katrina	Shifted	3.28	2100	RCP 8.5 (extreme)

CHAPTER 4. MODELS OF PORT FUNCTIONALITY

4.1. Port Configurations and operations

Port facilities, shown schematically in Figure 4-1, consist of coastal infrastructure (access channels, seawalls, breakwaters), terminal infrastructure (berths and docks), intermodal ground transportation (railway or roadway) connecting the port to inland markets, harbor superstructure (cranes, vehicles, warehouses), and operating facilities (buildings, water supply and power plant) (Bichou and Gray, 2005) that are necessary to handle the processes of port activities. Seaports can be privately or publicly owned and operated. Public and private terminals can be located in the same seaport and may share the same ground transportation and coastal infrastructure (Bichou, 2018).

Figure 4-1: The main infrastructure and superstructure components of the seaport.

The most common type of port in the U.S. throughout maritime cities involves owner terminals, where harbor infrastructure is under the authority of the state government (Bichou, 2018). As illustrated in Figure 4-1, when the vessels arrive at the seaport dock, goods and commodities are unloaded by crane, and then moved to storage at a warehouse or yard, awaiting shipment by surface transportation (roads, railways or river barges) to inland markets. These operations are extensive and seldom are handled by the port authority. Instead, some or all of the terminals, docks, and yards operations are leased to private companies using their own operating equipment such as cranes and container handling trucks to load/unload and move goods from dock to market and vice versa (Bichou and Gray, 2005; Becker and Caldwell, 2015).

4.2. Seaport components

Ports are usually classified by the nature of the goods and commodities that they handle, freight or category of the container. For example, there are dry bulk (cement, aggregates, agricultural and timber products, and unspecified bulk products) ports, liquid bulk (e.g. asphalt, petroleum products, chemical products, gas, water, and non-specified tankers) ports, and general freight ports.

Additional classifications break down ports into specific terminals, for instance, oil, containers and coal ports. Figure 4-2 illustrates functioning of a container port with some essential components, including berthing, ship to shore (STS) crane, storing, and gantry cranes. Berth's length and STS crane usually depend on the type of vessels and containers being handled (Bichou, 2018). As illustrated in Figure 4-2, an STS crane is used to deal with container loading/unloading to and from the vessels. Containers can be stacked either inside a warehouse or in an outdoor storage area (Figure 4-1). To allow

moving and storing cargos in the yard, container carriers are used with the help of the prime movers (Morris and Sempier, 2019). Gantry cranes are used basically to load/unload containers on the train or the trucks, after being retrieved from the warehouse or the yard by carriers, as shown in Figure 4-1 through train or truck cycles. There are two basic types of gantry cranes (Bichou, 2018; Morris and Sempier, 2019). The first is a rubber-tired gantry (RTG) crane, in which the crane moves on tires, can easily maneuver, and usually serve trucks (Figure 4-1). The second type (often called a rail-mounted gantry (RMG) crane (Thoresen, 2018) moves on rails and serves railway cars (Figure 4-1). Containers come in different sizes, but the most common standard size is the twenty-foot equivalent units (TEU) containers (Bichou, 2018).

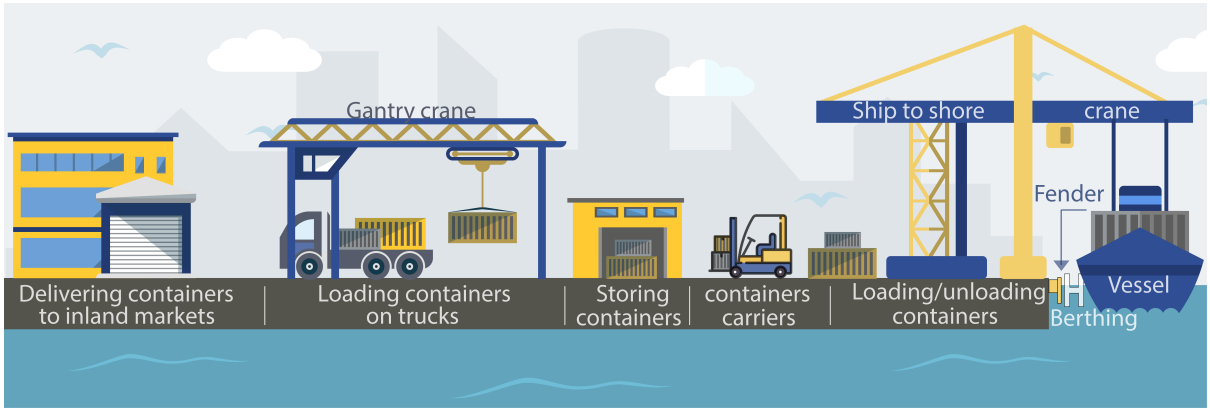

Figure 4-2: Container port with the most common throughput tasks.

Coal ports, which are considered as dry bulk ports, have the same tasks as container ports, except for not having warehouses to store coal products. The only way to store coal is to do so on the ground at the yard, as shown in Figure 4-3. Also, what differentiates coal ports over container ports, is that trains are the only way to deliver coal products from the yard to the market. A bulk handling crane is the only crane used

in dry bulk ports due to its ability to grab any raw bulk material which is not stored in containers.

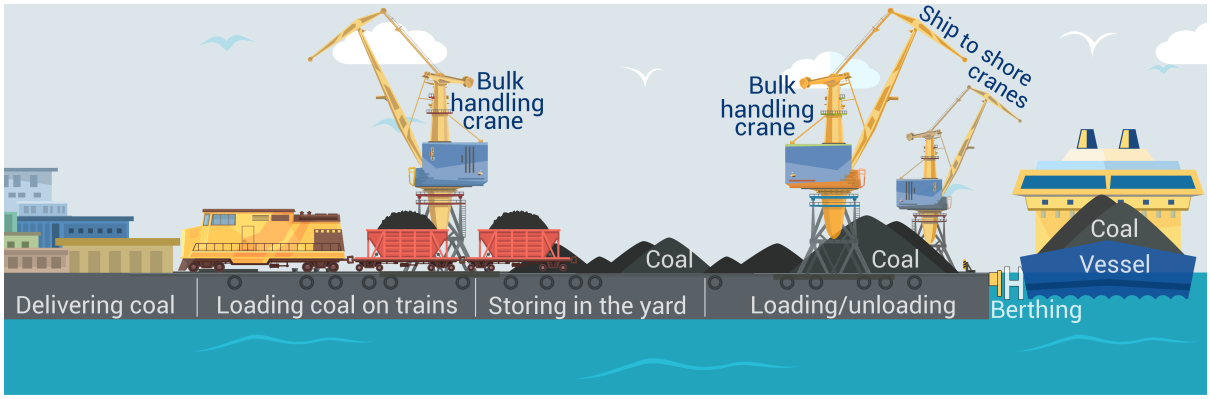

Figure 4-3: Traditional coal port with the most common throughput tasks.

4.3. Overview of the Port of Mobile

The Port of Mobile is an important node in Alabama's transport network and the South-Central Area of the U.S. by providing a connection between ocean-going cargo, a rail system and the I-10 interstate highway tunnel. The Port contributes $25 billion in annual financial activity to the State of Alabama state, creating direct and indirect jobs for around 153 thousand people (USACE, 2019). The Mobile port has an area of around 16 km^2 (Asdd, 2020), handles 59 million tons annually in goods and commodities, and ranks 11th among the top 100 U.S. ports in terms of total tonnage traffic across all categories (USACE, 2018). Figure 4-4 illustrates the commodities distribution at the Port of Mobile in 2018 (USACE, 2018). The Port is situated at the north end of Mobile Bay, which serves the port's vessel navigation requirements, has a triangle shape with a surface area of 1070 square kilometers and average depth of around 3 m (USACE, 2019).

A channel 12.2 m in depth is maintained by the USACE, and keeping the channel following extreme hurricanes is a necessary part of the port's resilience management.

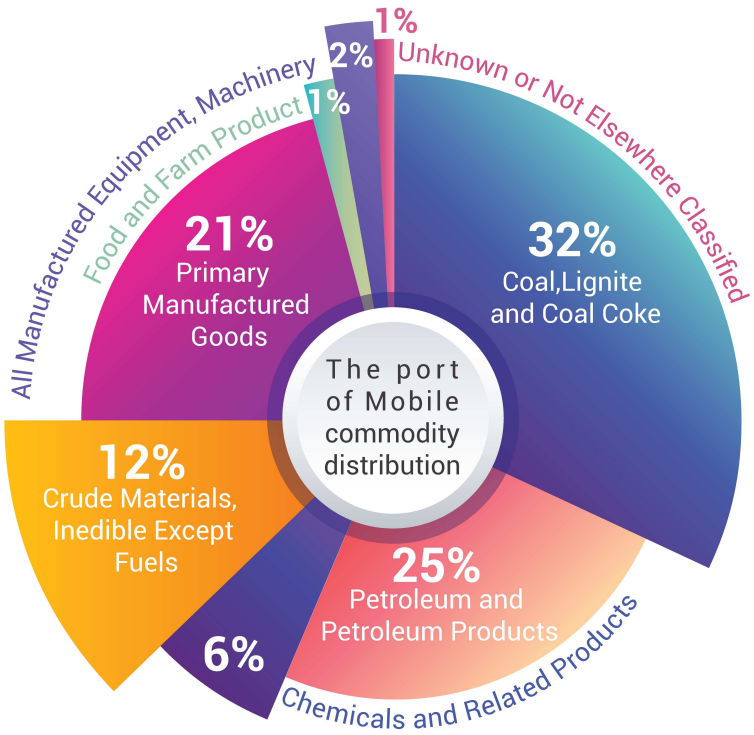

Figure 4-4: The distribution of products handled through the Port of Mobile (USACE, 2019).

The Port of Mobile has several terminals, some of which are owned by the Alabama State Port Authority (ASPA) or by private companies, while others are partially owned by either of the two sectors (USACE, 2019). Figure 4-5 shows the seven terminals owned and operated by the ASPA (Asdd, 2020). As shown in Figure 4-5, two terminals (the main complex and Blakeley Island Terminals) are located north of the I-10 (Wallace) tunnel, while the remaining five terminals are located south of it. Mobile middle bay port – Theodore is the only terminal that is far from others, as it located on the middle western shore of Mobile Bay, south of the Theodore Ship Channel (Asdd, 2020). There are 41 berths distributed within different terminals (the main complex, McDuffie Island, Choctaw

Point, and other terminals) under the ownership of the ASPA which is the largest public operator in the port (Asdd, 2020).

Among the upper two port terminals, the main complex is the most important one besides being the largest terminal in the Port of Mobile. Its container terminal has an approximate area of 2.3 km^2 with a 0.22 km^2 of storing space yard that allows handling up to 75 thousand TEUs annually of soybeans, forest products, iron, and steel products, roll-on/roll-off (Ro-Ro), and aluminum containers (USACE, 2019). The terminal also has a Bulk Handling Plant with an area of 0.089 km^2 located at the north part of the terminal.

For the five lower part terminals, APM Terminal Mobile and McDuffie Coal Terminal are the highest production terminals. APM is a terminal operated and managed by the A.P. Moller-Maersk Group company (Asdd, 2020). The container terminal has an approximate area of 0.47 km^2 (Figure 4-5) which allows handling 750 thousand TEUs annually and is projected to handle almost 2 million TEUs when the terminal expansion work is finished (USACE, 2019; APM, 2020). A $135 million international distribution center for Walmart opened 24 km from the terminal in 2018, which accounted for an additional 50 thousand TEUs of new annual containers throughput to the terminal (APM, 2020).

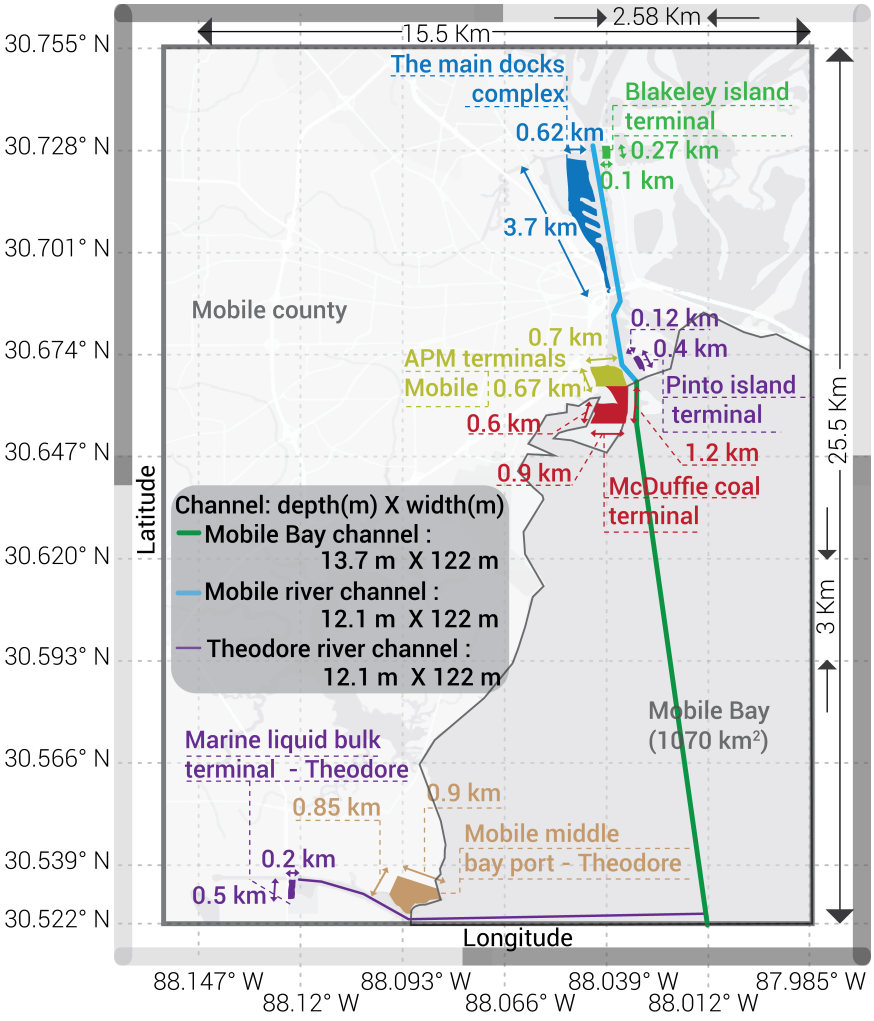

Figure 4-5: The operated terminals at the Port of Mobile.

The McDuffie Coal Terminal is one of the most important features of the Mobile harbor, as its three docks contribute a big share of the coal export from the U.S. (Harris et al., 2008). The terminal has an approximate area of 0.7 km^2 (Figure 4-5) that allows handling up to 30 million tons of coal annually, which makes it the third-largest coal export terminal in the U.S. (USACE, 2019; Asdd, 2020).

4.4. The Port of Mobile – Facilities, Operations and Functionality

As illustrated in the Port of Mobile overview (section 4.3), the port has seven distributed facilities/terminals within the Mobile county region operated by the ASPA. The berthing of vessels and ships through these facilities, besides all other tasks, that handle getting commodities to the inland market will be analyzed using FTA to evaluate the throughput of each facility and then to assess the functionality of the port. To do so, data available from different sources (USACE, 2019; APM, 2020; Asdd, 2020) were used to identify the location of berths in each facility as shown by a blue circle in Figure 4-6, and describe each berth along with its dimension as summarized in Table 4-1. One should notice that some locations has three berths as stated in Table 4-1.

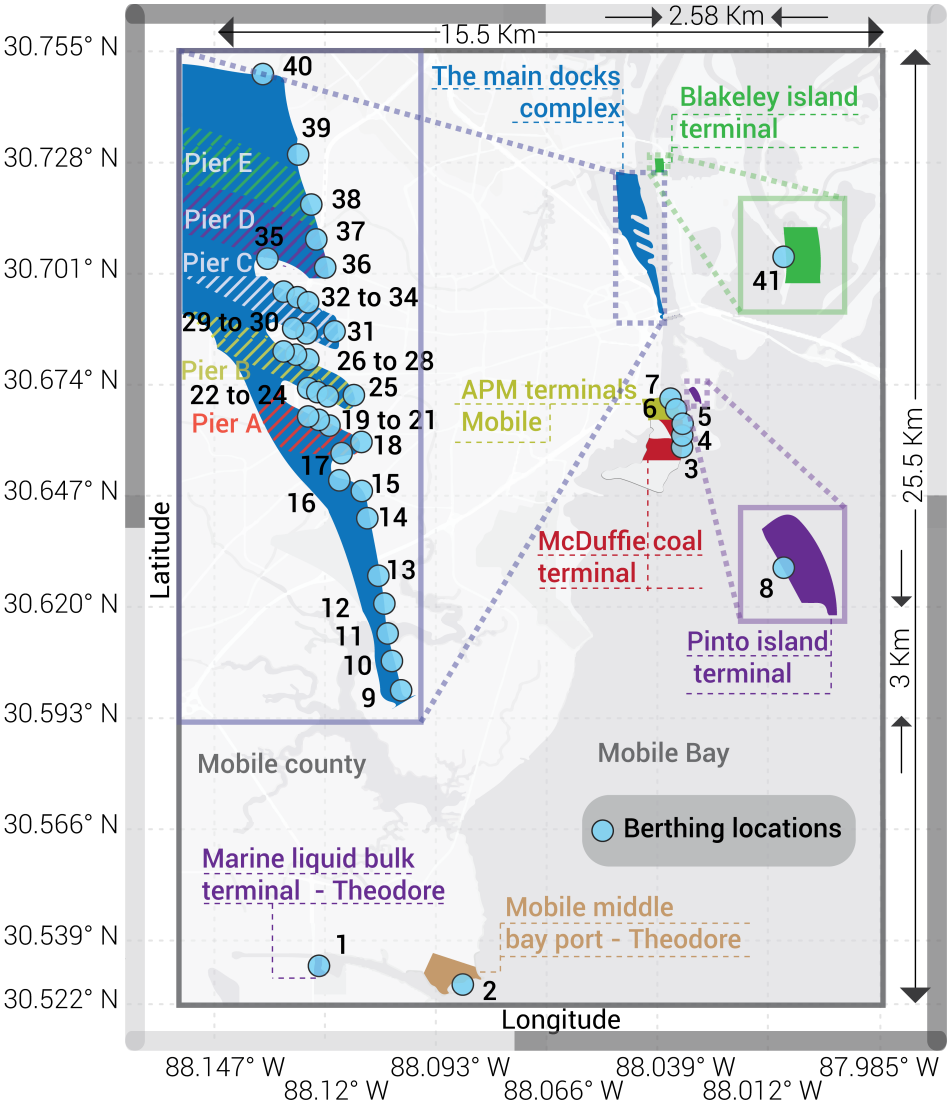

Figure 4-6: The 41 berth locations for the seven facilities at the Port of Mobile considered in this study.

Table 4-1: List of the 41 berth locations considered in this study along with the number of warehouse and other facilities associated with each berth

Berth location No	Description	Berth length (m)	Berth elevation (above MSL) (m)	No of Ware-houses	Piers and dock facilities
1	Marine liquid bulk terminal	335	3	-	-
2	Mobile middle bay port	183	3	-	-

3 to 5	McDuffie coal terminal		Berth 3: 267 Berth 4: 320 Berth 5: 275	4.57	-	6
6 to 7	APM terminals Mobile		Berth 6: 365 Berth 7: 365	2.75	-	6
8	Pinto island terminal		304	3.66	-	1
9	The main docks complex	Pier 2	302	3.35	-	-
10 to 13		Pier 3 to Pier 6	152.4	3.35	3	-
14		Pier 7	204.2	3.35	1	-
15		Roll-on/roll-off	39.6	3.35	1	-
16		Pier 8	176.8	3.35	1	-
17		Pier A South	173.7	3.35	1	1
18		Pier A river wharf	106.7	1.82	1	-
19 to 21		Pier A North **(3 berths)**	457	3.35	4	5
22 to 24		Pier B South **(3 berths)**	466	3.35	1	4
25		Pier B river wharf	198	3.35	-	-
26 to 28		Pier B North **(3 berths)**	491	3.35	1	-
29 to 30		Pier C South (**2 berths)**	467	3.35	1	1
31		Pier C river wharf	247.5	3.35	-	-
32 to 34		Pier C North **(3 berths)**	436.5	3.35	-	-
35		Pig Iron Dock	195	3.35	-	1
36		Pier D	244	3.35	1	1
37		Pier D-2	152	3.35	-	1
38		Pier E	335.3	3.65	2	16
39		Rail barge unloading	-	2.44	-	-
40		Bulk handling plant	470.3	2.89	3	-

41	Blakeley Terminal	Pier	152.4	3.35	1	1
Total		41 berths			22	44

As shown in Figure 4-6, terminals that belong to the Port of Mobile are spatially distributed within Mobile County, and each terminal is used to deal with specific commodity. Some of these seven terminals handle mixed products. For example, in the main dock complexes, most of the berths are used as a container terminal, except berths no 39 and 40, they are used as a dry/liquid bulk terminal. Others are used exclusively to handle specific commodities i.e., McDuffie coal terminal is used for coal products, and Pinto island terminal is used for steel products.

In order to estimate the damage cost due to the studied scenarios, the fixed assets in the port must be identified. Thus, Figure 4-7 is made using the port website (Asdd, 2020) and Google Satellite Images (Google, 2020) to locate all the warehouses or any other facilities (i.e., office buildings) used with every terminal. From Figure 4-7 and Table 4-1, one can notice that bulk terminals generally do not use warehouses or closed storage to store their products; instead, the products are stored on the ground, as shown in Figure 4-3 in section 4.2. However, for container terminals, warehouses are used with some terminals, i.e., in the main docks complex, and open storing is used with others, i.e., APM terminal Mobile.

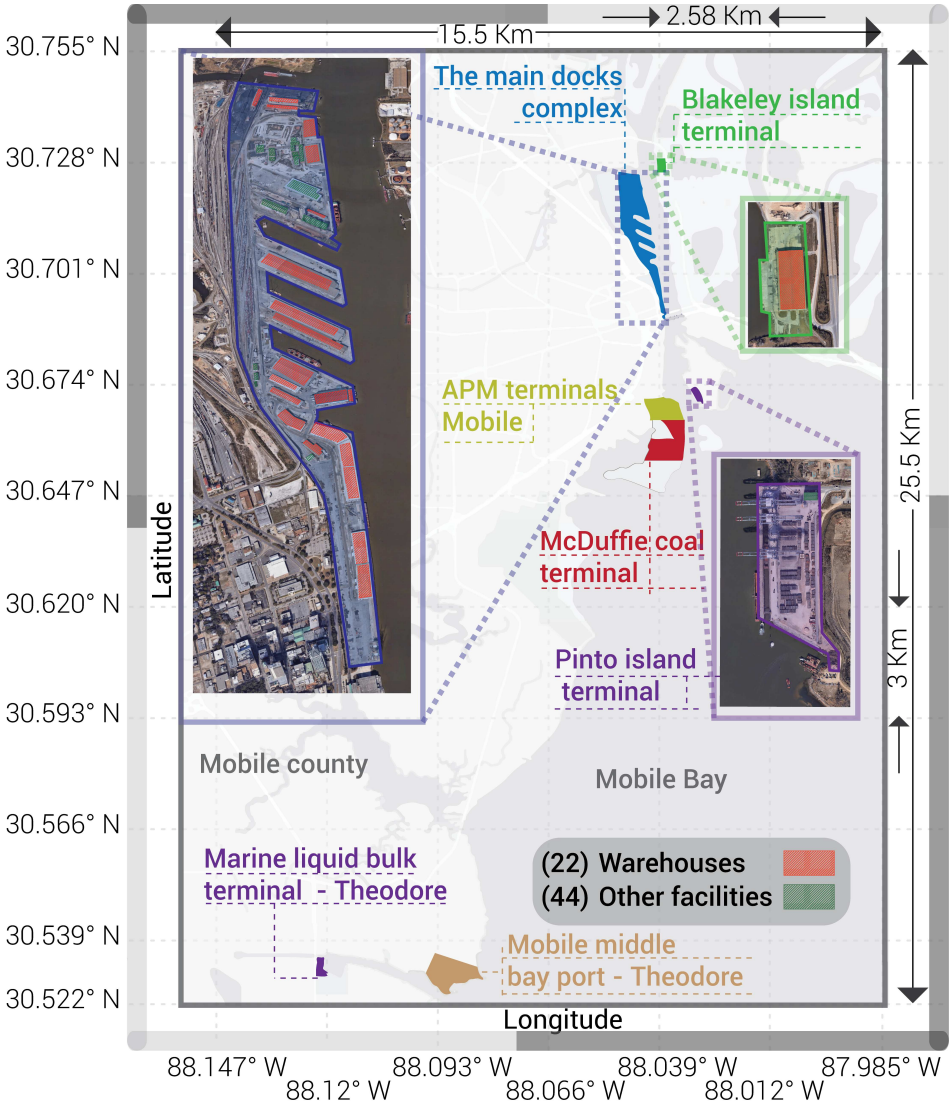

Figure 4-7: The locations for the 22 warehouses and some facilities within the selected six terminals at the Port of Mobile.

4.5. Resilience of seaports corresponding to SLR

The transportation systems sector was defined by the Presidential Policy Directive 21 (Department of Homeland Security, 2013) as one of the 16 primary infrastructure sectors. When a disaster hits a seaport, damage to harbor infrastructure can lead to a drop in functionality, which may lead to the port disruption and enormous financial losses. This loss in functionality, in turn, can spread to industries depending on the port

across distribution networks and have negative effects on the local, national and international markets. Therefore, seaport facilities must recover quickly and efficiently to pre-disaster rates after a severe environmental incident such as a hurricane.

Most previous research addressing resilience of ports have been aimed at the their performance during and following earthquakes (Na and Shinozuka, 2009; Shafieezadeh and Ivey Burden, 2014; Burden et al., 2016). For the calculation of interruption times and drop in performance, these investigators implemented a terminal modeling and a quay wharf and crane fragility curves. Several researchers have studied the impact of tropical cyclones on the seaport operational loss, but only from a wind engineering perspective (Esteban et al., 2012; Zhang and Lam, 2015; Cao and Lam, 2018). Regarding life cycle analysis for seaport post-hazard assessment, these studies did not illustrate the damage to physical components of the port; rather, they were focused mostly on the economic impact on the entire operation of the port. Only one study has addressed the resilience of each component of the seaport (Balbi. et. al 2018), which is necessary to deconstruct the various factors that impair port performance and lay a foundation for evaluating the reliability of port's components following a hurricane and its capability to recover from a natural disaster quantitatively. However, the Balbi study did not provide either a theoretical or logical model of port operations or functionality; nor did it address the interdependencies between its different components. These points are required to determine the functionality of the port during and after the occurrence of a tropical cyclone, accompanied by storm surge in an era of climate change. Thus, this thesis uses Fault tree analysis (FTA) to fill that gap and calculate the functionality of the port.

4.6. Fault tree analysis

Fault tree analysis (FTA) is a risk assessment technique based on logical analysis that has been used in different industries, early with nuclear power plants (Rasmussen 1974), and later in construction (Chi et al., 2014), railway systems (Liu et al., 2015), water supply (Lindhe et al., 2012), power plants (Doytchev and Szwillus, 2009), hospitals (Hassan and Mahmoud, 2019), and food security (Nozhati et al., 2019). As shown in Figure 4-8, the construction of a fault tree requires an understanding of how the various components of a complex system must function and interact together to achieve a performance goal, with top, intermediate, and basic events (Coudert and Madre, 1994). The probability of the top event is determined from a "bottoms-up" analysis. The probability of failure for each basic event generally can be computed from basic data or from engineering analysis; the probability of the intermediate and top events can be calculated from the basic events. The simplest fault tree models are constructed with only "OR" and "AND" gates. The AND gate requires all subsidiary events to occur for a major event occurrence, while with the "OR" gate, an event occurs if at least one of the subsidiary events occurs. Assuming a parallel or series model of system performance, the probability of occurrence of the higher-level event can be calculated per Eq. 4-1 and Eq. 4-2 for "AND" gate and "OR" gate, respectively.

$$P_{AND} = \prod_{k=1}^{i} P_k \quad (4\text{-}1)$$

$$P_{OR} = 1 - \prod_{k=1}^{i} (1 - P_k) \quad (4\text{-}2)$$

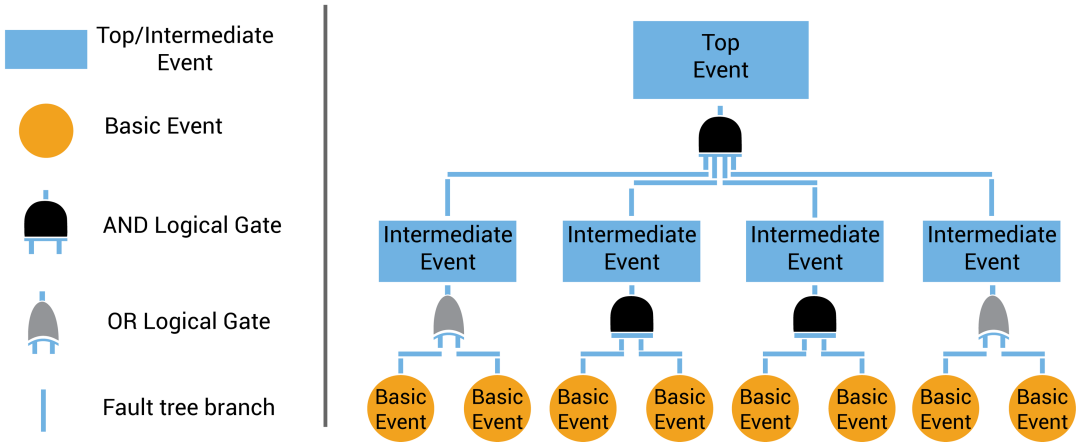

Figure 4-8: Description of FTA.

The Port of Mobile, as with most major seaports, has many docks prone to the same hurricane occurrence, which may present a broad spectrum of hazards, vulnerability, and exposure. To assess probability and future damage of the seaport under future scenarios, a quantitative evaluation by using fault tree analysis, is used (Figure 4-9). The FTA is a logical extension of the work by Balbi. et. al (2018), which provides most of the basic components for the operation of the port, combined with some common ideas regarding functionality from a previous study on hospitals by Hassan et. al (2019).

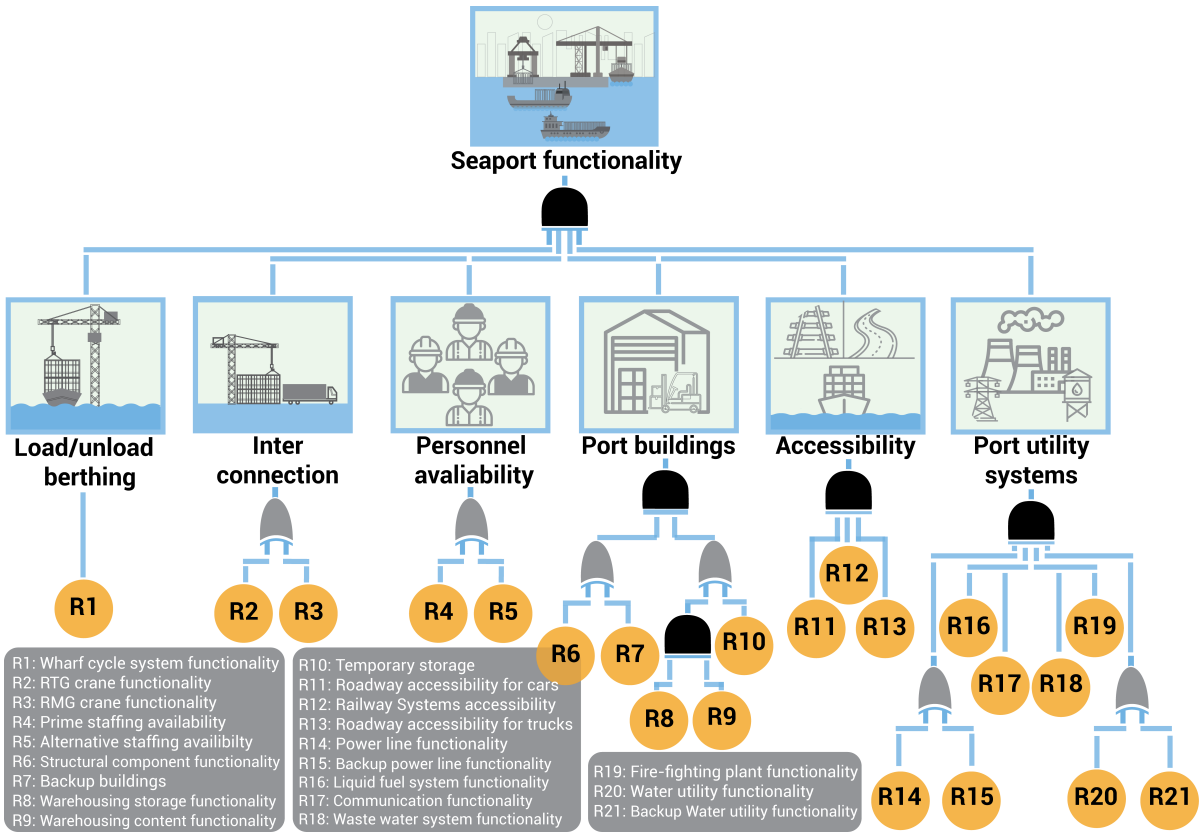

Figure 4-9: The fault tree chart considered for quantifying the functionality of the seaports.

The functionality of the port is defined by the throughput of the goods and commodities through the port, expressed as a fraction of the normal throughput, which averages 4,800 TEU/day (CEIC, 2016). In this thesis, we consider risk of terms of the response of the exposed physical components of the seaport to the damage associated with the studied SLR/hurricane scenarios. Therefore, depth-damage functions are required to identify the damage associated with each basic event of the FTA in response to different water depths. While damages due to hurricane wind pressures are not considered because storm surge is the major source of damages, the FTA could be easily modified to account for such damages.

As summarized in section 3.1, after obtaining the inundation map within the port area, and after determining the water depth at each component of the seaport, a risk assessment to quantify the functionality of the port operation can be performed. Adopting an approach for assessing damage to a particular harbor facility and its related industries (Tebodin, 1998), we have used depth damage curves for flooding in container and bulk terminals.

For the wharf cycle system functionality (element R1 in Figure 4-9), berthing requires that the cargo be safely and efficiently unloaded or loaded to and from ships. Thus, the initial reduction in berthing performance is a result of the increase in the inundation level due to storm surge (Figure 4-10). In this basic event, we consider the recommendation of Guyer (2018), in that the freeboard should not be less than 1 m, as shown in Figure 4-10 (a). However, in this study, it is assumed that loading/unloading can be conducted as long as the difference between the freeboard and dock elevation is not less than zero because it might be technically feasible to load/unload products for a short period of time if vessels are hocked to the dock in a stable manner. Thus, the functionality of the loading/unloading process depends on the mean sea level being at least at the same level as the dock elevation (Figure 4-10 (b)). R1 is considered non-functional if the increase of the storm surge is higher than the wharf elevation as shown in Figure 4-10 (c) and fully functional otherwise.

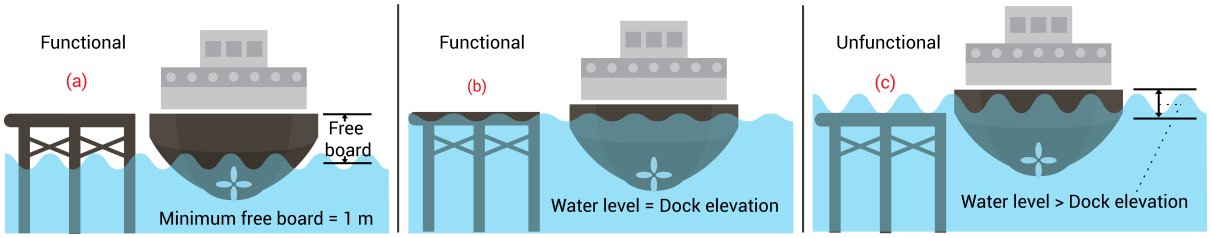

Figure 4-10: Functionality of R1 with (a) minimum recommended allowable freeboard, (b) minimum freeboard considered in this study, and (c) when a failure might occur.

For interconnection (Figure 4-9, R2 and R3) and warehousing content functionality (R9), the initial drop in their operations occurs when the exposed water depth exceeds the proper depth-damage function for container/bulk terminals (Figure 4-11). This fragility is extracted from a study conducted in The Netherlands (Tebodin, 1998) in which the performance of terminal installations was assessed for various water depths. Many types of installations were considered, including process equipment (i.e., tanks), utilities (i.e., pipes), mechanical equipment, control systems, inter transport (i.e., cranes and trucks), and storage system (i.e., racks and silos).

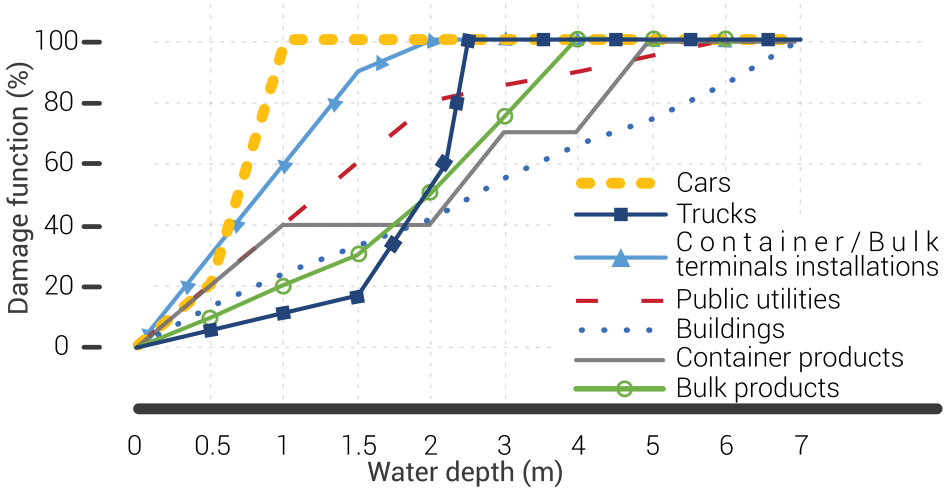

Figure 4-11: Depth-damage functions considered in this study.

Storage of goods and commodities is one of the crucial components in the port throughput functionality. Thus, the fault tree includes three primary events to represent storage: R8, R9, and R10 in Figure 4-9. Warehousing storage equipment and installations inside the warehouse to handle loading/unloading (R8 and R9) must function together in order to allow products to be stored securely. However, if their ability to store the products is affected by a natural hazard for a short period, temporary storage (R10) must be available to prevent the products from being damaged. The easiest way to allow temporary storage in the absence of the warehouse functionality is by stacking them on the dock of the port (see Figure 4-12). R8 and R9 functionalities are assessed by using buildings and installations depth-damage functions (Figure 4-11), respectively. For temporary storage (R10), the initial drop in this basic event is the result of the damage in the products stored on the dock by using depth-damage functions for either container or bulk products (see Figure 4-11).

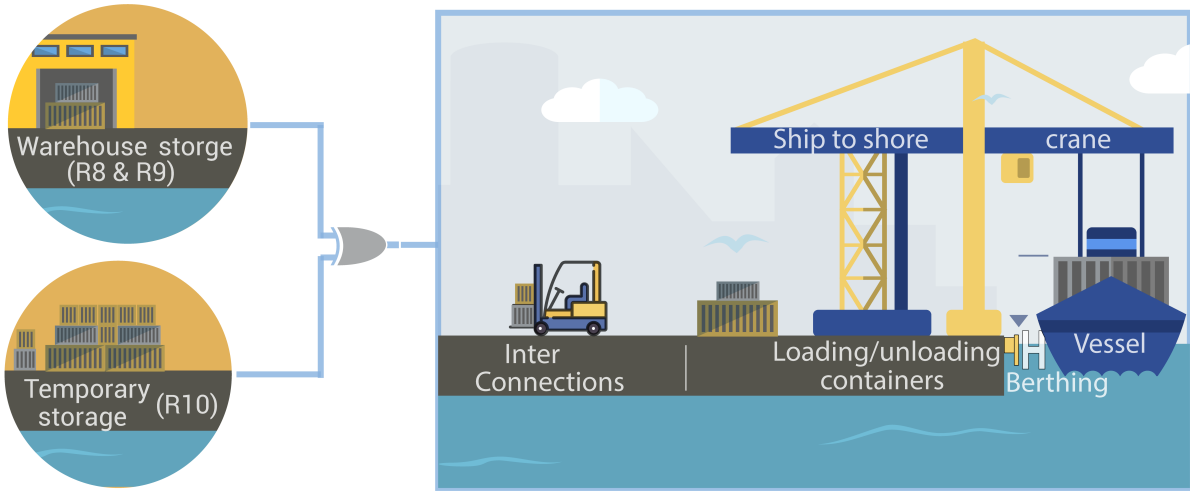

Figure 4-12: Illustration of the OR connection between warehouse storage and temporary storage basic events.

The functionality of the accessibility event depends on the accessibility of roadway for cars (R11), railways for trains (R12) and roadway for trucks (R13). The feasibility of employees' privately owned vehicles (POV) and commercial trucks reaching the port on roadways servicing the port following a hazard event is evaluated using vehicle depth-damage functions (Figure 4-11) obtained from HAZUS (Scawthorn et al., 2006). As shown in Figure 4-13, the thresholds for functionality of POV and trucks are 0.9 m and 2.40 m, respectively. For railway accessibility, we assume that if the water does not cover the rails (Figure 4-13), then the train is fully functional. Thus, the threshold for the train accessibility is chosen to be 0.2 m (see Figure 4-13), to represent the maximum height of the rail cross section.

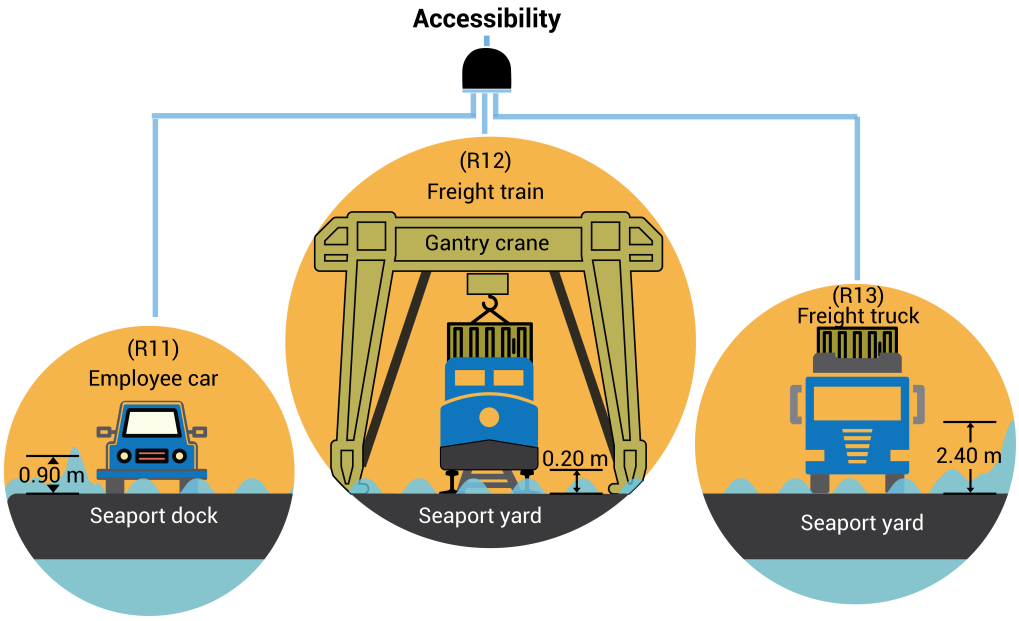

Figure 4-13: illustration of the AND connection between R11, R12, and R13.

Inundation by storm surge coupled with SLR has a variety of negative environmental and social effects, including the evacuation of residents (Levine et al., 2007). Thus, personnel availability for employment at the port (R4 and R5) is estimated

by evaluating damage to employees' residential homes by storm surge floods using depth-damage functions for building (Figure 4-11). The number of employees who work at the Port of Mobile is not available to the public. However, an online interview (Toner, 2015), with Alabama Port Authority executive director, revealed that the number of employees was 647 in 2015. Thus, we use that number to randomly select houses in Mobile and Baldwin counties out of 4565 houses obtained from the open-source collaborative project, OpenStreetMap (OSM), to represent the residency of these employees, as shown in Figure 4-14(a). Since the topography of the ground level at the selected houses varies even within the same region (see Figure 4-14 (b)), buildings in different areas must be assessed individually under different SLR/hurricane scenarios.

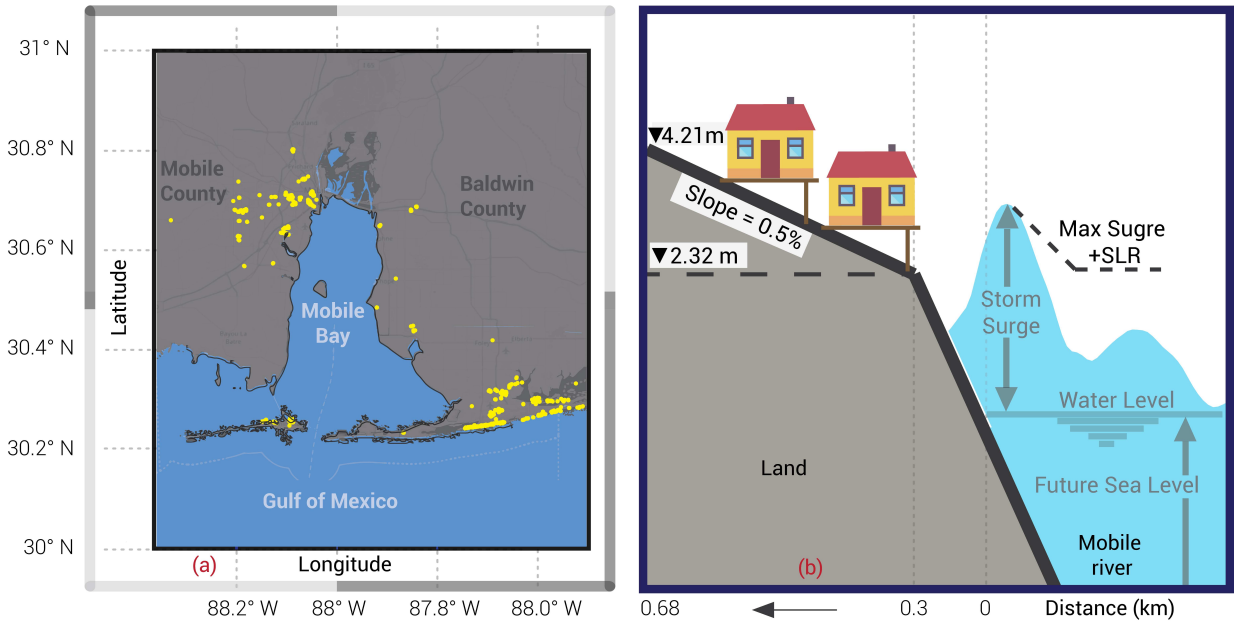

Figure 4-14: Random location of residences of port employees. (a) The location of the randomly selected houses shown in yellow, and (b) the variation in ground elevations for some of these houses

Utility systems (R14 to R21), such as electricity lines, water supply, wastewater pipelines, communication lines, liquid fuel supply, and fire-fighting facilities, are essential to enable the port to operate safely and efficiently. For the lack of information regarding the geodata of these facilities within the Port of Mobile, we assess the functionality of these facilities within each dock of the port. Depth-damage functions for public utilities (Tebodin, 1998) (Figure 4-11) were used to evaluate the initial drop in the functionality of these facilities due to the studied SLR/hurricane scenarios.

CHAPTER 5. RESULTS AND DISCUSSION

5.1. Validation of multi-hazard modeling

The accuracy of the storm surge model used in this study was tested using data obtained during Hurricane Katrina from the NOAA Tides and Currents (NOAA, 2020) stations at Dauphin Island (ID: 8735180) and at Pensacola, FL (ID: 8729840), as they were the only two stations that had recorded data during the hurricane. In Figure 5-1 (a), the predicted water levels at the Dauphin Island station capture the measured peak storm surge, although the predicted astronomical tides were slightly less than at the observation station. The model produces the same shape and duration of storm surge and tides at the Pensacola Station (Figure 5-1(b)), but it overestimates the peak surge by around 0.13m. This behavior can be attributed to the fact that this station is some distance from the hurricane track. The simulation also captures the peak storm surge of about 3.5m in downtown Mobile, which matches the FEMA high water marks at this location (FEMA, 2006). It is clear that this model can be used to simulate future hurricane storm surges, coupled with SLR, and to study the impact of different hazard scenarios on the region of interest.

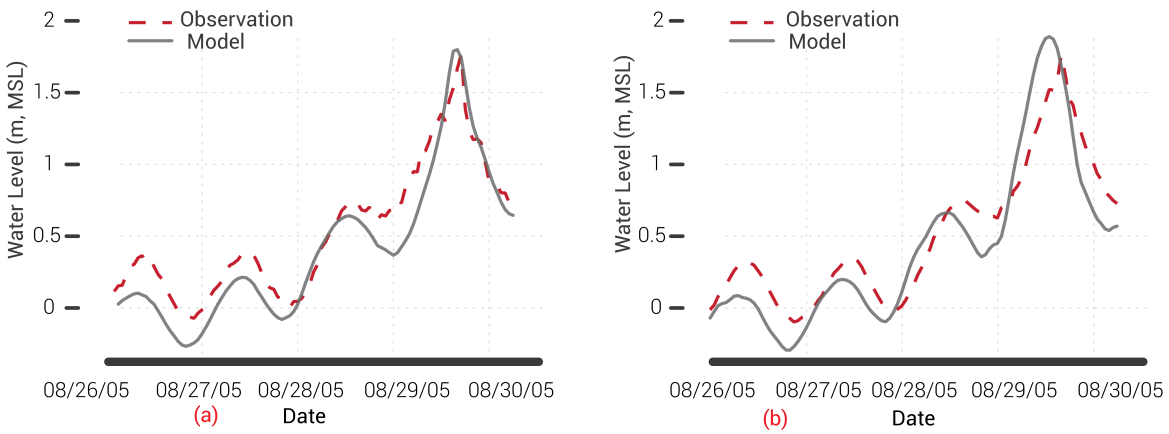

Figure 5-1: Comparison of water level from observation stations (red dots) and model simulation (blue lines) for baseline scenario (SKN005) at (a) Dauphin island and (b) Pensacola, FL observation stations.

A common method of quantifying model error is to calculate the average gap between the simulation model and observed data (Sutherland et al., 2004). Root-mean-squared-error (RMSE) (Emery and Thomson, 1997), bias, skill score (Plant et al., 2004), and mean absolute percentage error (MAPE) values were computed using the following equations:

$$\mathrm{RMSE} = \sqrt{\frac{1}{N}\sum_{i=1}^{n}(X_i - Y_i)^2} \quad (5\text{-}1)$$

$$\mathrm{Bias} = \frac{1}{N}\sum(X_i - Y_i) \quad (5\text{-}2)$$

$$\text{Skill score} = 1 - \frac{\sum_{i=1}^{n}(X_i - Y_i)^2}{\sum_{i=1}^{n}(Y_i - \overline{Y_i})^2} \quad (5\text{-}3)$$

$$\mathrm{MAPE} = \left(\frac{100}{N}\right)\sum_{i=1}^{n}\left(\frac{|Y_i - X_i|}{Y_i}\right) \quad (5\text{-}4)$$

where X_i, Y_i, and N are simulation model results, observation data values and the number of samples, respectively. The best agreement between model and observation is achieved when RMSE, bias, skill score, and MAPE equal to zero, zero, one, and 0%, respectively. A negative bias implies that the water in the observation is higher than the

model. Table 5-1 summarizes these metrics for the two observation stations. The RMSE values associated with Figure 5-1 (a) and (b) are 0.13 m and 0.19 m for the stations at the Dauphin Island and Pensacola, Fl, which is considered to be a good agreement for a study of this kind.

Table 5-1: Computed statistics for NOAA tides and currents stations

Station	RMSE (m)	Bias (m)	Skill score	MAPE (%)
Dauphin Island	0.13	-0.13	0.91	9
Pensacola, FL	0.19	-0.09	0.88	10.26

5.2. Flooding due to storm surge

The areal extent of peak storm surge flooding for each scenario is shown in Figure 5-2. Comparing flooding between original and shifted track, the area inundated by the shifted track (blue color in Figure 5-2 (b)) is 24% larger than the area inundated by the original track (blue color in Figure 5-2 (a)). That increase is derived by the increase in storm surge associated with the peaking of wind speed when the Katrina track is shifted. These simulations highlight the effect of SLR on the inundated area, where for the original track, the area flooded increased by 54% and 100%, respectively, for the NOAA-specified intermediate and extreme SLR events (see Figure 5-2). The inundation areas from the six scenarios are summarized in Table 5-2. Changing the landfall location so that the area of interest is impacted by the maximum wind speed not only contributes to

a higher storm surge, but also to a larger inundated area due to flooding. SLR with RCP 8.5, in combination with the hurricane, almost doubled the flooded area for the natural track and increased it by more than 65% for the shifted track, as shown in Figure 5-2 and Table 5-2.

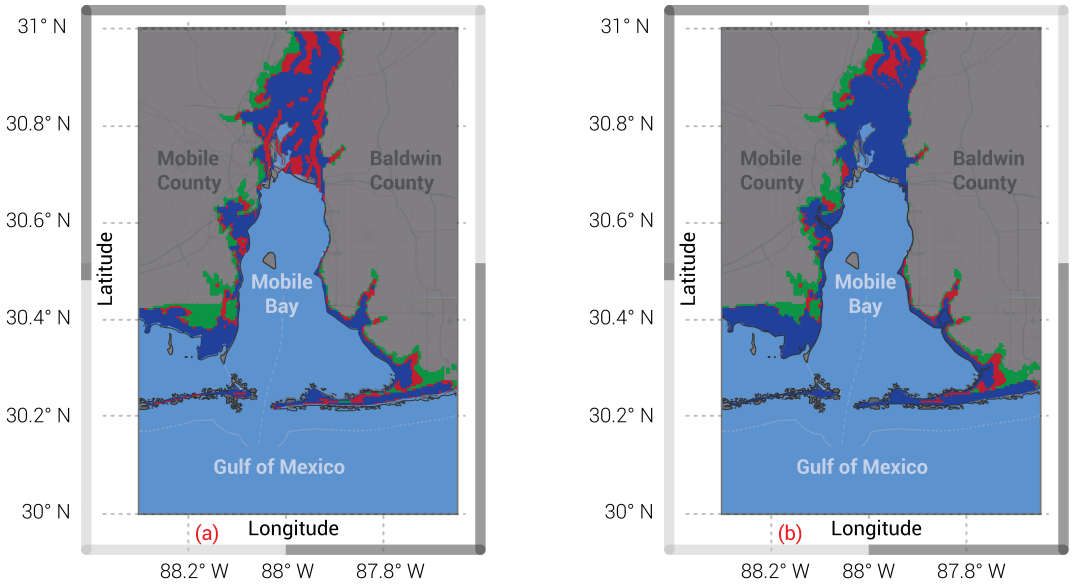

Figure 5-2 Sensitivity of inundation area to hurricane and SLR scenarios: (a) S_{KN2005} and (b) S_{KS2005}. Blue color dominates the area inundated only by (a) S_{KN2005} and (b) S_{KS2005}. The red represents the extra area flooded by (a) $S_{KN2100\text{-}4.5}$ and (b) $S_{KS2100\text{-}4.5}$. Green is the extra area inundated by (a) $S_{KN2100\text{-}8.5}$ and (b) $S_{KS2100\text{-}8.5}$.

Table 5-2: Inundation areas in Mobile and Baldwin counties under different scenarios.

Scenarios	Inundation area In Mobile and Baldwin counties	% Increase from baseline
S_{KN2005} (baseline)	775 km^2	-
S_{KS2005}	963 km^2	24%
$S_{KN2100\text{-}4.5}$	1196 km^2	54%
$S_{KS2100\text{-}4.5}$	1239 km^2	60%

$S_{KN2100\text{-}8.5}$	1537 km^2	100%
$S_{KS2100\text{-}8.5}$	1590 km^2	105%

NOAA has a gauge station at Mobile State Docks (ID: 8737048), which is near the Port of Mobile, to capture daily water level and tides (NOAA, 2020). This location (Figure 5-3 (a)) is used to assess the impact of the scenarios identified in Table 3-2 (Chapter 3) on the functionality of the Port.[2] The predicted future SLR would also have a substantial impact on the peak of storm surge, besides increasing the flooded area. Simulation outputs comparing the storm surge water levels for the six scenarios considered at the Mobile State Docks station are shown in Figure 5-3 (b). When water levels for the original and shifted tracks at the Mobile State Docks station are compared, the simulated peak storm surge from the shifted track (S_{KS2005} in Figure 5-3 (b)) is 15% larger than that from the original track (S_{KN2005} in Figure 5-3 (b)). Considering the intermediate and extreme SLR scenarios, the peak storm surge by the shifted track ($S_{KS2100\text{-}4.5}$ and $S_{KS2100\text{-}8.5}$ in Figure 5-3 (b)) is 15% and 20% larger than that by the original track ($S_{KN2100\text{-}4.5}$ and $S_{KN2100\text{-}8.5}$ in Figure 5-3 (b)), respectively. The maximum water levels from the six scenarios are summarized in Table 5-3. SLR with RCP 8.5, in combination with the hurricane, increase the maximum water level by 90% for the natural track and doubled it for the shifted track, as shown in in Figure 5-3 (b) and Table 5-3. The simulation outputs also show that the 15% increase of the maximum water level by the shifted Katerina (S_{KS2005}), resulted in a 25% increase

[2] This gauge station was functioning at the time of Hurricane Katrina, but failed four hours into recording and thus cannot be used for validating the hydrodynamic analysis of storm surge.

in the flooded area of the studied area. However, these results depend mainly on the changes in local land levels of the area of interest.

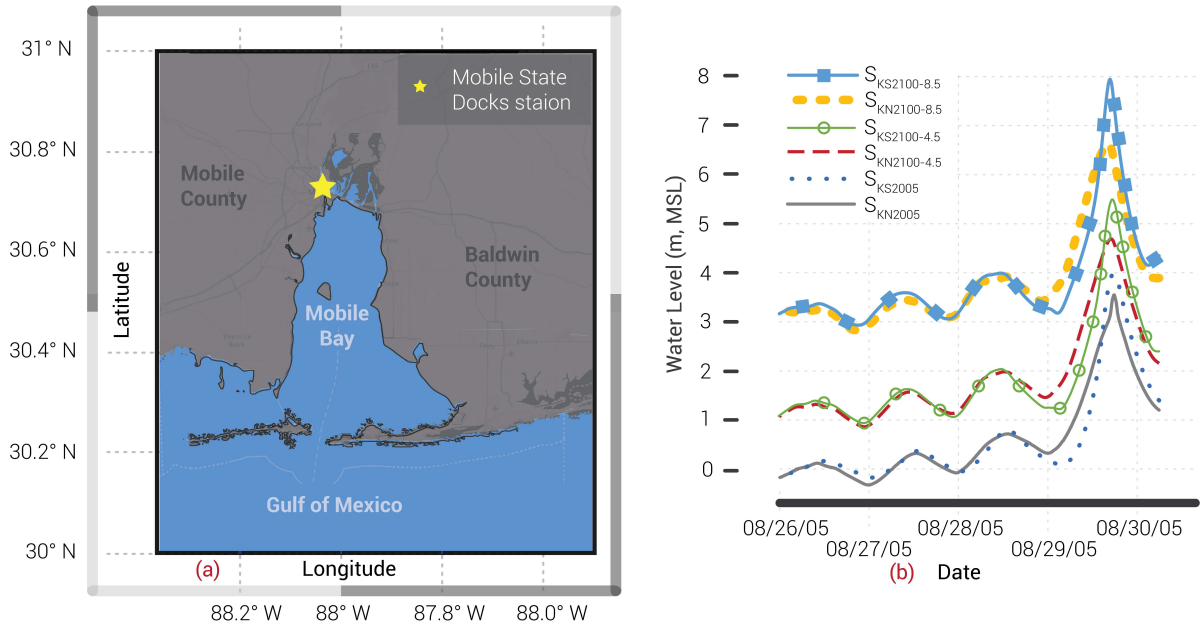

Figure 5-3: Comparison of storm surge at Mobile State Dock for different hazard scenarios. (a) Location for Mobile State Dock, and b) Comparison of the water level due to storm surge and SLR scenarios.

Table 5-3: The peak of storm surge at Mobile State Docks station under different scenarios

Scenarios	**Max water level In Mobile State Docks station**	**% Increase from baseline**
S_{KN2005} (baseline)	3.5 m	-
S_{KS2005}	4 m	15%
$S_{KN2100\text{-}4.5}$	4.7 m	34%
$S_{KS2100\text{-}4.5}$	5.5 m	57%
$S_{KN2100\text{-}8.5}$	6.64 m	90%
$S_{KS2100\text{-}8.5}$	8 m	128%

5.3. Damage Assessment for surge hazard

The impact of the proposed scenarios on the fixed assets of the port (see Table 4-1 and Figure 4-7) is considered using the simulation outputs from Table 5-3. The structural component values of ports and harbors from the flood model in the HAZUS-MH (2020) technical manual are utilized to calculate the losses to the physical components of the port. Figure 5-4, Figure 5-5, and Figure 5-6 show the heat map of the expected damage to the physical components of the studied port. In all three figures, damages caused by the shifted Katrina track (close to the Port region) are substantially higher than those caused by its natural track. Indeed, Hurricane Katrina on its natural track causes minimal damages to most of the fixed assets of the terminals of the port, with the exception of one berth that was vulnerable because of its low elevation (Figure 5-4(a)). The damage state for most terminals increases when the shifted track of Katrina is considered, from minimal to moderate or to extensive, as shown Figure 5-4(b). SLR with RCP 4.5, in combination with the hurricane, increases the damage states from minimal to extensive for the natural track and from moderate to significant for the shifted track, as shown in Figure 5-4 and Figure 5-5. Under RCP 8.5, the damage state of the port is changed to substantial by both tracks (Figure 5-4 and Figure 5-6).

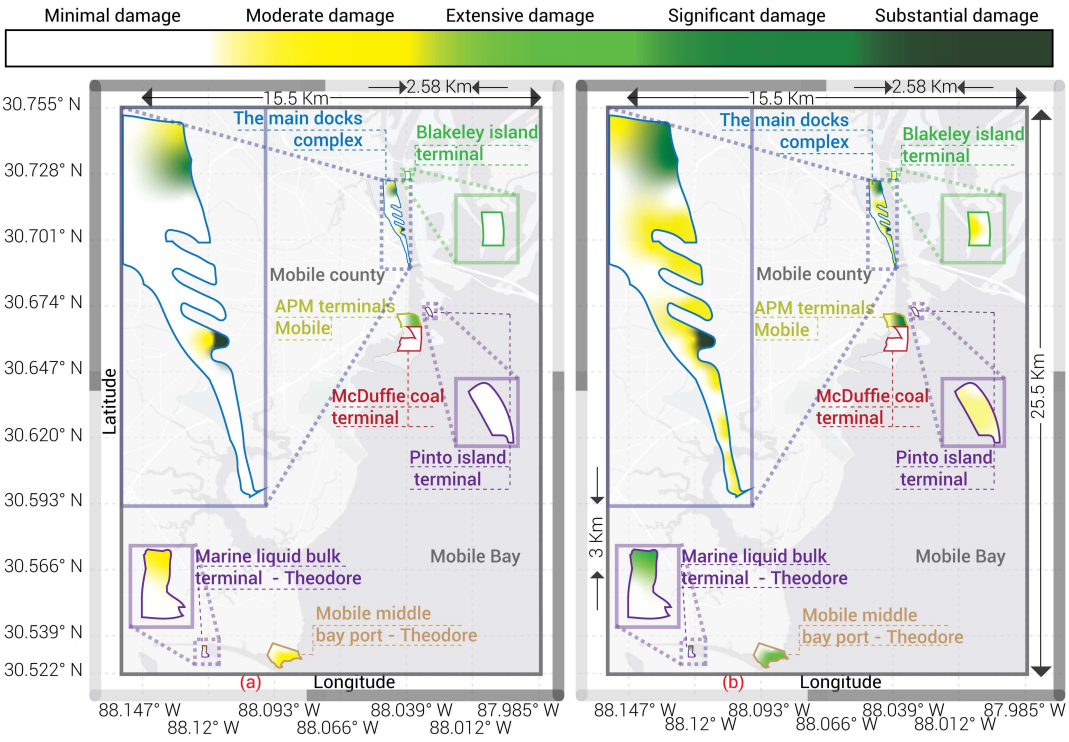

Figure 5-4: Expected damages for scenario a) S_{KN2005} and b) S_{KS2005}.

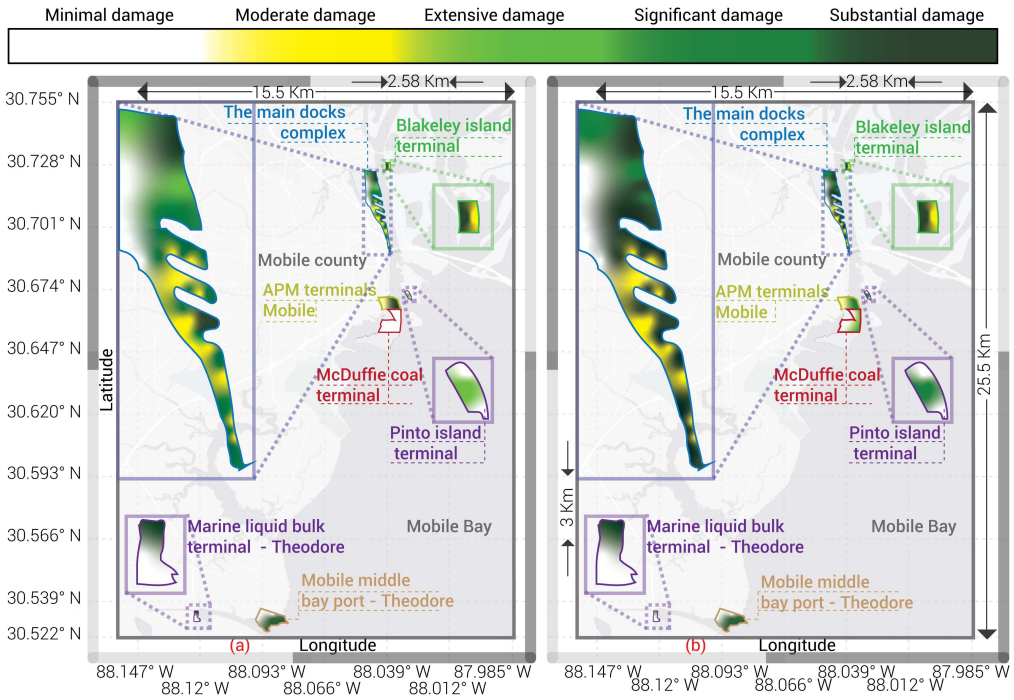

Figure 5-5: Expected damages for scenario a) $S_{KN2100\text{-}4.5}$ and b) $S_{KS2100\text{-}4.5}$.

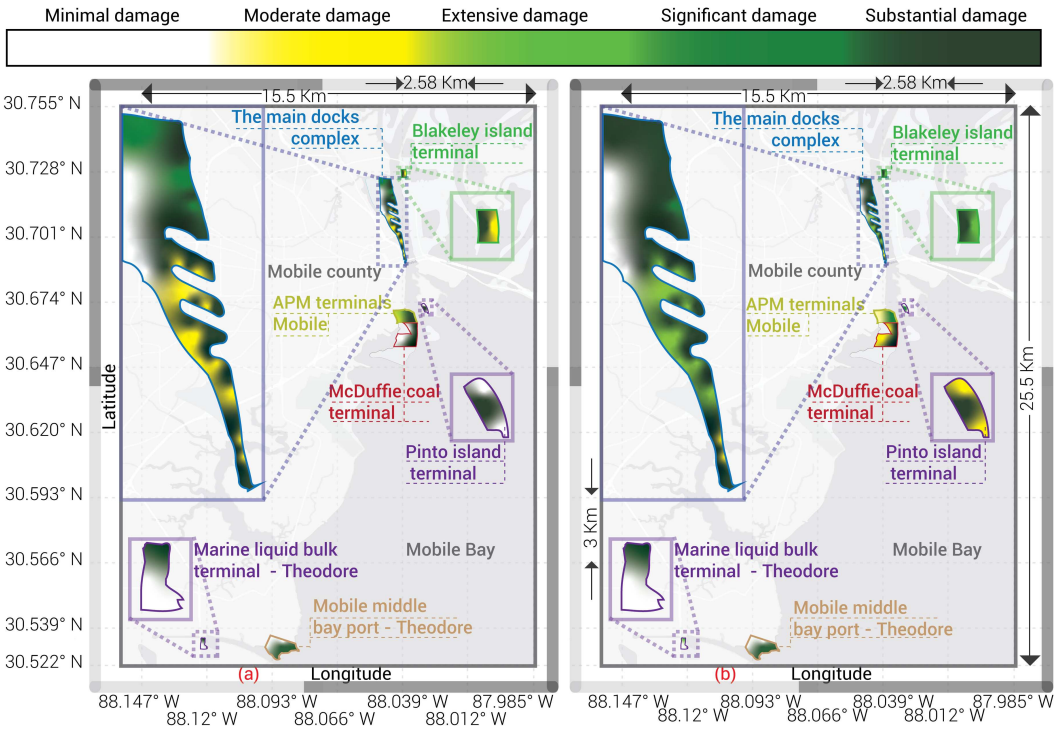

Figure 5-6: Expected damages for scenario a) $S_{KN2100\text{-}8.5}$ and b) $S_{KS2100\text{-}8.5}$.

One observation from these results is that the dock with handling equipment is highly vulnerable to an increase in water level, as the dock sustained substantial damage state by the shifted Karina coupled with RCP 4.5 of SLR (Figure 5-5(b)). However, the case is not the same with warehouses and other industrial buildings within the port region. For example, warehouses did not change from a minimal damage state even with the shifted Katrina track. Their damage scale started to change to a moderate level when only SLR is included with RCP 4.5 in both tracks (Figure 5-5). Even under extreme scenarios ($S_{KN2100\text{-}8.5}$ and $S_{KS2100\text{-}8.5}$), the damage states of warehouses were moderate or extensive under both natural and shifted Katrina hurricanes when coupled with RCP 8.5 of SLR, respectively.

The previous results show how some components of the port might be vulnerable to extreme hurricane events in the future. To illustrate more and to provide an overall picture of the impact of the studied scenarios on the port, Figure 5-7 is constructed to show the normalized physical damage cost to the whole port to the damage cost of the historical hurricane Katrina. The damage costs of the port fixed assets are tripled by only shifting the Katrina track to be closer to the port.

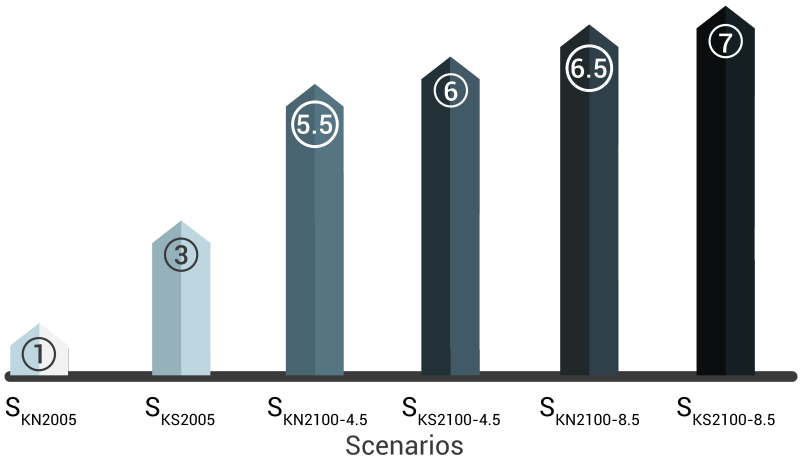

Figure 5-7: Physical assets damage costs normalized to the damage cost of the baseline scenario.

Coupling future SLR scenarios under RCP 4.5 with the hurricane, the damages are increased by 5.5 times for the natural track scenario and are doubled for the shifted track. The highest damage costs are reached by the results of the RCP 8.5 scenarios with both tracks. The shifted Katrina with RCP 8.5 increased the damage costs to the port seven times compared to the baseline scenario. Moreover, the damages are risen more than six times for the original track and are more than doubled for the shifted track by RCP 8.5 scenarios.

5.4. Fault tree analysis outputs

The costs of damage to the physical components are not the only losses to the port after a hurricane event. The shutdown of port operations that handle the products from arriving vessels and ships is another primary loss to the port after hurricane events. The outputs from the proposed fault tree analysis described previously can be used to assess losses due to the drop in the port functionality, First, the functionality of each terminal alone is examined using the FTA outputs; subsequently, the performance of the whole port is assessed in the following paragraphs.

5.4.1. The performance of individual terminals

Figure 5-8, Figure 5-9, and Figure 5-10 show the functionality of each terminal over time following the scenarios identified previously. Those figures only cover the initial drop in the functionalities without considering the recovery part. In all three figures, the initial drop in all terminals' functionalities caused by the natural track has occurred earlier than the shifted track. In other words, zero functionality for all terminals is reached using the natural track prior to being reached using the shifted track in all cases. The initial drop of the terminals' functionality (In all three figures), at around August 29th, is caused by the initial increase of the storm surge in all scenarios (as shown in Figure 5-3 (b)).

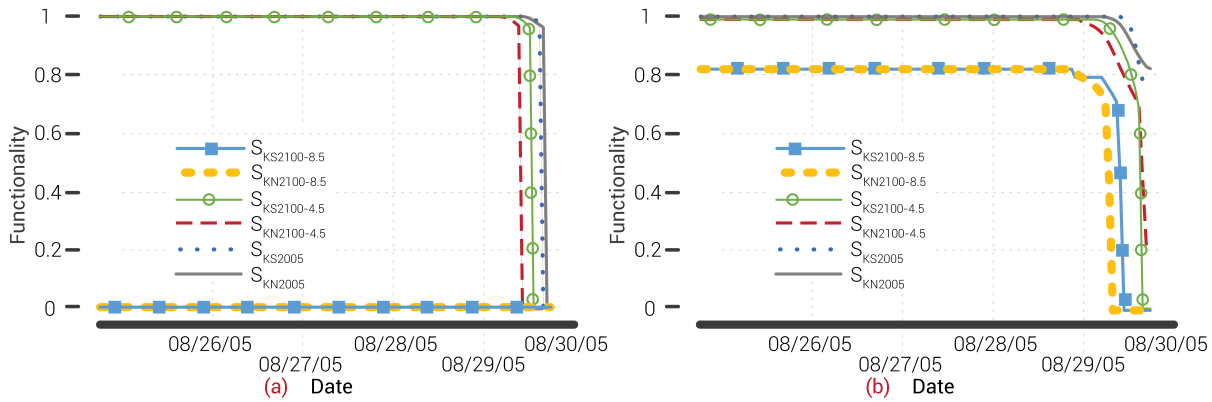

Figure 5-8: Estimated functionality for a) Theodore terminals and b) McDuffie coal terminal.

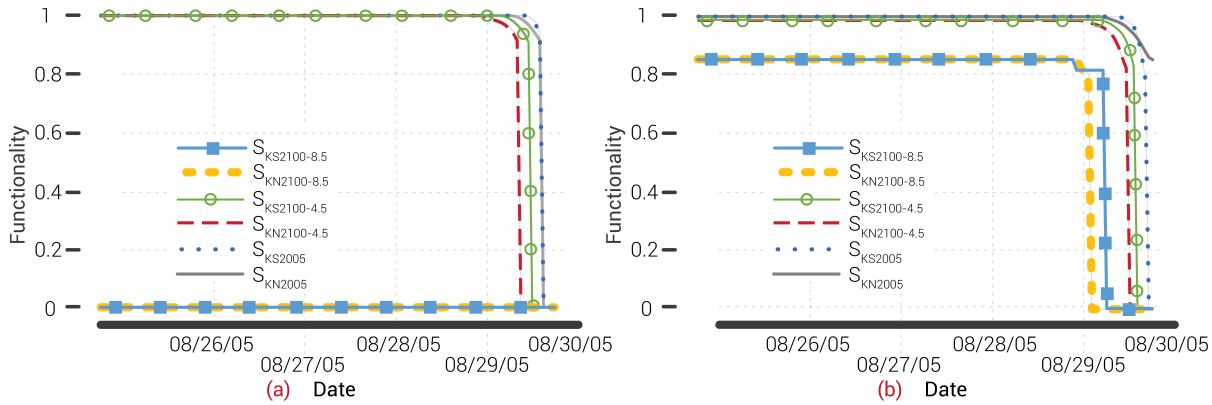

Figure 5-9: Estimated functionality for a) APM terminal and b) Pinto island terminal

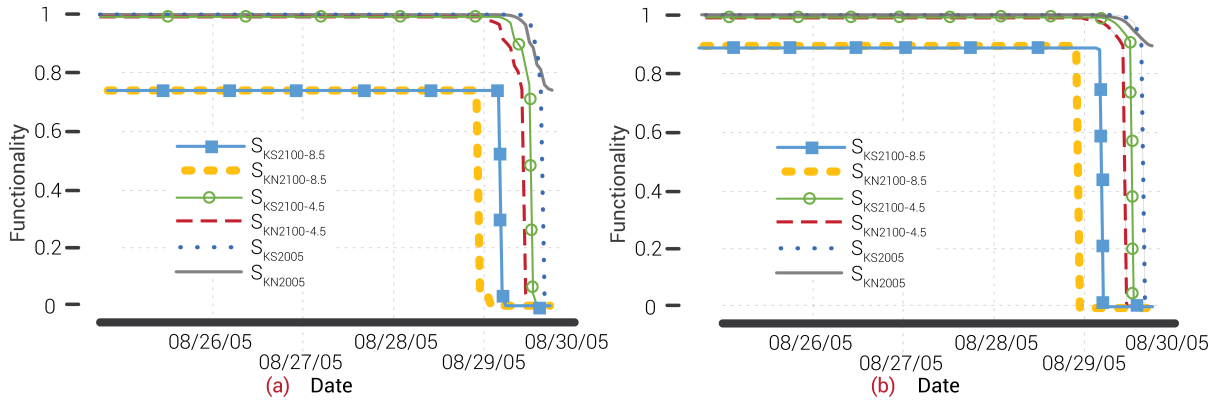

Figure 5-10: Estimated functionality for a) The main docks complex and b) Blakeley terminal

For all terminals, SLR with RCP 4.5 alone does not affect the operation of the port as it does when coupling it with the hurricane, as shown in Figure 5-8 to Figure 5-10. However, SLR with RCP 8.5, alone (the period before the hurricane storm surge), causes the functionality of the Theodore terminals (Figure 5-8(a)) and the APM terminal (Figure 5-9(a)) to drop by 100%, while decreasing it by around 20% for other terminals. In other words, SLR scenarios in the future might present a functionality issue to the port before the end of the 21st Century, irrespective of whether a hurricane occurs. The functionality of all terminals decreases to 0% in all the six scenarios except the natural track scenario. In the baseline scenario (S_{KN2005}), the functionality is dropped to 0% for the Theodore terminals (Figure 5-8(a)) and the APM terminal (Figure 5-9(a)), while it is decreased to around 80% for other terminals.

5.4.2. The performance of the port

Figure 5-11, Figure 5-12, and Figure 5-13 show the functionality for the 41 docks considered in this study with their mean functionality over time after the studied scenarios. Figure 5-14 shows a comparison between the considered scenarios for the mean functionality of the port. In Figure 5-11(a), the mean operation of the port dropped to 75% after the natural track (S_{KN2005}), as most of the docks have that behavior while few of them reach a complete shutdown. On the contrary, the shifted track causes an 85% drop in mean functionality of the port following the same trend for most docks, as shown in Figure 5-11(b). The drop in functionality of the port is decreased by 50% by only shifting the Katrina track to be close to the port, as shown in Figure 5-11.

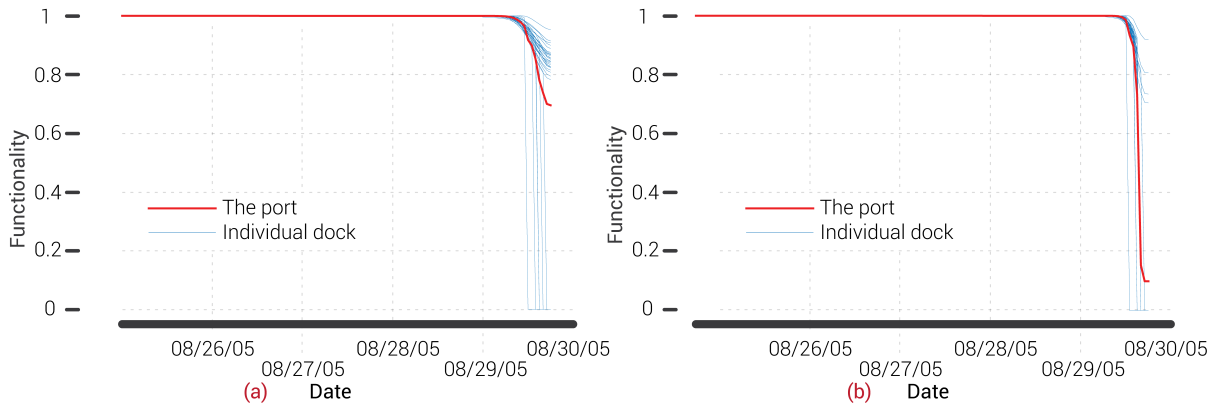

Figure 5-11: Estimated functionality of the port for scenario a) S_{KN2005} and b) S_{KS2005}.

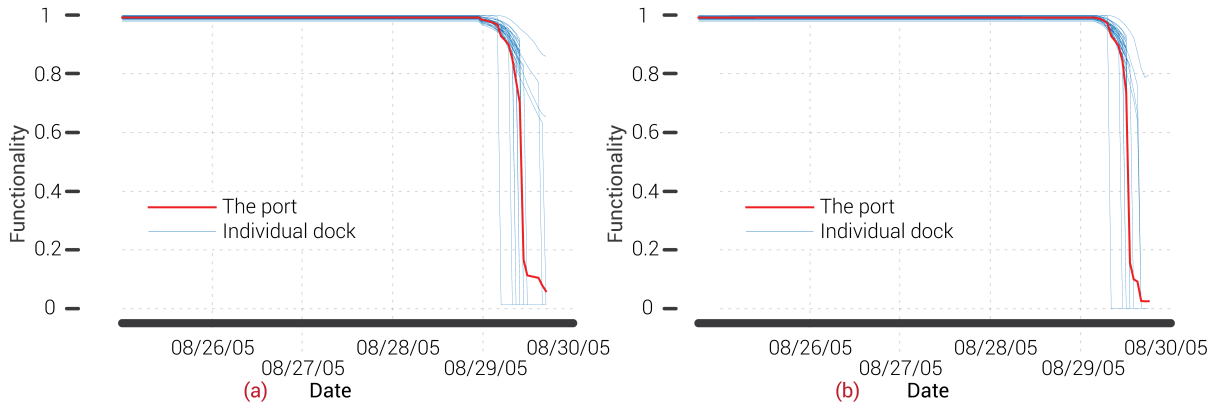

Figure 5-12: Estimated functionality of the port for scenario a) $S_{KN2100\text{-}4.5}$ and b) $S_{KS2100\text{-}4.5}$.

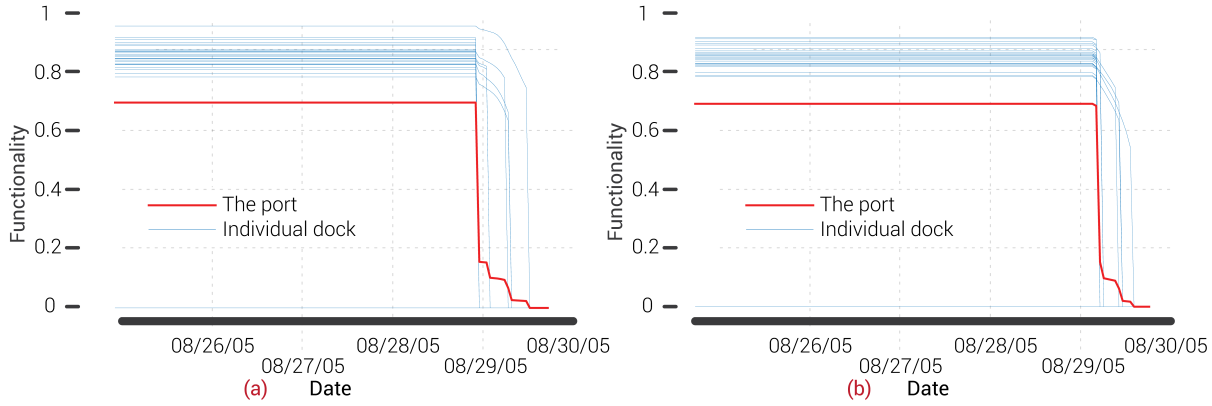

Figure 5-13: Estimated functionality of the port for scenario a) $S_{KN2100\text{-}8.5}$ and b) $S_{KS2100\text{-}8.5}$.

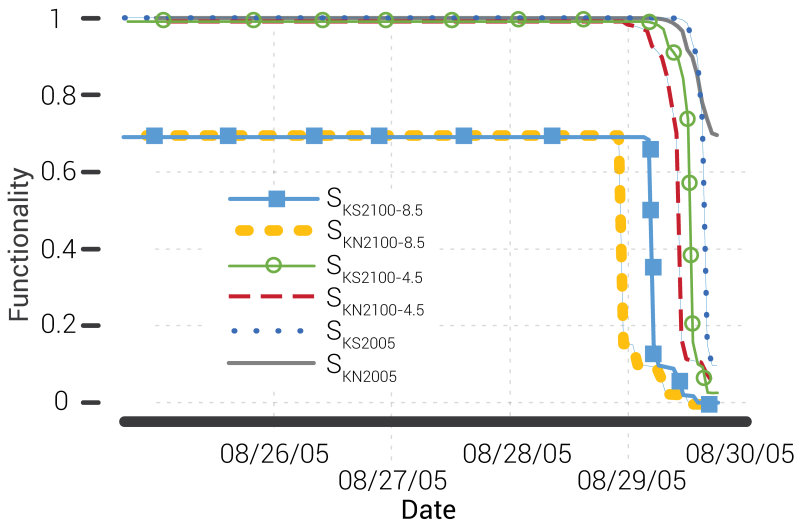

Figure 5-14: Estimated functionality of the port for all scenarios.

SLR, alone, for both tracks, does not affect the operation of the port with RCP 4.5, and it drops the functionality to 75% with RCP 8.5, as shown in Figure 5-14. By coupling future SLR scenarios of RCP 4.5 with the hurricane, the drop in functionality of the port is decreased by 65% for the natural track scenario and by around 10% for the shifted track. While, SLR with RCP 8.5, when coupled with the hurricane, drops the functionality to 0% for both tracks, as shown in Figure 5-13.

5.5. Recovery of the port functionality

We now consider the recovery of the port when subjected to two of the scenarios considered previously: natural (S_{KN2005}) and shifted Katrina (S_{KS2005}). In this approach, we didn't consider the recovery time for each component and the availability of repair crews. Instead, we used a random recovery trajectory. In other words, we assumed that the recovery for each of the basic events (R1 to R21) is a one-directional recovery randomly selected from 1000 generated samples that start from the initial drop of each R up to

value one. We used this procedure to find how many trials (time steps) each scenario needs to recover back to full recovery (i.e. a value one). The number of trials will indicate the recovery time for each scenario. Based on previous recovery (Grenzeback and Lukmann, 2007), time step (T) can vary from one week up to one year, depending on the available funds and repair crew members. The following equations summarize the methods used to calculate the recovery in this study:

$$R_i(T_{jk}) = \text{rand}\,(R_i(T_0), 1) \;\; \forall \;\; \text{Sample size} = 1000 \tag{5-1}$$

$$R_i(T_j{+}1) = R_i(T_{jk}) \;\; \forall \;\; R_i(T_j) < R_i(T_{jk}) \leq 1 \tag{5-2}$$

$$F_P(T_j) = \left(\frac{1}{n}\right) \sum_{i=1}^{n} \left(F_{dock}(T_j)\right) \tag{5-3}$$

$$F_{dock}(T_j)_{AND} = \prod_{i=1}^{n} R_i(T_j) \tag{5-4}$$

$$F_{dock}(T_j)_{OR} = 1 - \prod_{i=1}^{n} (1 - R_i(T_j)) \tag{5-5}$$

where, T, i, and j are the time step, the number of basic event (1 to 21), and number of trials (1 to inf.), respectively. K is the number of iteration (100), and n is the number of docks (41). Functionality of each dock and of the port are represented by F_{dock} and F_P. $R_i(T_0)$ is the initial drop of the basic event (R_i).

Table 5-4 summarize number of time step required for each scenario to recover along with the recovered values of each of the basic events corresponding to each time step. Figure 5-15 show the recovery timeline for each dock along with the mean of the docks to represent the recovery of the port. From Figure 5-15, shifted Katrina required triple the time for the natural Katrina to recover back to full functionality.

Table 5-4: Recovery time of the port for natural and shifted Katrina scenarios.

Basic event	Max drop In the mean functionality		Recovery timeline							
			S_{KN2005}		S_{KS2005}					
			T1	T2	T1	T2	T3	T4	T5	T6
	S_{KN2005}	S_{KS2005}								
R1	0.81	0.125	0.85	1	0.67	0.88	0.96	0.97	0.99	1
R2	0.93	0.62	0.98	1	0.84	0.93	0.97	0.99	0.99	1
R3	0.93	0.62	0.96	1	0.86	0.93	0.96	0.97	0.98	1
R4	0.85	0.78	0.94	1	0.91	0.95	0.97	0.98	0.99	1
R5	0.85	0.78	0.9	1	0.83	0.87	0.91	0.96	0.97	1
R6	0.97	0.84	0.99	1	0.958	0.984	0.995	0.998	0.99	1
R7	0.95	0.80	0.96	1	0.81	0.85	0.88	0.9	0.92	1
R8	0.97	0.84	0.98	1	0.944	0.989	0.99	1	1	1
R9	0.93	0.62	0.97	1	0.88	0.96	0.99	0.99	0.99	1
R10	0.96	0.77	0.97	1	0.93	0.98	0.99	0.99	0.99	1
R11	0.93	0.597	0.94	1	0.9	0.97	0.99	0.99	1	1
R12	0.84	0.125	0.85	1	0.70	0.83	0.95	0.98	0.99	1
R13	0.98	0.921	0.99	1	0.97	0.98	0.99	0.99	0.99	1
R14	0.92	0.72	0.97	1	0.92	0.97	0.99	0.99	1	1
R15	0.94	0.74	0.97	1	0.76	0.82	0.87	0.89	0.9	1
R16	0.91	0.71	0.97	1	0.93	0.97	0.98	0.99	0.99	1
R17	0.93	0.73	0.97	1	0.92	0.97	0.98	0.99	0.99	1
R18	0.95	0.75	0.97	1	0.88	0.93	0.97	0.99	0.99	1
R19	0.97	0.77	0.97	1	0.95	0.96	0.98	0.98	0.99	1
R20	0.90	0.70	0.98	1	0.84	0.88	0.93	0.96	0.99	1
R21	0.92	0.72	0.94	1	0.78	0.8	0.83	0.89	0.91	1

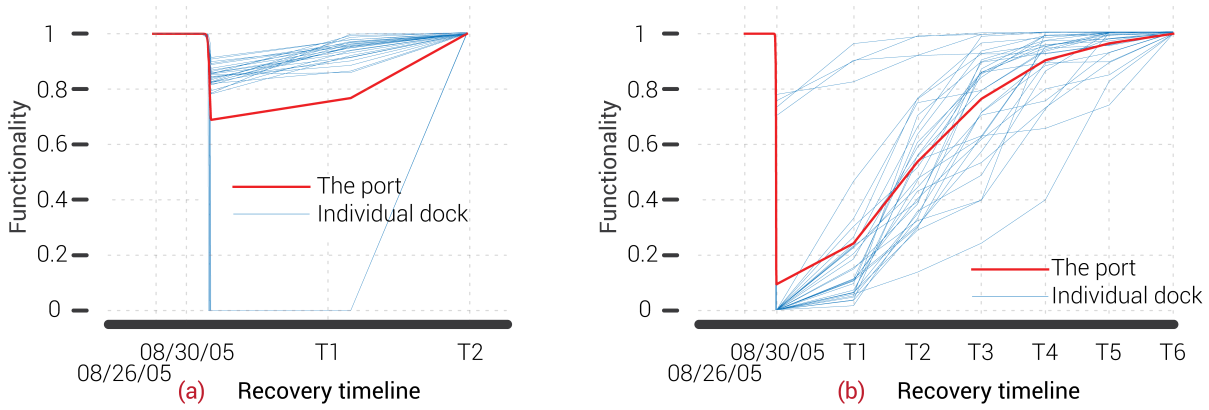

Figure 5-15: The recovery timeline of the port for (a) S_{KN2005} and (b) S_{KS2005}

CHAPTER 6. CONCLUSION AND FUTURE WORK

Increases in SLR during the remainder of the 21st Century is inexorable under present plausible scenarios of global climate change, and the associated impacts on coastal communities, such as coastal flooding and more severe hurricane or storm surge events should be anticipated and planned for in the future. SLR takes place slowly over time and communities have adequate time for preparation through adaptation. On the other hand, mitigation plans should be aimed at withstanding the intensity of future natural hazard events associated with SLR, such as storm surge and coastal inundation through embracing the concept of resilience.

6.1. Summary

In this study, a new method has been developed for quantifying the operation of seaports subject to SLR and tropical cyclones (hurricanes) to determine their functionality appropriately without solving complicated equations describing physical processes. Three main steps were taken in order to build the model. The first step was the setting up of a hydrodynamic model for forecasting storm surge in the presence of SLR under tropical cyclones and to validate this model using the historical measurements of the water levels on the Gulf Coast of the U.S. during past hurricanes. The second step was the development of a novel model of port operations and functionality, in the form of a fault tree that included the major components of port infrastructure, and their interdependencies, and could be used as a basis of quantitative analysis of port functionality during and following a severe natural hazard event. The third, and final, step was the identification of a set of plausible future SLR and storm

scenarios that in which hydrodynamic modeling in the Mobile Bay area had to be performed to get the storm surge values for each case. Once built, the three fundamental ingredients of this model were used to assess the functionality of the Port of Mobile, AL under several plausible hurricane and SLR scenarios, occurring in the presence of a changing climate.

The hydrodynamic model, Delft3D, was used to simulate the storm surge induced by hurricanes in the vicinity of Mobile Bay, AL. Three different resolutions structured mesh of 10 km, 2 km, and 0.38 km were used to cover the Gulf of Mexico, the northern part of the Gulf, and the Mobile Bay. A 90 m resolution bathymetry and topography were used in this study. Depending on the land cover on which the manning coefficient classification was chosen, varying hydraulic roughness was implemented. The Delft3D simulation was validated using water levels recorded at NOAA stations (Dauphin Island and Pensacola, FL) during Hurricane Katrina in 2005. The results of the validation show a simulation skill score of 0.91 and 0.88 at Dauphin and Pensacola stations. The simulation also captures the peak of storm surge at Mobile downtown, which is close to our study area.

Simulations subsequently were conducted for other scenarios involving Katrina-like hurricanes coupled with storm surge effects intensified by SLR under climate projections based on RCP 4.5 (moderate) and RCP 8.5 (severe) warming over the remainder of the 21st century. An overview of how the vulnerability of the Port of Mobile might be measured in the sense of physical damage under various hurricane and global warming scenarios was presented. The recovery from a post-disaster damages after a

hurricane depends on several socio-economic variables beyond the reach of this initial analysis.

6.2. Major Findings

Our analysis of various hurricanes and climate change scenarios on the performance of coastal industrial community has demonstrated that decision-making at the port authority level is essential. The findings in the following paragraphs can help the decision-makers to decrease hurricanes' threat and adjust to climate change by establishing reasonable infrastructure mitigations for existing terminals and by considering future SLR for designing new ones.

Model results show that, with SLR of RCP 4.5 and RCP 8.5, there would be an increase of 54% and 100% of the inundated area, respectively, if Katrina landed with its historical path and intensity. For the shifted track, the increase of inundated area would be 29% and 65%. In addition to the region getting submerged, we also observed that the amount of storm surges would rise if the natural and shifted tracks of Katrina were to exist under the projected future SLR scenarios.

Damage assessment of the port shows that historical Hurricane Katrina with SLR of RCP 4.5 and RCP 8.5 increases the damage cost of the port 5.5 times and 6.5 times. With the shifted Katrina track the damage cost is doubled and more than doubled with SLR of RCP 4.5 and RCP 8.5. The findings from FTA reveal that the port capability to operate is decreased by 50% if the Katrina track is moved closer to the terminals. SLR with RCP 8.5, alone, causes the functionality of the Theodore terminals and the APM terminal to drop by 100%. SLR alone does not affect the port activity with RCP 4.5, while SLR decreases it with RCP 8.5 by 25% for both tracks. The reduction in port

performance in the presence of RCP 4.5 (SLR) scenario with Katrina falls by 65% for the natural track and by about 10% for the shifted one. SLR with RCP 8.5 reduces the performance to 0 percent on both tracks when paired with the hurricane. Shifted Katrina took the normal Katrina triple time to get back to full functionality.

6.3. Recommendations and future work

Further work is suggested in the following areas on the basis of the main findings and the limitations of the current analysis:

- The damages to some port equipment are very sensitive to storm surge water elevation, requiring an accurate estimate of water depth. Evaluating the damages to employees' residential homes and roadways around the port depends on the inundation extent by the storm surge. For the hydrodynamic model, higher bathymetry and topography resolution data (i.e., at least 10 meters) will be necessary for a better simulation of overland inundation. Accordingly, a higher mesh resolution would be needed to capture the detailed resolution data, and maybe using unstructured mesh would be better in this case. However, higher resolution will also result in more computational time.
- The wind field (velocity and pressure deficit) are the major factors determining storm surge. Alternative methods for modeling the hurricane wind profile are required to determine the sensitivity of storm surge to this effect. One limitation of the current approach is that it does not take into account the dissipation of energy that occurs as the hurricane makes land fall.

- More detailed fragilities to estimate the component and subcomponent damages of the port due to storm surge, wave and wind action are required to augment the depth-damage relations used in this study. For better damage assessment of the port, an accurate geodata for the port facilities is required to estimate each dock's elevation.
- A detailed analysis for estimating the post-disaster recovery of port components and systems is needed in place of the random trajectories assumed to illustrate the analysis in Chapter 5 and to mitigate future SLR with hurricane events.

REFERENCES

AAPA (2018). National Economic Impact of the U.S. Coastal Port System: Executive Summary. Available at: https://www.aapa-ports.org/advocating/PRDetail.aspx?ItemNumber=22306 [Accessed September 16, 2019].

Adhikari, P., Abdelhafez, M., Dong, Y., Guo, Y., Mahmoud, H. N., and Ellingwood, B. R. (2020). ACHIEVING RESIDENTIAL COASTAL COMMUNITIES RESILIENT TO TROPICAL CYCLONES AND CLIMATE CHANGE. Spec. issue Front. Worsening Trop. Cyclone Impact Cities.

APM (2020). APM Mobile Terminal. Available at: https://www.apmterminals.com/en/mobile/about/our-terminal [Accessed June 20, 2020].

Asdd (2020). The Alabama State Port Authority. Available at: http://www.asdd.com [Accessed June 20, 2020].

Balbi, A., Repetto, M. P., Kammouh, O., and Cimellaro, G. P. (2018). Resilience framework for seaport infrastructure: Theory and application. in Maintenance, Safety, Risk, Management and Life-Cycle Performance of Bridges - Proceedings of the 9th International Conference on Bridge Maintenance, Safety and Management, IABMAS 2018.

Bates, P. D., and De Roo, A. P. J. (2000). A simple raster-based model for flood inundation simulation. J. Hydrol. doi:10.1016/S0022-1694(00)00278-X.

Becker, A., and Caldwell, M. R. (2015). Stakeholder Perceptions of Seaport Resilience Strategies: A Case Study of Gulfport (Mississippi) and Providence (Rhode Island). Coast. Manag. doi:10.1080/08920753.2014.983422.

Becker, A. H., Acciaro, M., Asariotis, R., Cabrera, E., Cretegny, L., Crist, P., et al. (2013). A note on climate change adaptation for seaports: A challenge for global ports, a challenge for global society. Clim. Change 120, 683–695. doi:10.1007/s10584-013-0843-z.

Becker, A., Inoue, S., Fischer, M., and Schwegler, B. (2012). Climate change impacts on international seaports: Knowledge, perceptions, and planning efforts among port administrators. Clim. Change. doi:10.1007/s10584-011-0043-7.

Bhattachan, A., Jurjonas, M. D., Moody, A. C., Morris, P. R., Sanchez, G. M., Smart, L. S., et al. (2018). Sea level rise impacts on rural coastal social-ecological systems and the implications for decision making. Environ. Sci. Policy.

doi:10.1016/j.envsci.2018.10.006.

Bichou, K. (2018). “Introduction to Port Systems,” in Encyclopedia of Maritime and Offshore Engineering doi:10.1002/9781118476406.emoe192.

Bichou, K., and Gray, R. (2005). A critical review of conventional terminology for classifying seaports. Transp. Res. Part A Policy Pract. doi:10.1016/j.tra.2004.11.003.

Bilskie, M. V., Hagen, S. C., Alizad, K., Medeiros, S. C., Passeri, D. L., Needham, H. F., et al. (2016). Dynamic simulation and numerical analysis of hurricane storm surge under sea level rise with geomorphologic changes along the northern Gulf of Mexico. Earth’s Futur. doi:10.1002/2015EF000347.

Blain, C. A., Linzell, R. S., Chu, P., and Massey, C. (2010). Validation Test Report for the ADvanced CIRCulation. Security.

Blake, E. S., Kimberlain, T. B., Berg, R. J., Cangialosi, J. P., and Beven, J. L. (2013). Tropical Cyclone Report Hurricane Sandy. J. Chem. Inf. Model. doi:10.1017/CBO9781107415324.004.

Bloetscher, F., Polsky, C., Bolter, K., Mitsova, D., Garces, K. P., King, R., et al. (2016). Assessing potential impacts of sea level rise on public health and vulnerable populations in Southeast Florida and providing a framework to improve outcomes. Sustain. doi:10.3390/su8040315.

Booij, N., Ris, R. C., and Holthuijsen, L. H. (1999). A third-generation wave model for coastal regions 1. Model description and validation. J. Geophys. Res. Ocean. doi:10.1029/98JC02622.

Bruneau, M., Chang, S. E., Eguchi, R. T., Lee, G. C., O’Rourke, T. D., Reinhorn, A. M., et al. (2003). A Framework to Quantitatively Assess and Enhance the Seismic Resilience of Communities. Earthq. Spectra. doi:10.1193/1.1623497.

Burcharth, H. F., Lykke Andersen, T., and Lara, J. L. (2014). Upgrade of coastal defence structures against increased loadings caused by climate change: A first methodological approach. Coast. Eng. doi:10.1016/j.coastaleng.2013.12.006.

Burden, L. I., Rix, G., and Werner, S. (2016). Development of a risk framework for forecasting earthquake losses in port systems. Earthq. Spectra. doi:10.1193/043013EQS117M.

Caldwell, R. L., and Edmonds, D. A. (2014). Delft3D-Flow: Simulation of Multi-Dimensional Hydrodynaminc Flows and Transport Phenomena, Including Sediments-User Manual. J. Geophys. Res. Earth Surf. doi:10.1002/2013JF002965.

Cao, X., and Lam, J. S. L. (2018). Simulation-based catastrophe-induced port loss

estimation. Reliab. Eng. Syst. Saf. doi:10.1016/j.ress.2018.02.008.

Cazenave, A., and Cozannet, G. Le (2014). Sea level rise and its coastal impacts. Earth's Futur. doi:10.1002/2013ef000188.

CEIC (2016). Weekly Container Throughput (2010-2016). Available at: CEIC Database [Accessed July 20, 2020].

Chhetri, P., Corcoran, J., Gekara, V., Maddox, C., and McEvoy, D. (2015). Seaport resilience to climate change: mapping vulnerability to sea-level rise. J. Spat. Sci. doi:10.1080/14498596.2014.943311.

Chi, C. F., Lin, S. Z., and Dewi, R. S. (2014). Graphical fault tree analysis for fatal falls in the construction industry. Accid. Anal. Prev. doi:10.1016/j.aap.2014.07.019.

Choate, A., Evans, C., Rodehorst, B., Saavedra, R., Snow, C., and Snyder, J. (2014). Impacts of climate change and variability on transportation systems and infrastructure: The Gulf Coast study, phase 2. US Department of Transportation. Report No. FHWA-HEP-14-033. Available at: https://www.fhwa.dot.gov/environment/sustainability/resilience/ongoing_and_current_research/gulf_coast_study/phase2_task3/task_3.1/phase2task3.pdf [Accessed April 17, 2020].

Church, J. A., Clark, P. U., Cazenave, A., Gregory, J. M., Jevrejeva, S., Levermann, A., et al. (2013). Sea level change. Clim. Chang. 2013 Phys. Sci. Basis. Contrib. Work. Gr. I to Fifth Assess. Rep. Intergov. Panel Clim. Chang. doi:10.1017/CB09781107415315.026.

Clough, J., Polaczyk, A., and Propato, M. (2016). Modeling the potential effects of sea-level rise on the coast of New York: Integrating mechanistic accretion and stochastic uncertainty. Environ. Model. Softw. 84, 349–362. doi:10.1016/j.envsoft.2016.06.023.

Coudert, O., and Madre, J. C. (1994). MetaPrime: An Interactive Fault-Tree Analyzer. IEEE Trans. Reliab. doi:10.1109/24.285125.

DeConto, R. M., and Pollard, D. (2016). Contribution of Antarctica to past and future sea-level rise. Nature. doi:10.1038/nature17145.

Deltares (2020). Delft3d FM. Available at: https://oss.deltares.nl/web/delft3dfm [Accessed May 10, 2020].

Department of Homeland Security (2013). Presidential Policy Directive - Critical Infrastructure Security and Resilience, PPD-21. White House, Washington, DC.

Doytchev, D. E., and Szwillus, G. (2009). Combining task analysis and fault tree analysis for accident and incident analysis: A case study from Bulgaria. Accid. Anal. Prev.

doi:10.1016/j.aap.2008.07.014.

Egbert, G. D., Bennett, A. F., and Foreman, M. G. G. (1994). TOPEX/POSEIDON tides estimated using a global inverse model. J. Geophys. Res. doi:10.1029/94jc01894.

Egbert, G. D., and Erofeeva, S. Y. (2002). Efficient inverse modeling of barotropic ocean tides. J. Atmos. Ocean. Technol. doi:10.1175/1520-0426(2002)019<0183:EIMOBO>2.0.CO;2.

Emanuel, K. A. (2013). Downscaling CMIP5 climate models shows increased tropical cyclone activity over the 21st century. Proc. Natl. Acad. Sci. U. S. A. doi:10.1073/pnas.1301293110.

Emery, W. J., and Thomson, R. E. (1997). Data analysis methods in physical oceanography. doi:10.2307/1353059.

Esteban, M., Thao, N. D., Takagi, H., and Shibayama, T. (2012). "Increase in Port Downtime and Damage in Vietnam Due To a Potential Increase in Tropical Cyclone Intensity," in Climate Change Management doi:10.1007/978-3-642-22266-5_7.

FEMA (2006). High Water Mark Collection for Hurricane Katrina in Alabama. FEMA-1605-DR-AL, Task Orders 414 and 421.

FEMA (2008). Hurricane Ike Impact Report. Available at: https://www.fema.gov/pdf/hazard/hurricane/2008/ike/impact_report.pdf [Accessed September 20, 2019].

Fretwell, P., Pritchard, H. D., Vaughan, D. G., Bamber, J. L., Barrand, N. E., Bell, R., et al. (2013). Bedmap2: Improved ice bed, surface and thickness datasets for Antarctica. Cryosphere. doi:10.5194/tc-7-375-2013.

Gattuso, J. P., Magnan, A., Billé, R., Cheung, W. W. L., Howes, E. L., Joos, F., et al. (2015). Contrasting futures for ocean and society from different anthropogenic CO 2 emissions scenarios. Science (80-.). doi:10.1126/science.aac4722.

GEBCO (2010). (General Bathymetric Chart of the Ocean), Gridded bathymetry data. Available at: https://www.gebco.net/.

Golnaraghi, M., Etienne, C., Sapir, D. G., and Below, R. (2014). Atlas of Mortality and Economic Losses from Weather, Climate and Water Extremes (1970–2012), WMO-No. 1123. Geneva, Switzerland.

Google (2020). Google earth pro. ver.7.3.3.7699. Available at: https://www.google.com/earth/ [Accessed July 1, 2020].

Graham, S., and Riebeek, H. (2006). Hurricanes: The Greatest Storms on Earth. https://earthobservatory.nasa.gov/Features/Hurricanes/.

doi:10.1017/CBO9781107415324.004.

Grenzeback, L. R., and Lukmann, A. T. (2007). Case Study of the Transportation Sector ' s Response to and Recovery from Hurricanes Katrina and Rita. Heal. (San Fr.

Guha-Sapir, D., Vos, F., and Below, R. (2014). EM-DAT: International Disaster Database of Disasters.

Hall, J. A., Gille, S., Obeysekera, J., Sweet, W., Knuuti, K., and Marburger, J. (2016). Regional Sea Level Scenarios for Coastal Risk Management: Managing the Uncertainty of Future Sea Level Change and Extreme Water Levels for Department of Defense Coastal Sites Worldwide. 224pp.

Hanson, S., Nicholls, R., Ranger, N., Hallegatte, S., Corfee-Morlot, J., Herweijer, C., et al. (2011). A global ranking of port cities with high exposure to climate extremes. Clim. Change 104, 89–111. doi:10.1007/s10584-010-9977-4.

Harris, G. A., Holden, A. R., Schroer, B. J., and Moeller, D. P. F. (2008). A simulation approach to evaluating productivity improvement at a seaport coal terminal. Transp. Res. Rec. doi:10.3141/2062-03.

Hassan, E. M., and Mahmoud, H. (2019). Full functionality and recovery assessment framework for a hospital subjected to a scenario earthquake event. Eng. Struct. doi:10.1016/j.engstruct.2019.03.008.

Hauer, M. E. (2017). Migration induced by sea-level rise could reshape the US population landscape. Nat. Clim. Chang. doi:10.1038/nclimate3271.

Hauer, M. E., Evans, J. M., and Mishra, D. R. (2016). Millions projected to be at risk from sea-level rise in the continental United States. Nat. Clim. Chang. doi:10.1038/nclimate2961.

HAZUS (2020). Multi-hazard Loss Estimation Methodology, Flood Model, Hazus –MH 2.1 Technical Manual. Dept. of Homeland Security, FEMA Mitigation Divison. Washington, D.C.

Heberger, M., Cooley, H., Moore, E., and Herrera, P. (2012). The impacts of sea level rise on the San Francisco Bay. 1–32.

Heming, J. T., Chan, J. C. L., and Radford, A. M. (1995). A new scheme for the initialisation of tropical cyclones in the UK Meteorological Office global model. Meteorol. Appl. doi:10.1002/met.5060020211.

Holland, G. (2008). A revised hurricane pressure-wind model. Mon. Weather Rev. doi:10.1175/2008MWR2395.1.

Holland, G. J. (1980). An analytic model of the wind and pressure profiles in hurricanes.

Mon. Weather Rev. doi:10.1175/1520-0493(1980)108<1212:AAMOTW>2.0.CO;2.

Horton, R., Little, C., Gornitz, V., Bader, D., and Oppenheimer, M. (2015). New York City Panel on Climate Change 2015 Report Chapter 2: Sea Level Rise and Coastal Storms. Ann. N. Y. Acad. Sci. doi:10.1111/nyas.12593.

IPCC (2007). Climate Change 2007 Synthesis Report. doi:10.1256/004316502320517344.

IPCC (2014). Climate Change 2014: Synthesis Report. Contribution of Working Groups I, II and III to the Fifth Assessment Report of the Intergovernmental Panel on Climate Change . IPCC, Geneva, Switzerland, 151 pp. In IPCC AR5 Synthesis Report website. Available at: https://www.ipcc.ch/report/ar5/syr/.

Irish, J. L., Resio, D. T., and Ratcliff, J. J. (2008). The influence of storm size on hurricane surge. J. Phys. Oceanogr. doi:10.1175/2008JPO3727.1.

Isobe, M. (2013). Impact of global warming on coastal structures in shallow water. Ocean Eng. doi:10.1016/j.oceaneng.2012.12.032.

J. Paul Guyer, P. E. R. A. (2018). An Introduction to Planning for Piers and Wharves. Guyer Partners Available at: https://books.google.com/books?id=bmVLDwAAQBAJ.

Kane, H. H., Fletcher, C. H., Frazer, L. N., and Barbee, M. M. (2015). Critical elevation levels for flooding due to sea-level rise in Hawai‘i. Reg. Environ. Chang. doi:10.1007/s10113-014-0725-6.

Knabb, R. D., Rhome, J. R., and Brown, D. P. (2006). Tropical Cyclone Report: Hurricane Katrina. Natl. Hurric. Cent. doi:10.1017/CBO9781107415324.004.

Koliou, M., van de Lindt, J. W., McAllister, T. P., Ellingwood, B. R., Dillard, M., and Cutler, H. (2018). State of the research in community resilience: progress and challenges. Sustain. Resilient Infrastruct. doi:10.1080/23789689.2017.1418547.

Kopp, R. E., Hay, C. C., Little, C. M., and Mitrovica, J. X. (2015). Geographic Variability of Sea-Level Change. Curr. Clim. Chang. Reports 1, 192–204. doi:10.1007/s40641-015-0015-5.

Kopp, R. E., Horton, R. M., Little, C. M., Mitrovica, J. X., Oppenheimer, M., Rasmussen, D. J., et al. (2014). Probabilistic 21st and 22nd century sea-level projections at a global network of tide-gauge sites. Earth’s Futur. doi:10.1002/2014ef000239.

Le Bars, D., Drijfhout, S., and De Vries, H. (2017). A high-end sea level rise probabilistic projection including rapid Antarctic ice sheet mass loss. Environ. Res. Lett. doi:10.1088/1748-9326/aa6512.

Le Cozannet, G., Rohmer, J., Cazenave, A., Idier, D., van de Wal, R., de Winter, R., et al. (2015). Evaluating uncertainties of future marine flooding occurrence as sea-level rises. Environ. Model. Softw. doi:10.1016/j.envsoft.2015.07.021.

Lesser, G. R., Roelvink, J. A., van Kester, J. A. T. M., and Stelling, G. S. (2004). Development and validation of a three-dimensional morphological model. Coast. Eng. doi:10.1016/j.coastaleng.2004.07.014.

Leuliette, E., and Nerem, S. (2016). Contributions of Greenland and Antarctica to Global and Regional Sea Level Change. Oceanography 29, 154–159. doi:10.5670/oceanog.2016.107.

Levine, J. N., Esnard, A. M., and Sapat, A. (2007). Population displacement and housing dilemmas due to catastrophic disasters. J. Plan. Lit. doi:10.1177/0885412207302277.

Lin, N., Kopp, R. E., Horton, B. P., and Donnelly, J. P. (2016a). Hurricane Sandy's flood frequency increasing from year 1800 to 2100. Proc. Natl. Acad. Sci. doi:10.1073/pnas.1604386113.

Lin, P., Wang, N., and Ellingwood, B. R. (2016b). A risk de-aggregation framework that relates community resilience goals to building performance objectivess. Sustain. Resilient Infrastruct. doi:10.1080/23789689.2016.1178559.

Lindhe, A., Norberg, T., and Rosén, L. (2012). Approximate dynamic fault tree calculations for modelling water supply risks. Reliab. Eng. Syst. Saf. doi:10.1016/j.ress.2012.05.003.

Liu, P., Yang, L., Gao, Z., Li, S., and Gao, Y. (2015). Fault tree analysis combined with quantitative analysis for high-speed railway accidents. Saf. Sci. doi:10.1016/j.ssci.2015.06.017.

Luettich, R. A., Jr., J. J. W., and Scheffner, N. W. (1992). ADCIRC: an advanced three-dimensional circulation model for shelves coasts and estuaries, report 1: theory and methodology of ADCIRC-2DDI and ADCIRC-3DL. Dredg. Res. Progr. Tech. Rep. DRP-92-6, U.S. Army Eng. Waterw. Exp. Station. Vicksburg, MS, 137p.

Luettich, R., and Westerink, J. (2015). ADCIRC: A (parallel) ADvanced CIRCulation model for oceanic, coastal and estuarine waters.

Mattocks, C., and Forbes, C. (2008). A real-time, event-triggered storm surge forecasting system for the state of North Carolina. Ocean Model. doi:10.1016/j.ocemod.2008.06.008.

McInnes, K. L., Hubbert, G. D., Abbs, D. J., and Oliver, S. E. (2002). A numerical modelling study of coastal flooding. Meteorol. Atmos. Phys. doi:10.1007/s007030200027.

Miller, K. G., Kopp, R. E., Horton, B. P., Browning, J. V., and Kemp, A. C. (2013). A geological perspective on sea-level rise and its impacts along the U.S. mid-Atlantic coast. Earth's Futur. doi:10.1002/2013ef000135.

Morris, L. L., and Sempier, T. (2019). "The Ports Resilience Index," in Risk Communication and Community Resilience (Routledge), 179–197. doi:10.4324/9781315110042-14.

Moss, R. H., Edmonds, J. A., Hibbard, K. A., Manning, M. R., Rose, S. K., van Vuuren, D. P., et al. (2010). The next generation of scenarios for climate change research and assessment. Nature 463, 747–756. doi:10.1038/nature08823.

Na, U. J., and Shinozuka, M. (2009). Simulation-based seismic loss estimation of seaport transportation system. Reliab. Eng. Syst. Saf. doi:10.1016/j.ress.2008.07.005.

Nakicenovic, N., and N., and Swart, R. (2000). IPCC. 2000. Special Report: Emissions Scenarios. Cambridge, UK Cambridge Univ. Press.

National Research Council (2012). Disaster Resilience: A National Imperative. Washington, D.C.: National Academies Press doi:10.17226/13457.

Neumann, B., Vafeidis, A. T., Zimmermann, J., and Nicholls, R. J. (2015). Future coastal population growth and exposure to sea-level rise and coastal flooding - A global assessment. PLoS One. doi:10.1371/journal.pone.0118571.

Ng, A., Becker, A., Cahoon, S., Chen, S. L., Earl, P., and Yang, Z. (2016). Climate Change and Adaptation Planning for Ports. London: Routledge doi:https://doi.org/10.4324/9781315756813.

NHC (2020). Storm Surge Overview. Available at: https://www.nhc.noaa.gov/surge/ [Accessed April 10, 2020].

NOAA. (2001). National Geophysical Data Center. U.S. Coastal Relief Model - Central Gulf of Mexico. doi:doi:10.7289/V54Q7RW0.

NOAA (2012). National Hurricane Center. Hurricanes in History. Available at: http://www.nhc.noaa.gov/outreach/history/ [Accessed September 20, 2019].

NOAA (2013). National coastal population report: Population trends from 1970 to 2020. NOAA State Coast Rep. Ser. Available at: https://coast.noaa.gov/digitalcoast/training/populationreport.html [Accessed April 10, 2020].

NOAA (2014). National Hurricane Center's (NHC). Available at: http://www.aoml.noaa.gov/hrd/ hurdat/Data_Storm.html.

NOAA (2018a). National Centers for Environmental Information (NCEI) Costliest U.S.

Tropical Cyclones Tables Updated. National Hurricane Center. Available at: https://www.nhc.noaa.gov/news/UpdatedCostliest.pdf [Accessed September 20, 2019].

NOAA (2018b). What is high tide flooding? National Ocean Service website.

NOAA (2019a). FIND YOUR LOCAL TIDES AND CURRENTS. Available at: https://www.co-ops.nos.noaa.gov/map/index.html [Accessed August 5, 2019].

NOAA (2019b). Historical Hurricane Tracks. Natl. Ocean. Atmos. Adm. US Dep. Commer. doi:10.1002/eco.

NOAA (2019c). Trends in Atmospheric Carbon Dioxide. Available at: https://www.esrl.noaa.gov/gmd/ccgg/trends/monthly.html [Accessed September 12, 2019].

NOAA (2020). Tides & Currents. Available at: http://tidesandcurrents.noaa.gov/ [Accessed April 17, 2020].

Nozhati, S., Ellingwood, B. R., and Mahmoud, H. (2019). Understanding Community Resilience from a PRA Perspective Using Binary Decision Diagrams. Risk Anal. doi:10.1111/risa.13321.

Parris, A., Bromirski, P., Burkett, V., Cayan, D., Culver, M., Hall, J., et al. (2012). Global Sea Level Rise Scenarios for the US National Climate Assessment. NOAA Tech Memo OAR CPO.

PEER (2006). Joint Legislative Committee on Performance Evaluation and Expenditure Review. The impact of hurricane Katrina on Mississippi's commercial public ports and opportunities for expansion of the ports. Available at: https://www.peer.ms.gov/ [Accessed October 10, 2019].

Peltier, W. R. (2004). GLOBAL GLACIAL ISOSTASY AND THE SURFACE OF THE ICE-AGE EARTH: The ICE-5G (VM2) Model and GRACE. Annu. Rev. Earth Planet. Sci. doi:10.1146/annurev.earth.32.082503.144359.

Perrette, M., Landerer, F., Riva, R., Frieler, K., and Meinshausen, M. (2013). A scaling approach to project regional sea level rise and its uncertainties. Earth Syst. Dyn. doi:10.5194/esd-4-11-2013.

Phadke, A. C., Martino, C. D., Cheung, K. F., and Houston, S. H. (2003). Modeling of tropical cyclone winds and waves for emergency management. Ocean Eng. doi:10.1016/S0029-8018(02)00033-1.

Plant, N. G., Holland, K. T., Puleo, J. A., and Gallagher, E. L. (2004). Prediction skill of nearshore profile evolution models. J. Geophys. Res. C Ocean. doi:10.1029/2003jc001995.

Rajabalinejad, M., and Demirbilek, Z. (2013). A Bayesian probabilistic approach for impacts of sea level rise on coastal engineering design practice. Ocean Eng. 71, 66–73. doi:10.1016/j.oceaneng.2013.05.001.

Rappaport, E. N. (2014). Fatalities in the united states from atlantic tropical cyclones: New data and interpretation. Bull. Am. Meteorol. Soc. doi:10.1175/BAMS-D-12-00074.1.

Rego, J. L., and Li, C. (2009). On the importance of the forward speed of hurricanes in storm surge forecasting: A numerical study. Geophys. Res. Lett. doi:10.1029/2008GL036953.

Revell, D. L., Battalio, R., Spear, B., Ruggiero, P., and Vandever, J. (2011). A methodology for predicting future coastal hazards due to sea-level rise on the California Coast. Clim. Change. doi:10.1007/s10584-011-0315-2.

Sánchez-Arcilla, A., Sierra, J. P., Brown, S., Casas-Prat, M., Nicholls, R. J., Lionello, P., et al. (2016). A review of potential physical impacts on harbours in the Mediterranean Sea under climate change. Reg. Environ. Chang. doi:10.1007/s10113-016-0972-9.

Santella, N., Steinberg, L. J., and Sengul, H. (2010). Petroleum and hazardous material releases from industrial facilities associated with hurricane katrina. Risk Anal. doi:10.1111/j.1539-6924.2010.01390.x.

Scawthorn, C., Flores, P., Blais, N., Seligson, H., Tate, E., Chang, S., et al. (2006). HAZUS-MH flood loss estimation methodology. II. Damage and loss assessment. Nat. Hazards Rev. doi:10.1061/(ASCE)1527-6988(2006)7:2(72).

Shafieezadeh, A., and Ivey Burden, L. (2014). Scenario-based resilience assessment framework for critical infrastructure systems: Case study for seismic resilience of seaports. Reliab. Eng. Syst. Saf. doi:10.1016/j.ress.2014.07.021.

Sharma, N., Tabandeh, A., and Gardoni, P. (2017). Resilience analysis: a mathematical formulation to model resilience of engineering systems. Sustain. Resilient Infrastruct. doi:10.1080/23789689.2017.1345257.

Shi, W., and Li, K. X. (2017). Themes and tools of maritime transport research during 2000-2014. Marit. Policy Manag. doi:10.1080/03088839.2016.1274833.

Smith, A. B., and Katz, R. W. (2013). US billion-dollar weather and climate disasters: Data sources, trends, accuracy and biases. Nat. Hazards. doi:10.1007/s11069-013-0566-5.

Smith, J. M. K., Cialone, M. A., Wamsley, T. V., and McAlpin, T. O. (2010). Potential impact of sea level rise on coastal surges in southeast Louisiana. Ocean Eng. doi:10.1016/j.oceaneng.2009.07.008.

Smythe, T. C. (2014). Assessing the impacts of Hurricane Sandy on the port of New York and New Jersey's maritime responders and response infrastructure. doi:https://doi.org/doi:10.7282/T30R9MMM.

Stelling, G. S. (1996). A non-hydrostatic flow model in cartesian coordinates, Technical note Z0901-10, WL | Delft Hydraulics, The Netherlands.

Strunsky, S. (2013). Port Authority puts Sandy damage at $2.2 billion, authorizes $50 million to power wash PATH tunnels. Available at: https://www.nj.com/news/2013/10/port_authority_sandy_22billion_outlines_recovery_measures.html [Accessed September 20, 2019].

Sutherland, J., Peet, A. H., and Soulsby, R. L. (2004). Evaluating the performance of morphological models. Coast. Eng. doi:10.1016/j.coastaleng.2004.07.015.

Sweet, W. V., Dusek, G., and Obeysekera (2018). PATTERNS AND PROJECTIONS OF HIGH TIDE FLOODING ALONG THE U.S. COASTLINE USING A COMMON IMPACT THRESHOLD.

Sweet, W., Park, J., Marra, J., Zervas, C., and Gill, S. (2014). NOAA Technical Report NOS CO-OPS 073: Sea Level Rise and Nuisance Flood Frequency Changes around the United States. doi:10.13140/2.1.3900.2887.

Sweet, W. V. (NOAA), Kopp, R. E. (Rutgers U. ., Weaver, C. P. (EPA), Obeysekera, J. (South F. W. M. D., Horton, R. M. (Columbia U. ., Thieler, E. R. (Geological S., et al. (2017). Global and regional sea level rise scenarios for the United States. 75. Available at: https://tidesandcurrents.noaa.gov/publications/techrpt83_Global_and_Regional_SLR_Scenarios_for_the_US_final.pdf.

Talke, S. A., Orton, P., and Jay, D. A. (2014). Increasing storm tides in New York Harbor, 1844-2013. Geophys. Res. Lett. doi:10.1002/2014GL059574.

Tebaldi, C., Strauss, B. H., and Zervas, C. E. (2012). Modelling sea level rise impacts on storm surges along US coasts. Environ. Res. Lett. doi:10.1088/1748-9326/7/1/014032.

Tebodin (1998). Schade bij inundatie van buitendijkse industrie. Tebodin Consult. Eng., Document no 334393 (in Dutch).

Teng, J., Jakeman, A. J., Vaze, J., Croke, B. F. W., Dutta, D., and Kim, S. (2017). Flood inundation modelling: A review of methods, recent advances and uncertainty analysis. Environ. Model. Softw. doi:10.1016/j.envsoft.2017.01.006.

The Hurricane Disaster—Potential Scale (1974). Weatherwise 27, 169–186. doi:10.1080/00431672.1974.9931702.

The Saffir-Simpson Hurricane wind scale (1970). Available at: https://www.nhc.noaa.gov/aboutsshws.php.

Thoresen, C. A. (2018). Port Designer's Handbook. ICE Publishing doi:10.1680/pdhbfe.63075.

Toner, C. (2015). Explore the Alabama Port Authority's $31.6 million payroll. Available at: https://www.al.com/news/2015/08/explore_the_alabama_port_autho.html?appSession=6YSXLA57WI44RT1BP8SOCC53897E0AXH2997ZQ39X1OC7C6V2Y38J9T7R6SL8XD0CQ4WIOLN34A9X410JDS167GZU22BO3E99SL74K7BWC6TP46V963859Z64F860S14 [Accessed June 30, 2020].

Trenberth, K. E., Fasullo, J. T., and Balmaseda, M. A. (2014). Earth's Energy Imbalance. J. Clim. 27, 3129–3144. doi:10.1175/JCLI-D-13-00294.1.

U.S. EPA. (2017). Evaluating Urban Resilience to Climate Change: A Multi-Sector Approach (Final Report). U.S. Environmental Protection Agency, Washington, D.C., EPA/600/R-16/365F, 2017. Tema-Journal L. Use Mobil. Environ.

UNISDR (2013). (The United Nations International Strategy for Disaster Reduction), From Shared Risk to Shared Value –The Business Case for Disaster Risk Reduction.

USACE (2013). Incorporating Sea level Changes in Civil Works Programs. ER 1100-2-8162.

USACE (2018). The U.S. Waterway System: 2018 Transportation Facts & Information. System.

USACE (2019). Mobile Harbor, Mobile, Alabama: Integrated General Reevaluation Report With Supplemental Environmental Impact Statement. Available at: https://hdl.handle.net/11681/34633.

USACE (2020). Sea Level Change Curve Calculator (Version 2019.21). Available at: http://corpsmapu.usace.army.mil [Accessed April 10, 2020].

USDOT (2008). U.S. Department of Transportation, Maritime Administration, Glossary of shipping terms. 111. Available at: https://www.maritime.dot.gov/sites/marad.dot.gov/files/docs/resources/3686/glossaryfinal.pdf [Accessed September 20, 2019].

van Vuuren, D. P., Edmonds, J., Kainuma, M., Riahi, K., Thomson, A., Hibbard, K., et al. (2011). The representative concentration pathways: An overview. Clim. Change. doi:10.1007/s10584-011-0148-z.

Veeramony, J., Condon, A., Linzell, R., and Watson, K. (2016). Validation of Delft3D as a Coastal Surge and Inundation Prediction System; Naval Research Laboratory Stennis Space Center. Hancock County, MA, USA.

Veeramony, J., Condon, A., and van Ormondt, M. (2017). Forecasting storm surge and inundation: Model validation. Weather Forecast. doi:10.1175/WAF-D-17-0015.1.

Vermeer, M., and Rahmstorf, S. (2009). Global sea level linked to global temperature. Proc. Natl. Acad. Sci. doi:10.1073/pnas.0907765106.

Webb, B. M. (2017). A Primer on Modeling in the Coastal Environment. U.S. Department of Transportation. Federal Highway Administration. Report No. FHWA-HIF-18-002. 71. Available at: https://www.fhwa.dot.gov/engineering/hydraulics/pubs/hif18002.pdf [Accessed April 10, 2020].

Weisberg, R. H., and Zheng, L. (2006). Hurricane storm surge simulations for Tampa Bay. Estuaries and Coasts. doi:10.1007/BF02798649.

Williams, J. (1997). The Weather Book. Vintage Books Available at: https://books.google.com/books?id=kVn0WdBDMkcC.

Yang, Z., Wang, T., Voisin, N., and Copping, A. (2015). Estuarine response to river flow and sea-level rise under future climate change and human development. Estuar. Coast. Shelf Sci. doi:10.1016/j.ecss.2014.08.015.

Yin, J., Yu, D., Lin, N., and Wilby, R. L. (2017a). Evaluating the cascading impacts of sea level rise and coastal flooding on emergency response spatial accessibility in Lower Manhattan, New York City. J. Hydrol. 555, 648–658. doi:10.1016/j.jhydrol.2017.10.067.

Yin, K., Xu, S., Huang, W., and Xie, Y. (2017b). Effects of sea level rise and typhoon intensity on storm surge and waves in Pearl River Estuary. Ocean Eng. doi:10.1016/j.oceaneng.2017.03.016.

Zhang, Y., and Lam, J. S. L. (2015). Estimating the economic losses of port disruption due to extreme wind events. Ocean Coast. Manag. doi:10.1016/j.ocecoaman.2015.08.009.